Strong Field Interactions with Molecules at High Pressure: Quantum Wakes and Flying Proteins

High Pressure Chemistry at 10^{13} W cm^{-2}:

- Laser Filamentation Control of Vibrational and Rotational Coherence in Air

- fs Laser Vaporization of Intact Proteins from Solids, Liquids and Surfaces

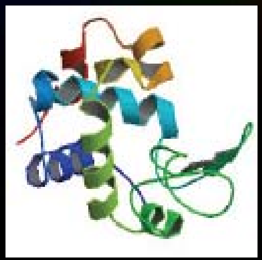

Laser Control of Chemical Reactions 4 August 2012

Robert J. Levis
Center for Advanced Photonics Research
Temple University
Philadelphia, PA

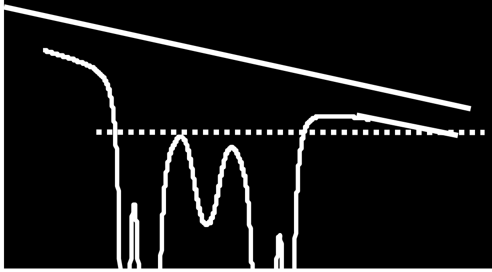

Cast


Johanan Odhner, Dmitri Romanov, Erin McCole, John Brady
Elizabeth Judge, Paul Flanigan, Johnny Perez
GAP

Intense Laser Pulse-Molecule Interactions

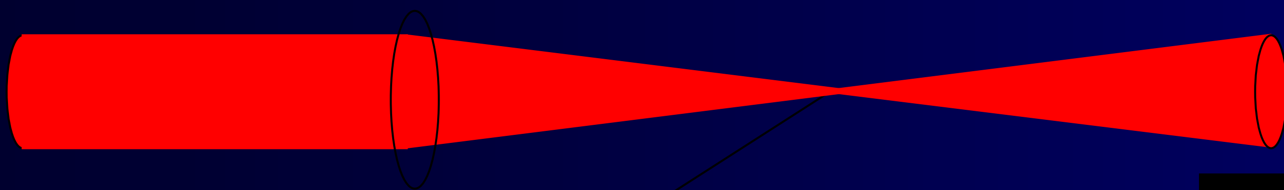

Given 1mJ, 60fs focused to 100 micron diameter:
photon density **~10^9 photons/cubic wavelength**
electric field strength **~6 Volts per Angstrom**.

Butadiene in a Strong Laser Field

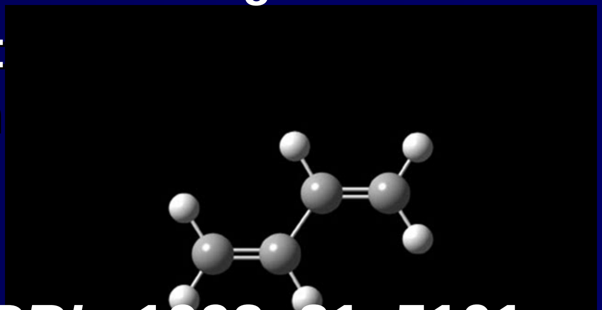

The Laser Molecule

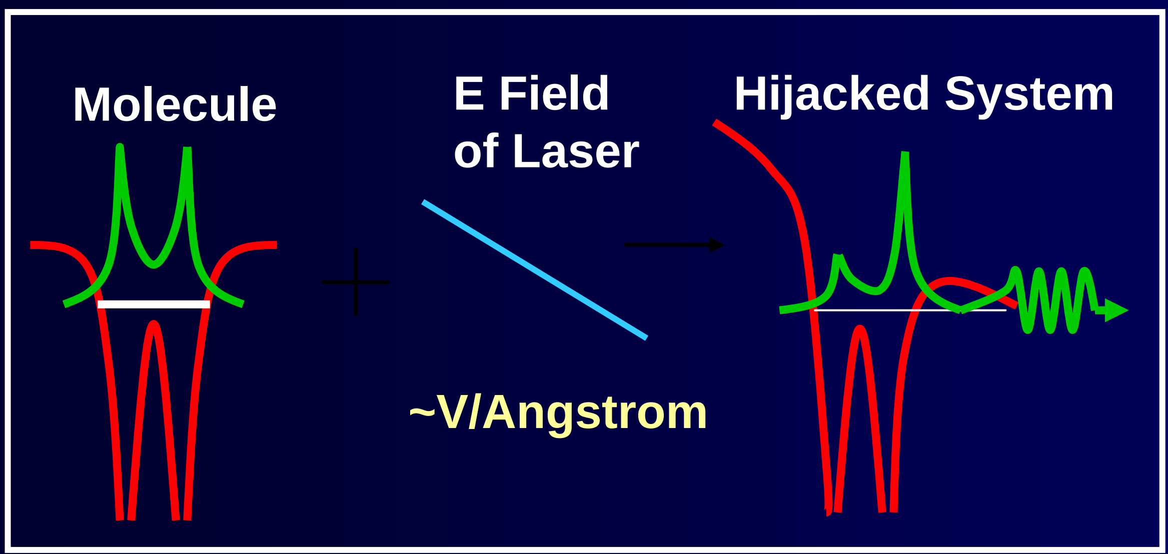

***PRL*, 1998, <u>81</u>, 5101**
***Science*, 2001, <u>292</u>, 709**
***PRL*, 2004, <u>92</u>, 063001**
***PRL*, *2006*, <u>96</u>, 163002**
***PRL*, 2009, <u>102</u>, 155004**
***PRL*, 2009, <u>103</u>, 075005**
***PRL*, 2009, <u>103</u>, 205001**
PRL, 2010, <u>105,</u> 125001
PNAS*, 2011, *<u>108</u>, 12217
***PRL*, 2012, <u>109</u>, 065003**

Laser Filaments Form Near Single Cycle Pulses

Pre-Filament
- Kerr lensing → high intensity
- High intensity → self phase modulation

Filament
- High intensity → ionization (10^{16} e^- cm^{-3})
- Ionization → intensity clamping 10^{13} W cm^{-2}
- Spatial temporal focusing → self shortening
- Self shortening → < 10 fs pulses

2 mJ 45 fs laser pulse

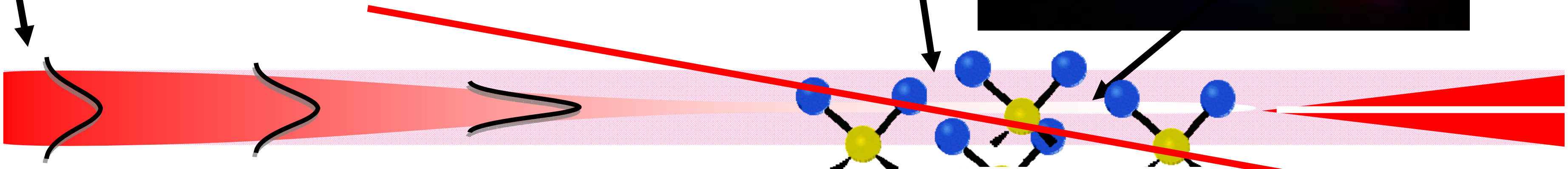

Short intense pulse provides impulsive rotational and vibrational excitation

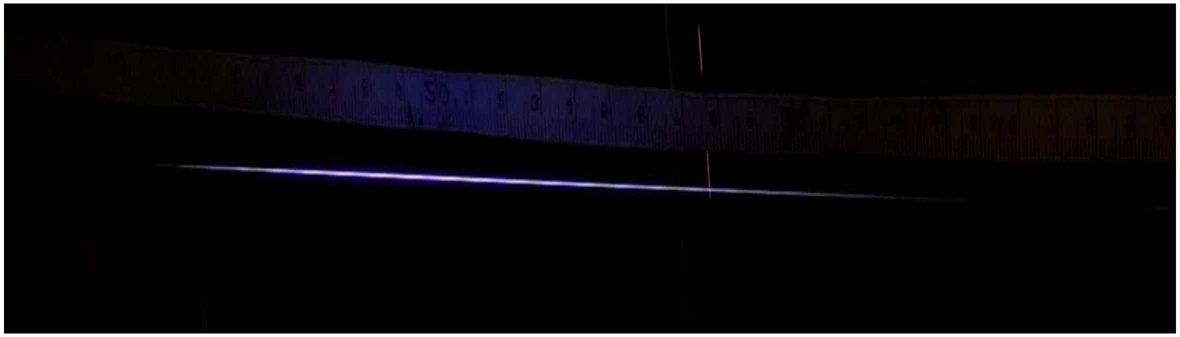

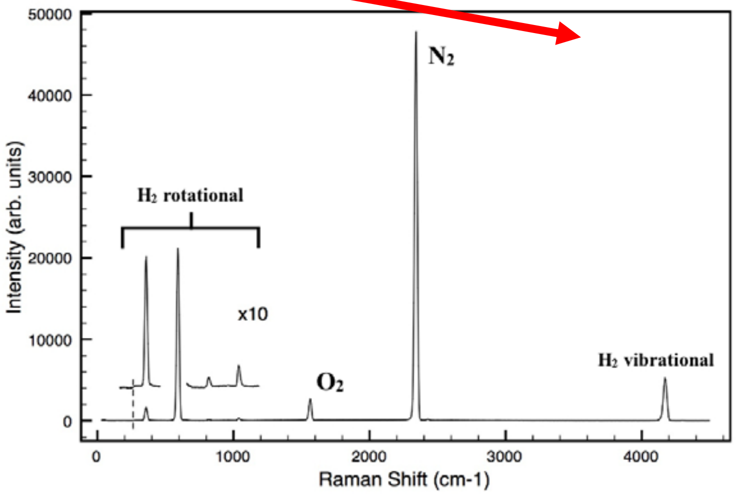

The Spatio-Temporal Dynamics Forming the Filament

electric field envelope

diffraction

group velocity dispersion

$$\frac{\partial E_{fil}}{\partial z} - \alpha k_0 \frac{\partial E_{fil}}{\partial t} = \frac{i}{2k_0}\Delta_\perp E_{fil} - \frac{i}{2}\beta k_0 \frac{\partial^2 E_{fil}}{\partial t^2} +$$

$$\frac{6\pi i \omega_0^2}{k_0 c^2}\chi^{(3)}\left|E_{fil}\right|^2 E_{fil} - \frac{12\pi\omega_0}{k_0 c^2}\left(\frac{\partial}{\partial t} + \frac{i}{2\omega_0}\frac{\partial^2}{\partial t^2}\right)\chi^{(3)}\left|E_{fil}\right|^2 E_{fil},$$

group velocity

Kerr lensing

Self-steepening

Spatial and Temporal Kerr Nonlinear Effects

From 100 oscillations of the electro-magnetic field to two!

Self Compression In Pulse

Spatio-temporal characterization of few-cycle pulses obtained by filamentation

A. Zaïr[1*], A. Guandalini[1], F. Schapper[1], M. Holler[1], J. Biegert[1,1], L. Gallmann[1], A. Couairon[2], M. Franco[3], A. Mysyrowicz[3], and U. Keller[1]

As the broad band pulse propagates, the system self-compresses to ultrashort (~5 fs) features

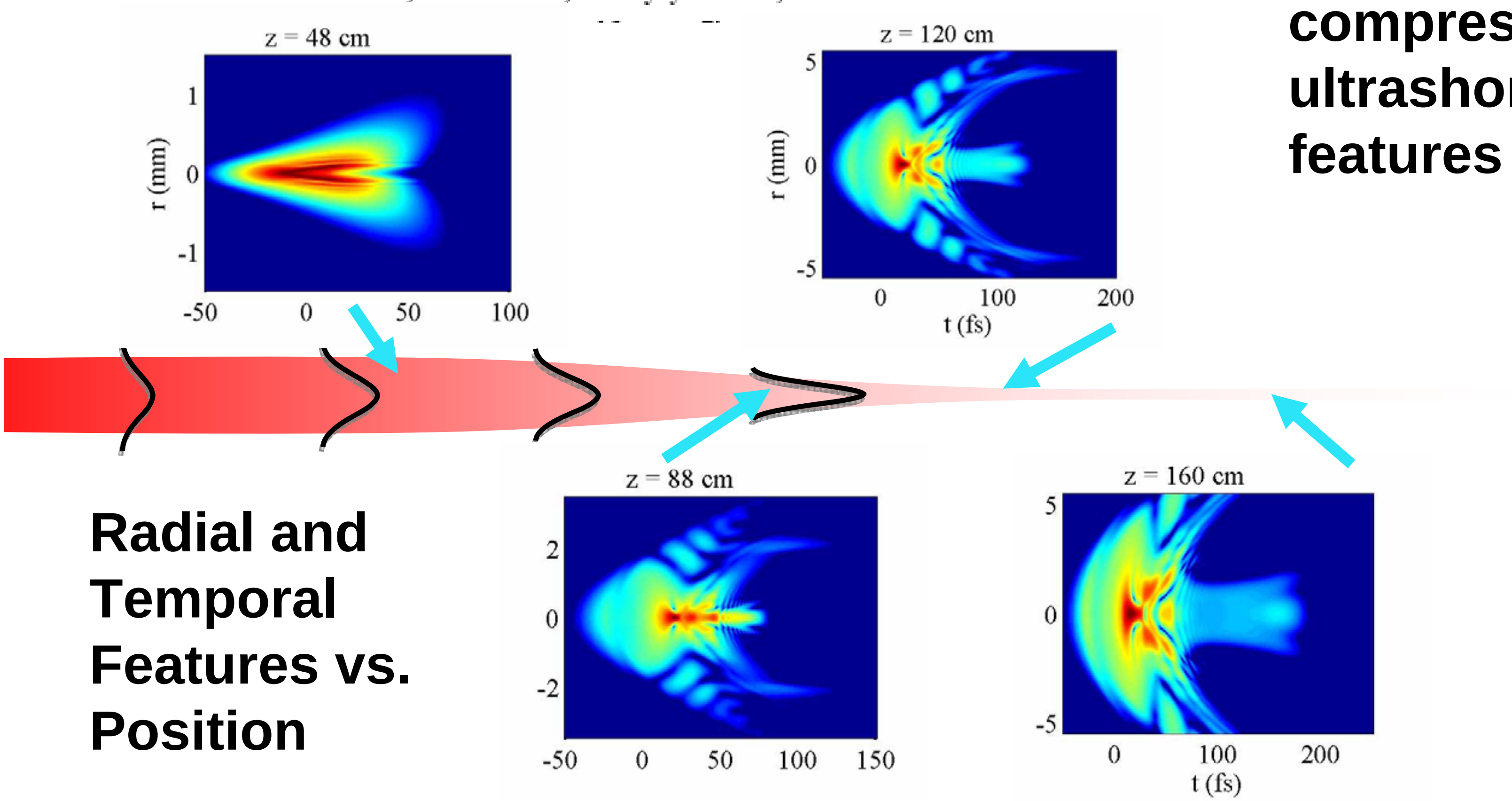

Radial and Temporal Features vs. Position

30 April 2007 / Vol. 15, No. 9 / OPTICS EXPRESS 5396

Measuring Filament Propagation in Air

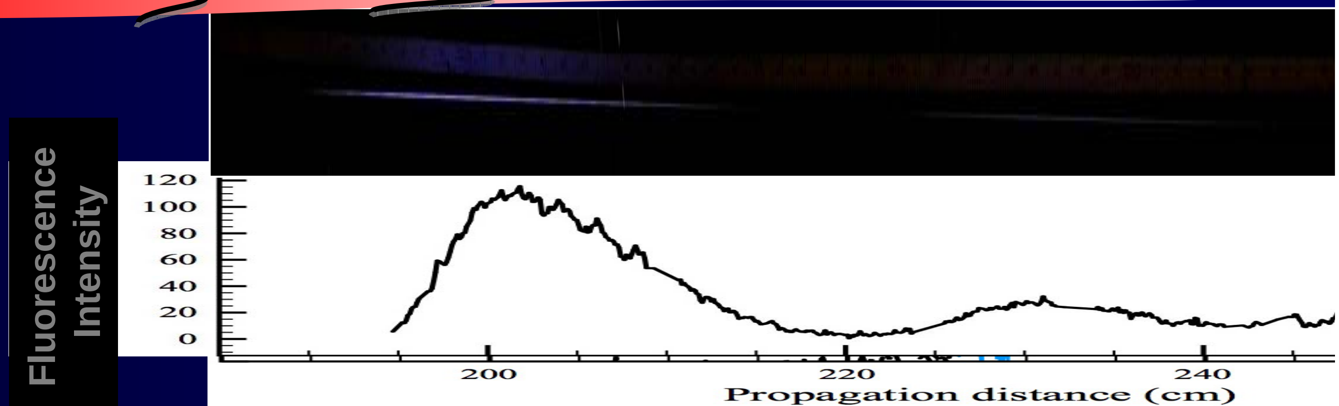

Bree et al. Opt. Ex.

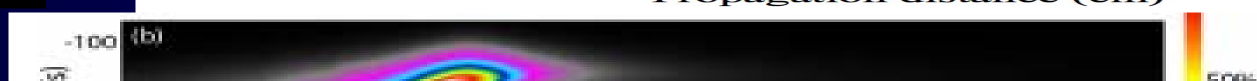

Probing filamentation dynamics is problematic due to high intensity 10^{13} W cm^{-2}

Fluorescence: Talebpour, Optics Communications **171**, 285 (1999).

Acoustic: Yu, Applied Optics **42**, 7117 (2003).

Conductivity: Eisenmann, Physical Review Letters **98**, (2007).

Post Filament SPIDER: Stibenz, Optics Letters **31**, 274 (2006).

Probing Filament Dynamics via Impulsive Raman Spectroscopy

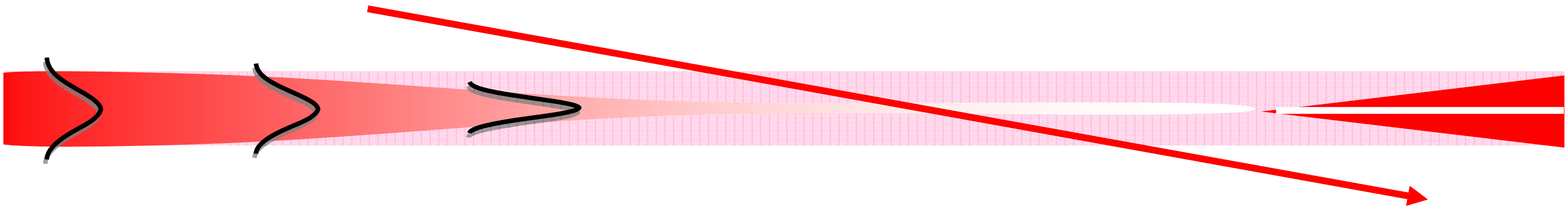

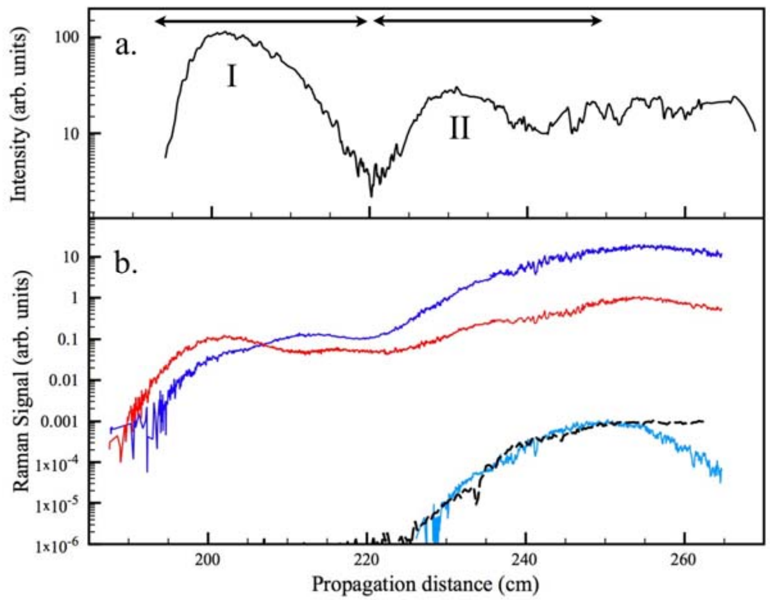

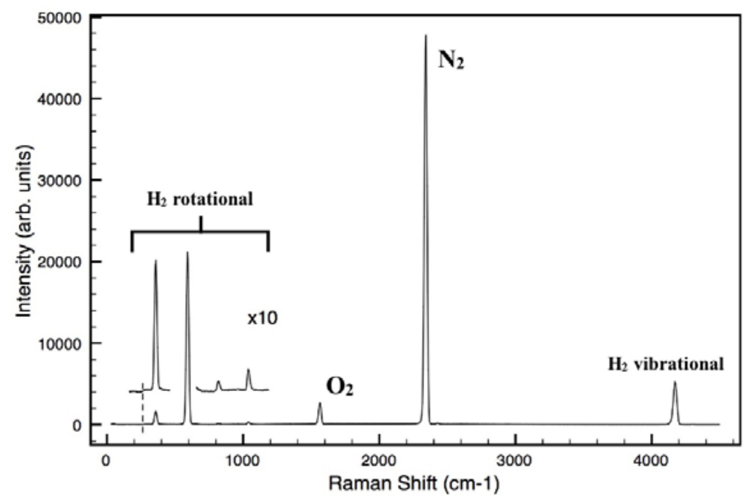

Criteria for Impulsive Vibrational Excitation

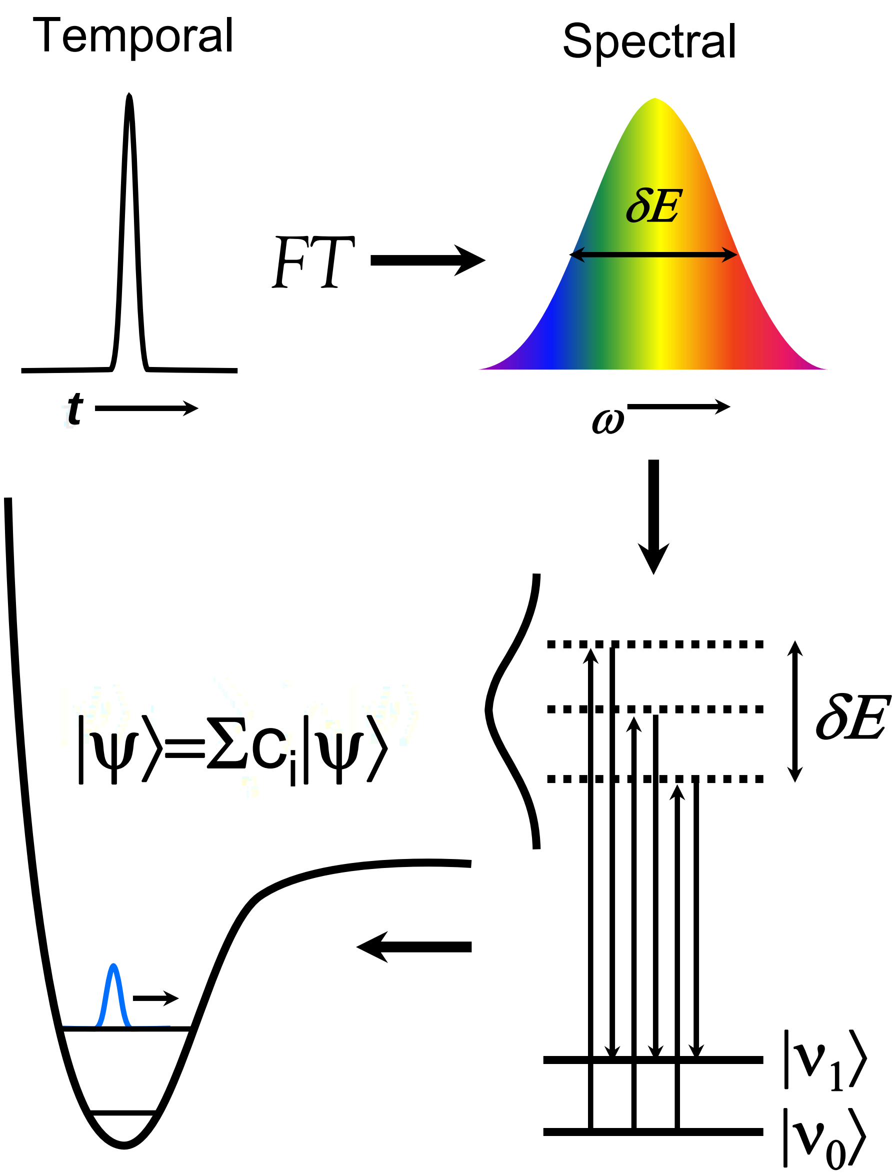

Irradiating a molecule with a sufficiently short pulse results in:
i, a superposition of vibrational states
ii, a time-dependent wavepacket
iii, a time-dependent polarizability

XFROG Characterization of Filament

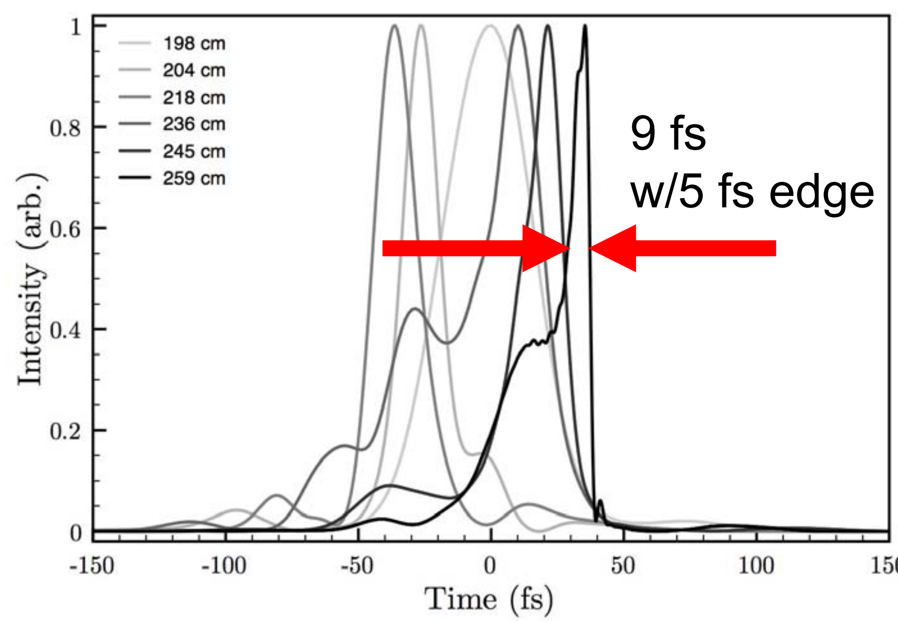

Impulsive Raman "Time-Domain" Detection

2922 OPTICS LETTERS / Vol. 33, No. 24 / December 15, 2008

Molecular rotovibrational dynamics excited in optical filamentation

F. Calegari,* C. Vozzi, S. De Silvestri, and S. Stagira
National Laboratory for Ultrafast and Ultraintense Optical Science–CNR-INFM, Dipartimento di Fisica, Politecnico di Milano, Piazza Leonardo da Vinci 32, I-20133 Milano, Italy

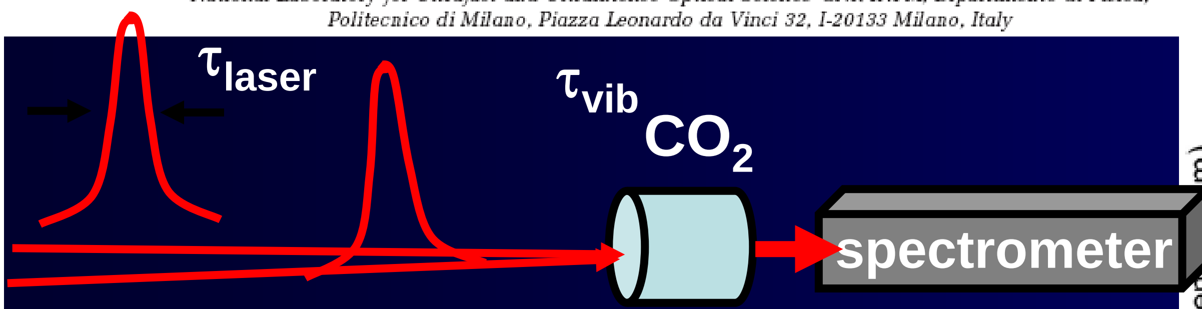

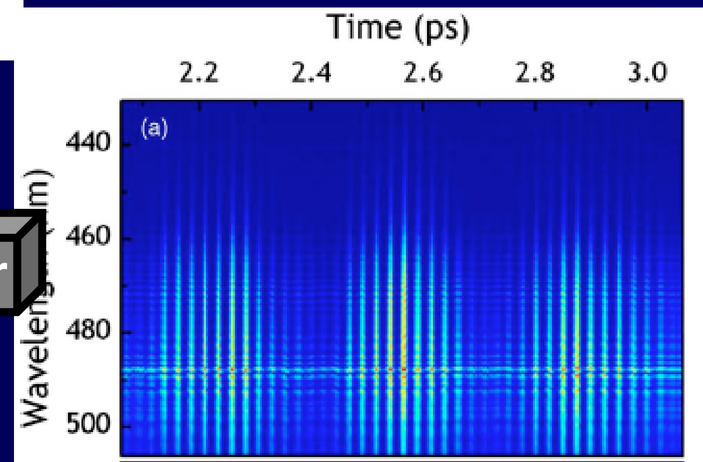

$\tau_{laser,\,1} = \tau_{laser,\,2} < \tau_{vib}$

Fourier Transform

$$\Delta\omega(t) = -\frac{\partial}{\partial t}\Delta\phi(t)$$

$$\Delta\phi(t) \propto n(t)$$

Impulsive Raman “Frequency-Domain” Detection

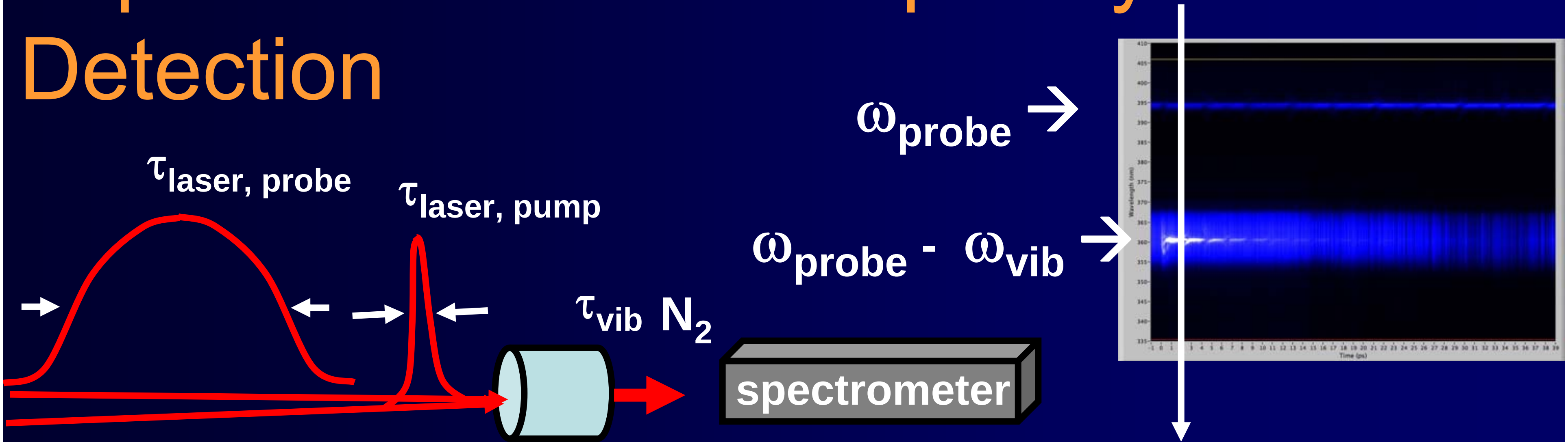

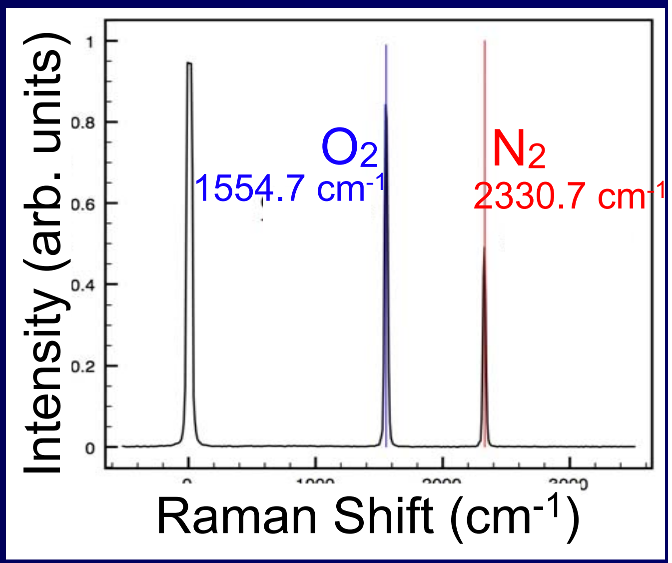

$$\tau_{laser,\ pump} < \tau_{vib} << \tau_{laser,\ probe}$$

$$\omega_{probe} \rightarrow \omega_{probe} \pm \omega_{vib}$$

pump prepares coherence

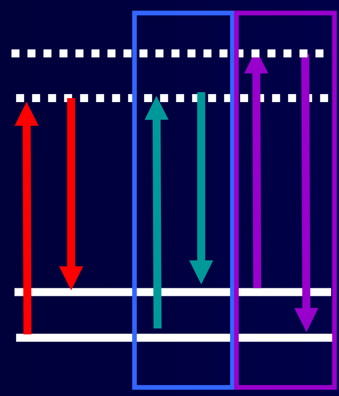

Stokes and anti-Stokes

Impulsive Stimulated Raman Spectrum in Air

An 800 nm drives both the impulsive filament pulse (2 mJ) and the weak (1.65 uJ) 400 nm probe pulse

Impulsive Raman Spectrum ~1.5 ps delay

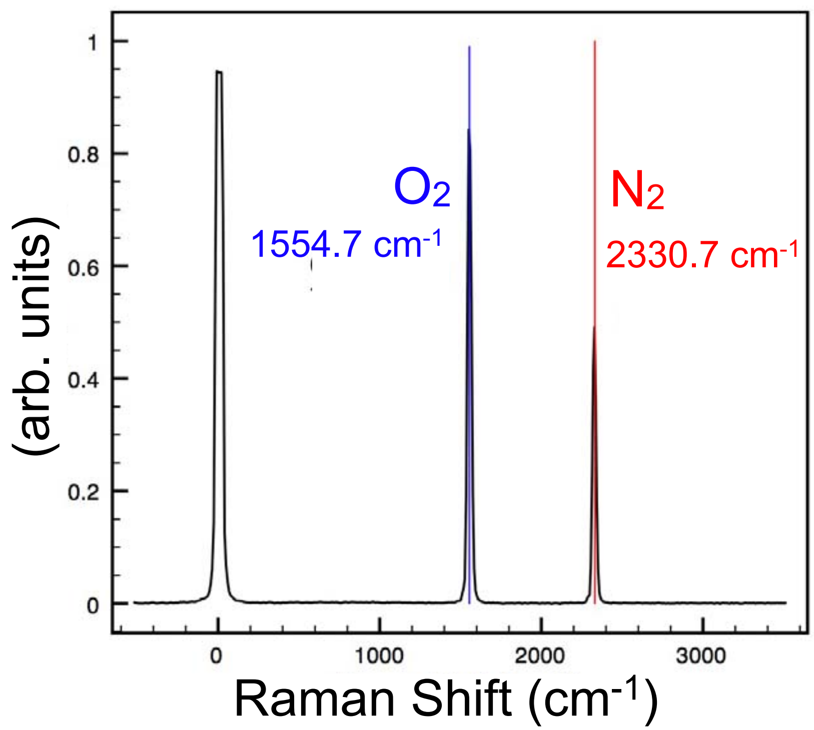

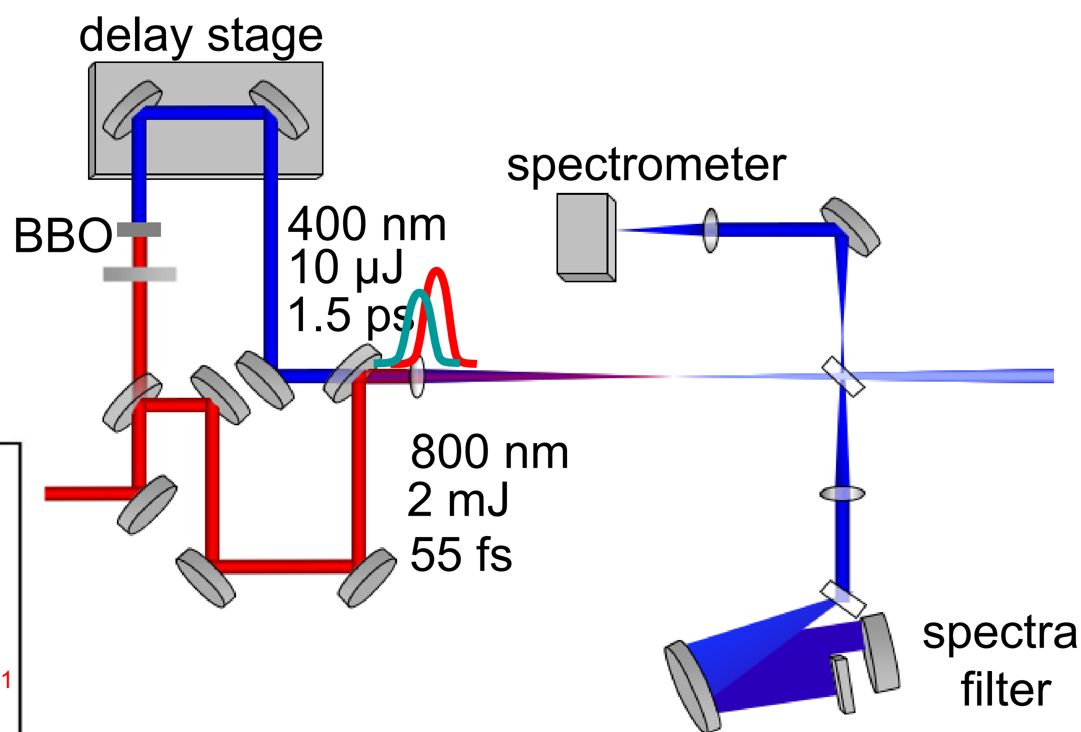

Spatial filter removes 400 nm probe

Impulsive Raman provides high sensitivity, rapid acquisition time (10 ms), few laser shots (10).

Time Scales for Molecular Motion Determine Pulse Duration for Impulsive Excitation

- Protein Backbone 500 femtosecond to ps
- CO_2 vibration 30 femtosecond
- O_2 vibration 21 femtosecond
- N_2 vibration 14 femtosecond
- C-H, O-H Stretch 10 fs
- H_2 vibration 8 femtosecond

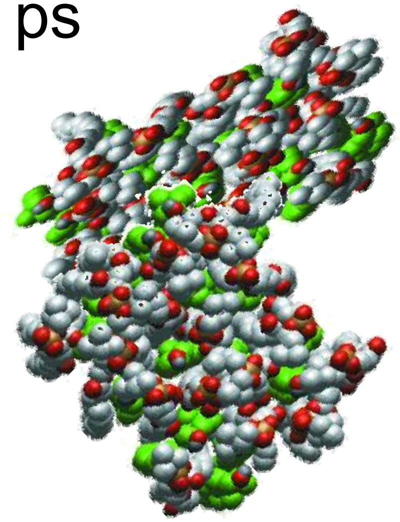

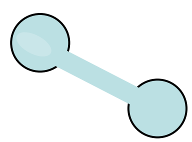

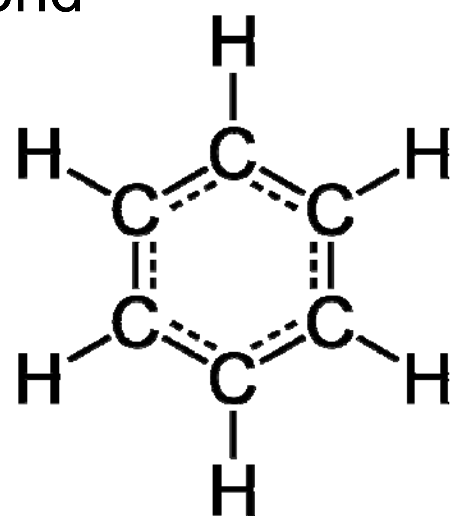

Measuring the Pulse Duration as a Function of Distance in Filament Using ISRS

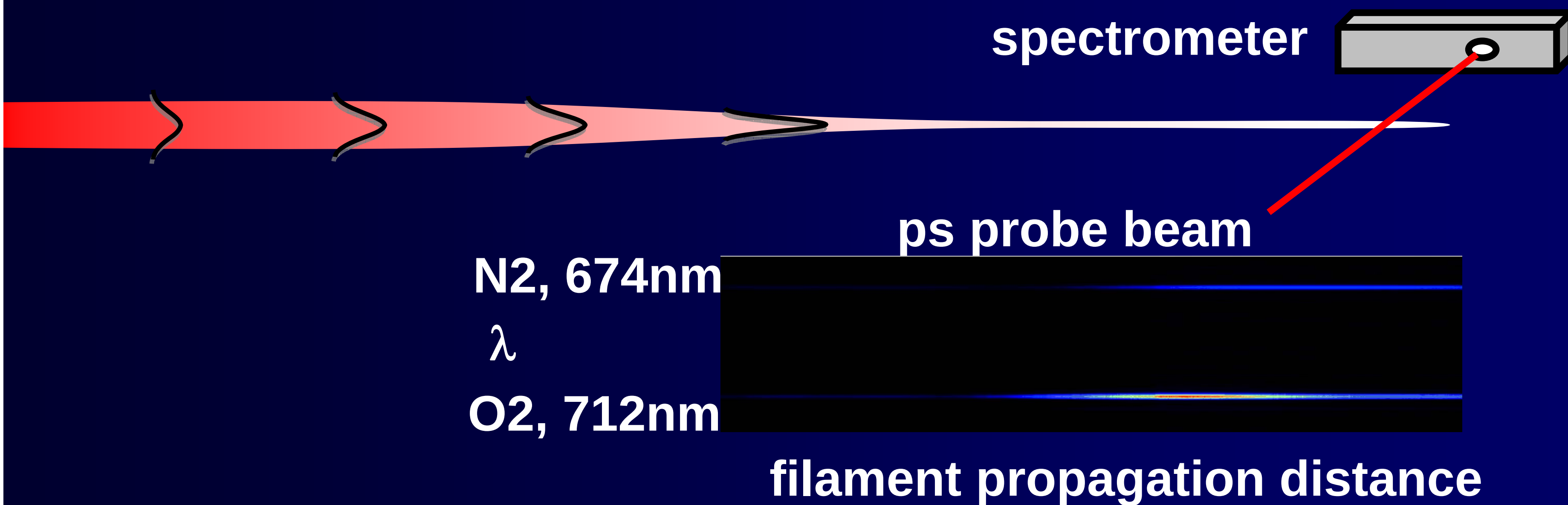

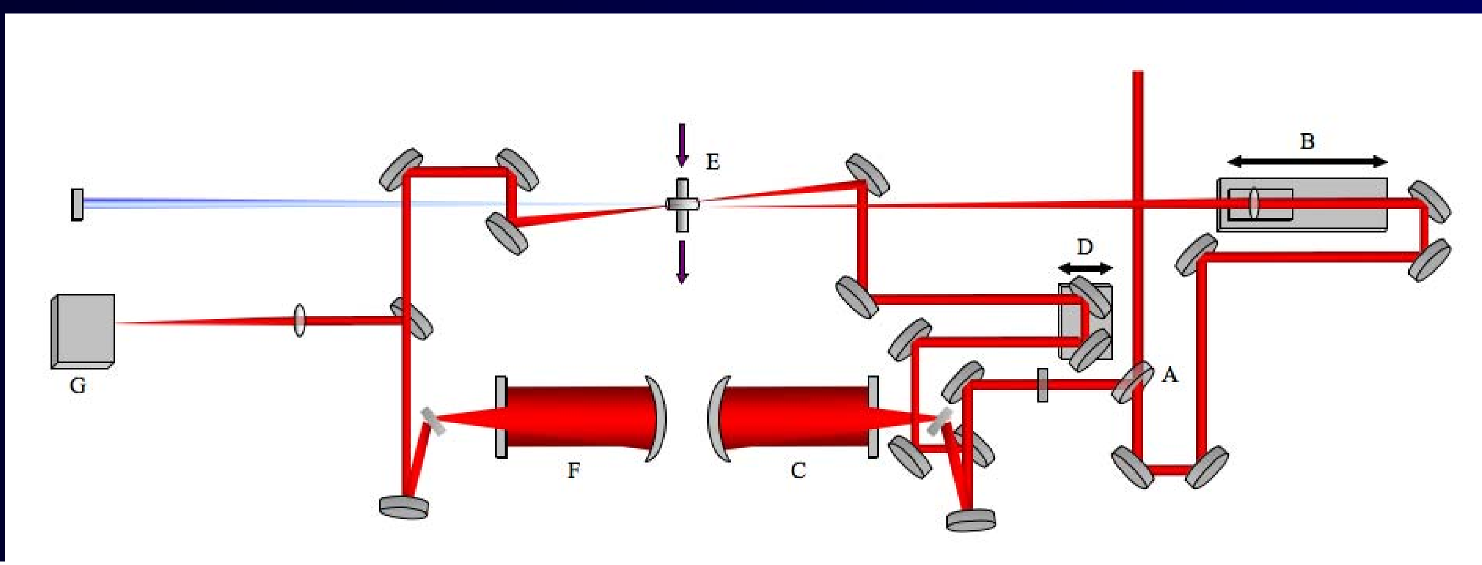

Filament Profile: Fluorescence and ISRS

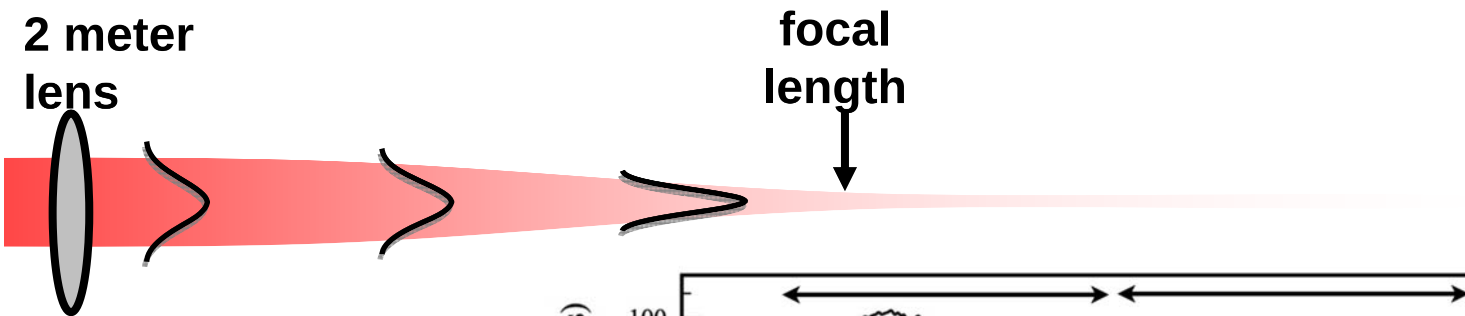

Filament Fluorescence

Impulsive Raman Scattering Intensity

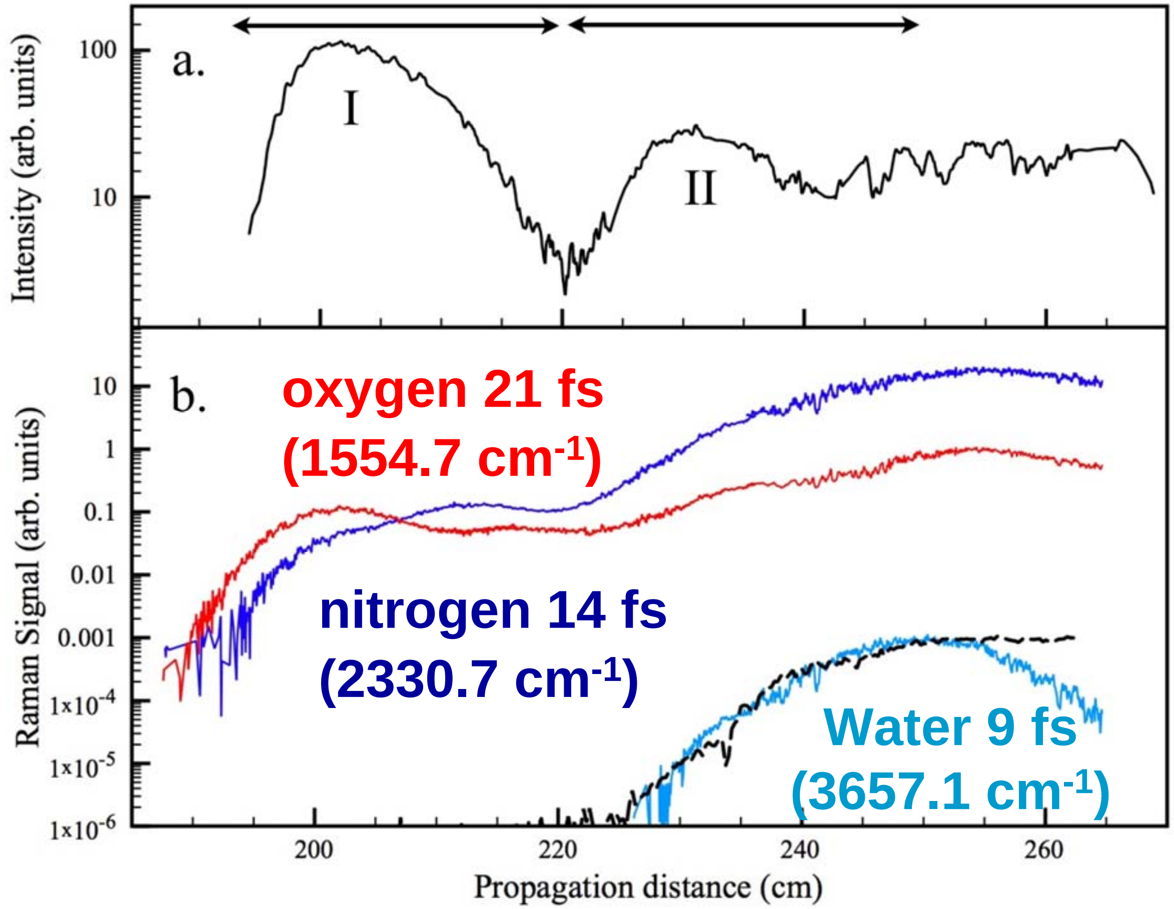

PRL 105, 125001 (2010)

Filament Profiling: Underpinnings

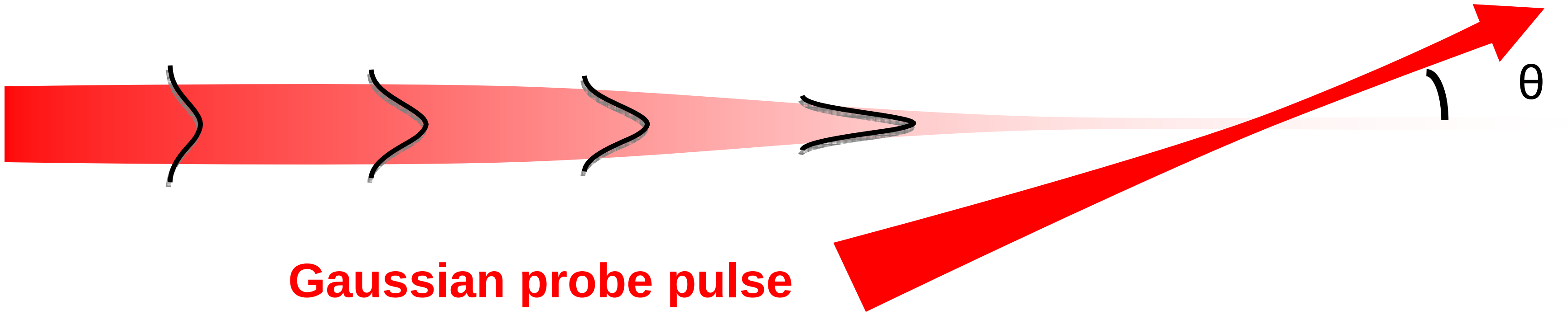

$$E_{probe}\left(t,\rho'\right)=E_{probe}e^{-\frac{\left(t-t_0\right)^2}{2\sigma}}e^{-\frac{\left(\rho'\right)^2}{2R^2}}\approx E_{probe}e^{-\frac{\left(t-t_0\right)^2}{2\sigma}}e^{-\frac{z^2\sin^2\theta}{2R^2}}$$

The resulting polarization

$$P\left(\omega_{obs},\mathbf{k},z\right)\approx\frac{N\tilde{E}_{probe}}{15\left(2\pi\right)^3\hbar^3}\frac{R\sqrt{2\pi}}{\sin\theta}\sum_{n,m,l}\frac{1}{\omega_{lg}}\frac{\mu_{mn}\mu_{ng}\;\mu_{ml}\;\mu_{lg}}{\left(\omega_{ng}-\omega_{obs}\right)\left(\omega_{mg}+\omega_{probe}-\omega_{obs}\right)}\times$$

$$e^{-\frac{R^2\left(k_z-k_{probe}\cos\theta\right)^2}{2\sin^2\theta}}\int d^2r_\perp\int_{-\infty}^{\infty}d\omega'\tilde{E}_{fil}\left(\omega',z,\mathbf{r}_\perp\right)\tilde{E}_{fil}\left(\omega_{obs}-\omega_{probe}-\omega',z,\mathbf{r}_\perp\right)$$

Filament Dynamics Via ISRS

Phys. Rev. Lett. 103, 075005 (2009)
Phys. Rev. Lett. 105, 125001 (2010)

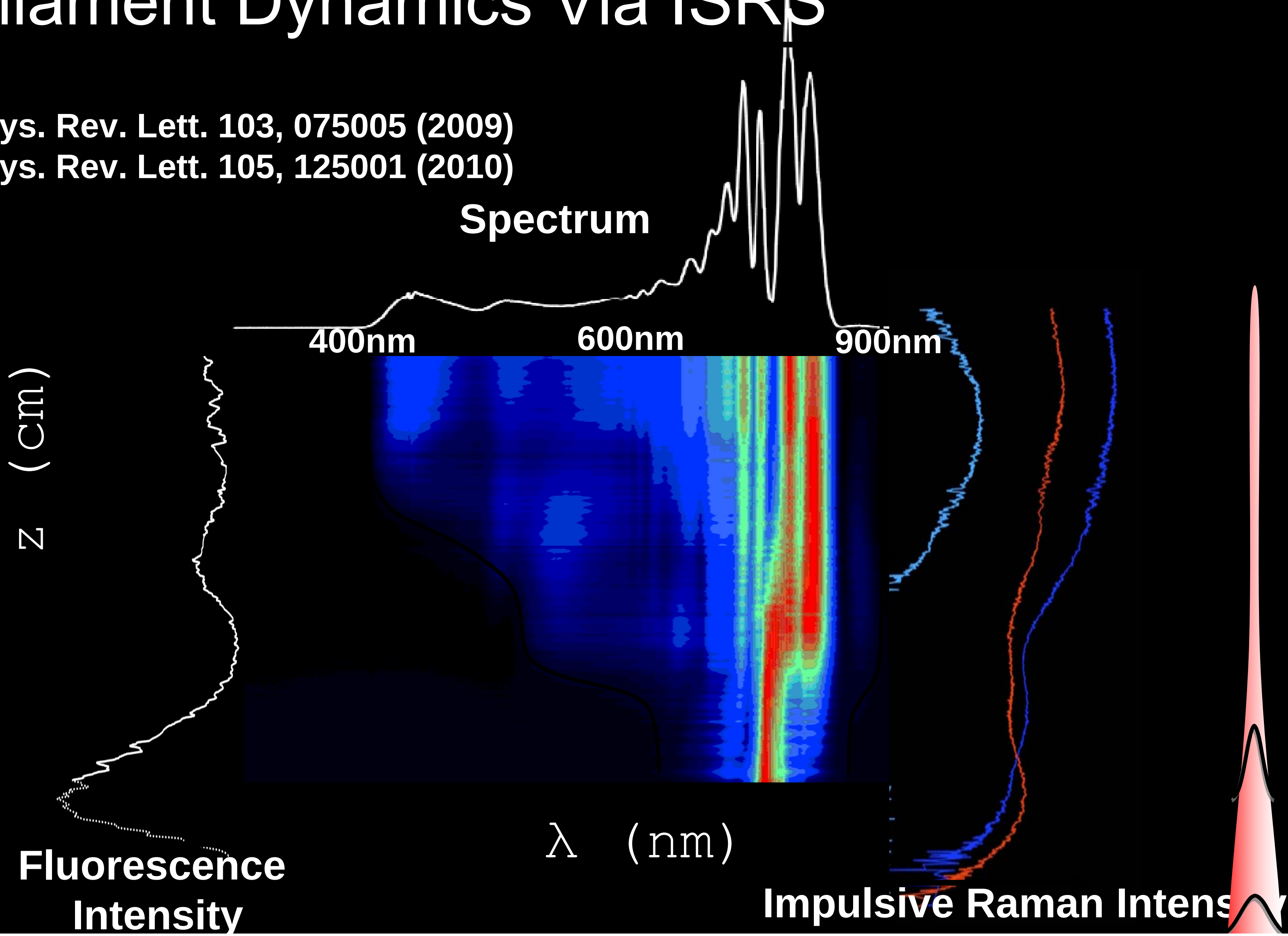

Temporal Dynamics of N2 Raman Reveals Temp

Optical Response as a function of time-delay between pump and probe

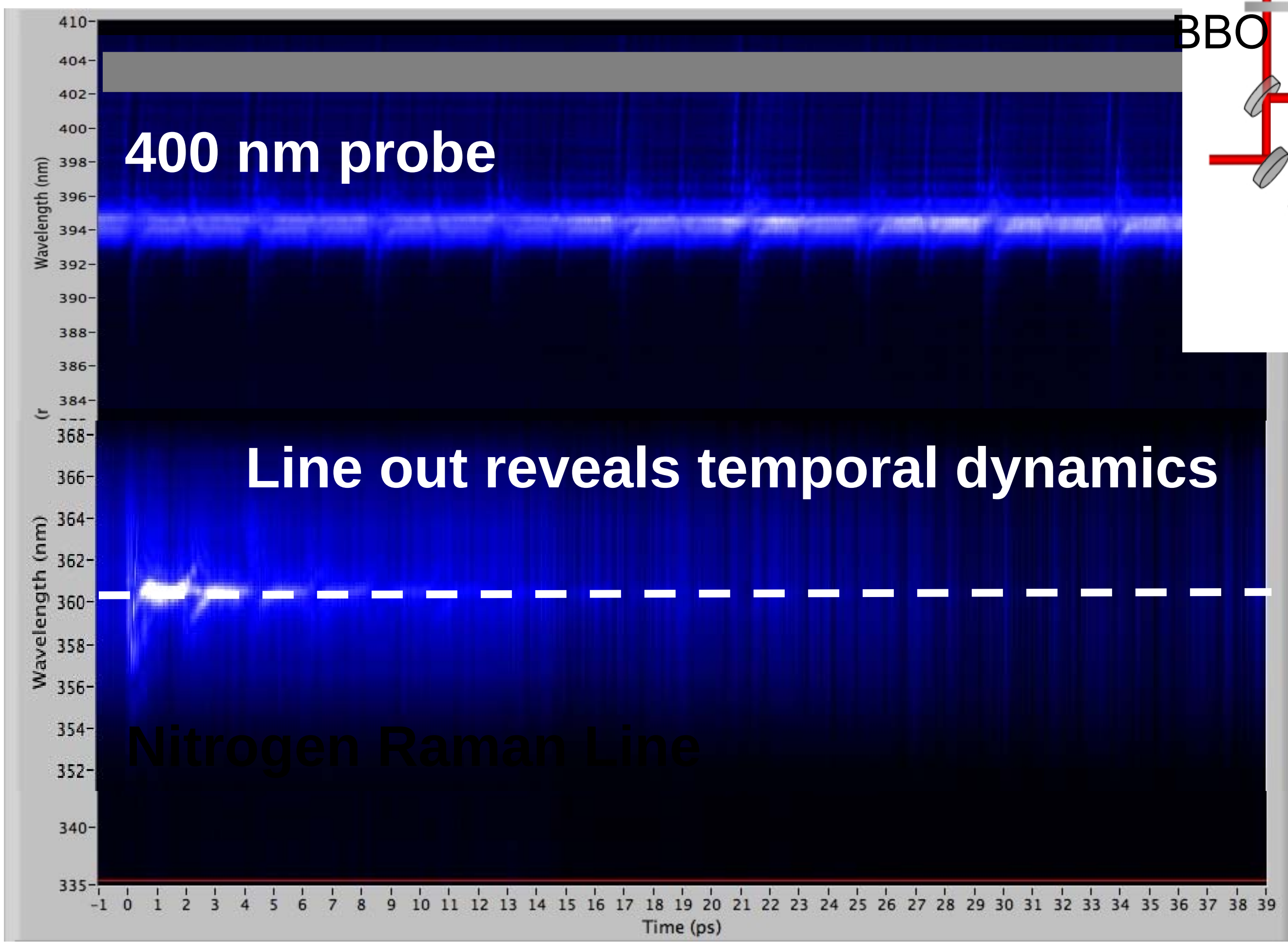

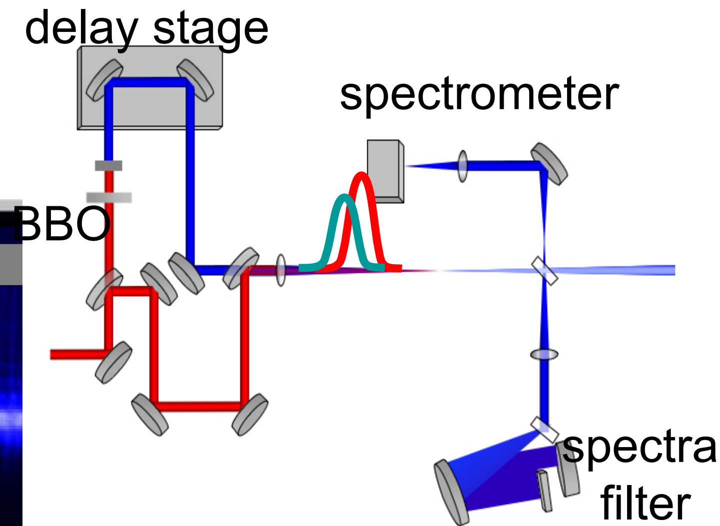

Temporal dynamics of N_2

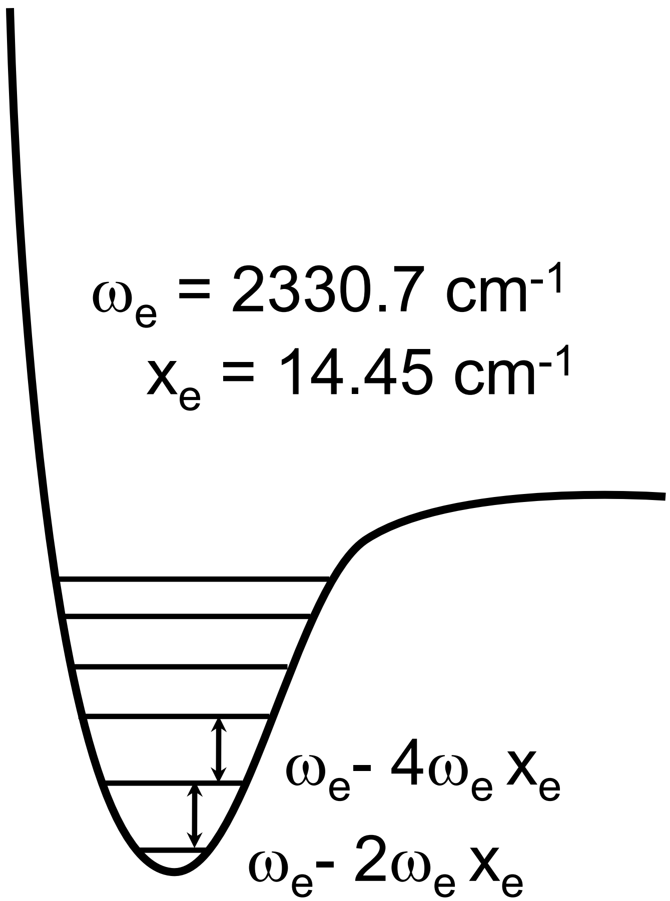

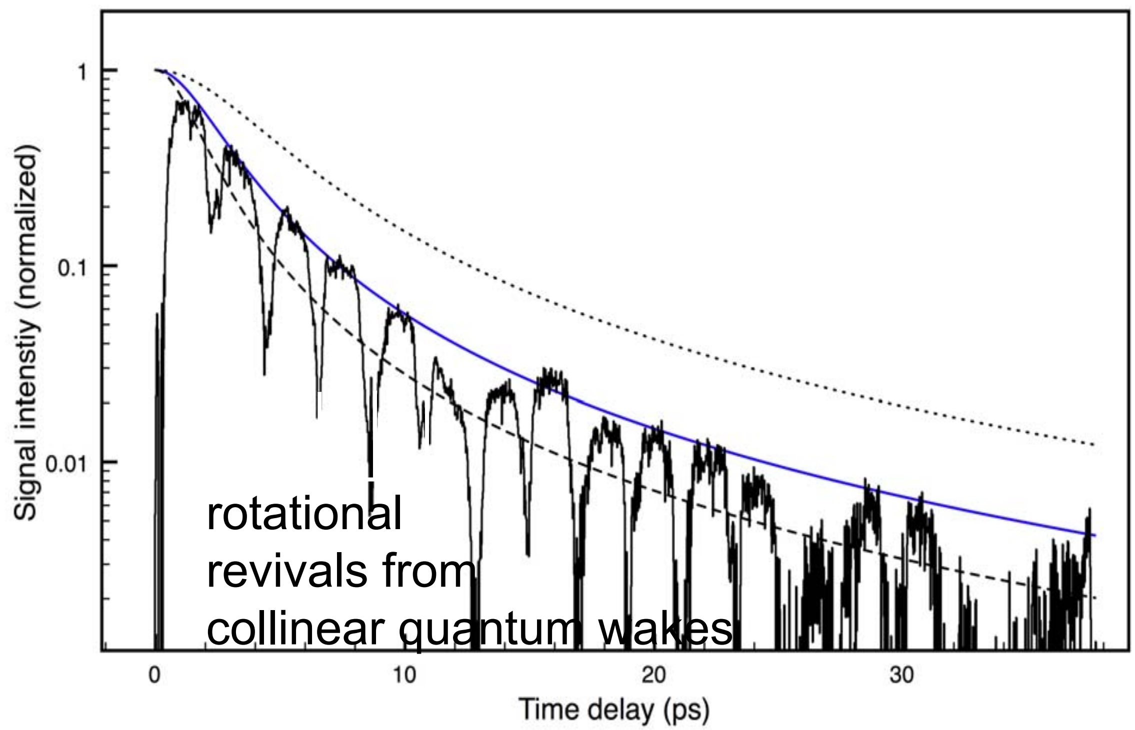

Time-dependent polarization:

$$P(t) = \sum_{v=0}^{v_{max}} A_v(T) \cos[(\omega_e - 2\omega_e x_e(v+1))t]$$

Dispersion of the Rotational-Vibrational Wavepacket

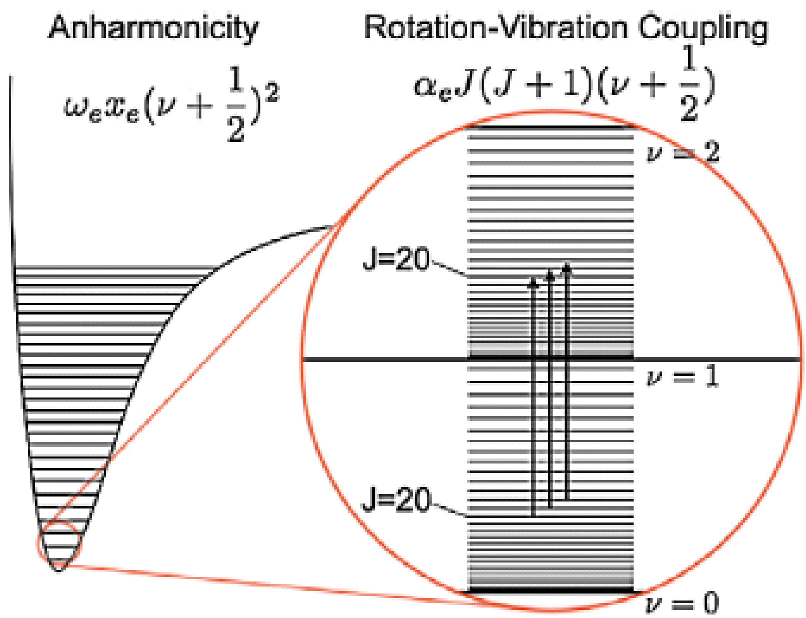

Excite multiple ro-vibrational states that are initially in phase.
With increasing time the coherent wave packet disperses via:

rotational constant

rotation-vibration coupling

$$I_S(t_d) \sim \frac{\left(\exp\left(\frac{2B_e}{kT}\right)+\frac{1}{2}\right)^2 - \sin^2\left(\frac{\alpha_e}{\hbar}t_d\right)}{\left(1+\left(\frac{\alpha_e T}{B_e \hbar}t_d\right)^2\right)\left(\sinh^2\left(\frac{\hbar\omega_e}{2kT}\right)+\sin^2\left(\omega_e x_e t_d\right)\right)}$$

vibrational frequency

anharmonicity

Temporal Dynamics at High Temperature

Temporal Dispersion of Diatomic Vibrational Wavepackets

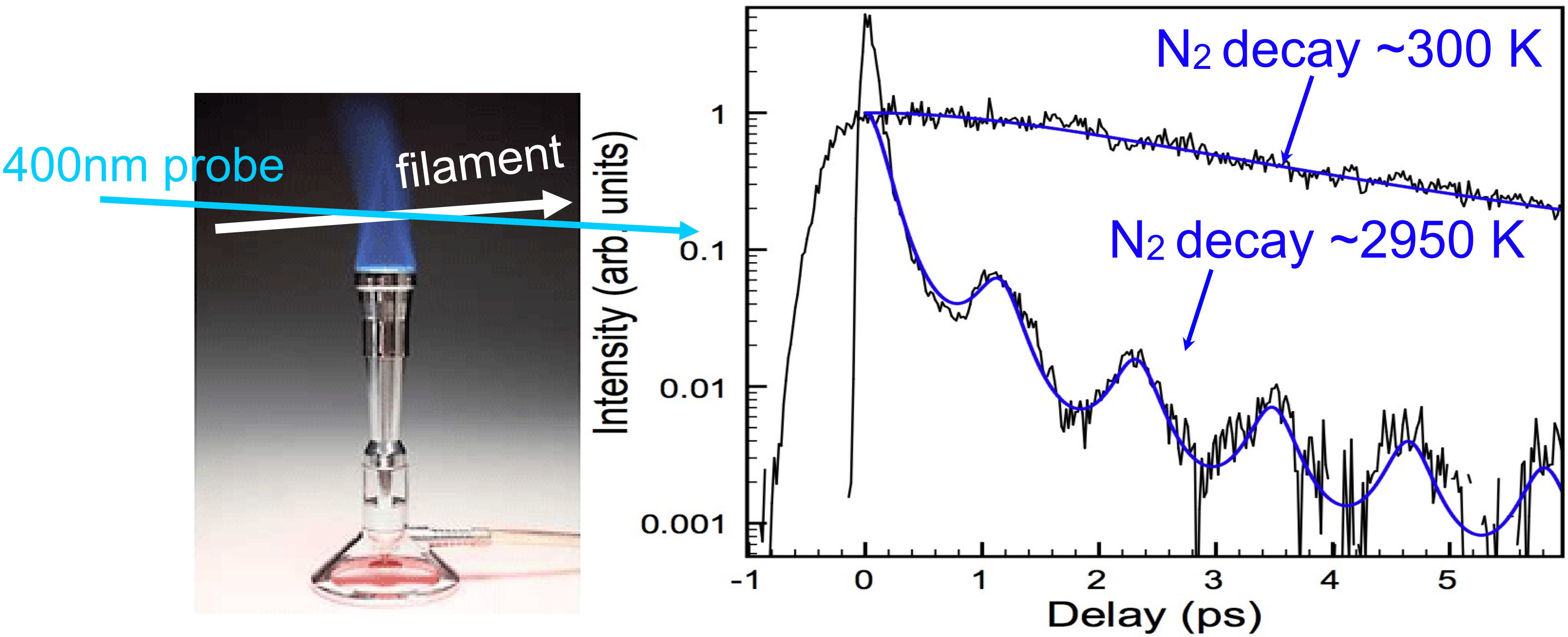

Bunsen Burner

Phys. Rev. Lett. 103, 075005 (2009)

$1/e^2$ dispersion times are on the order of ~10 ps.

Near Single Cycle Features in Filaments Enables Detection of *All* Raman Active Molecules

Single Shot Measurement from 300cm^{-1} to 4155cm^{-1}

Filament With H_2 Source

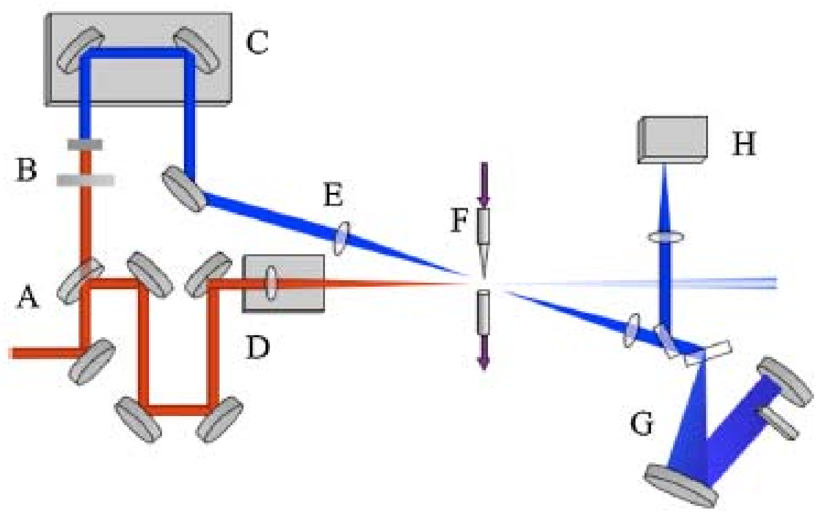

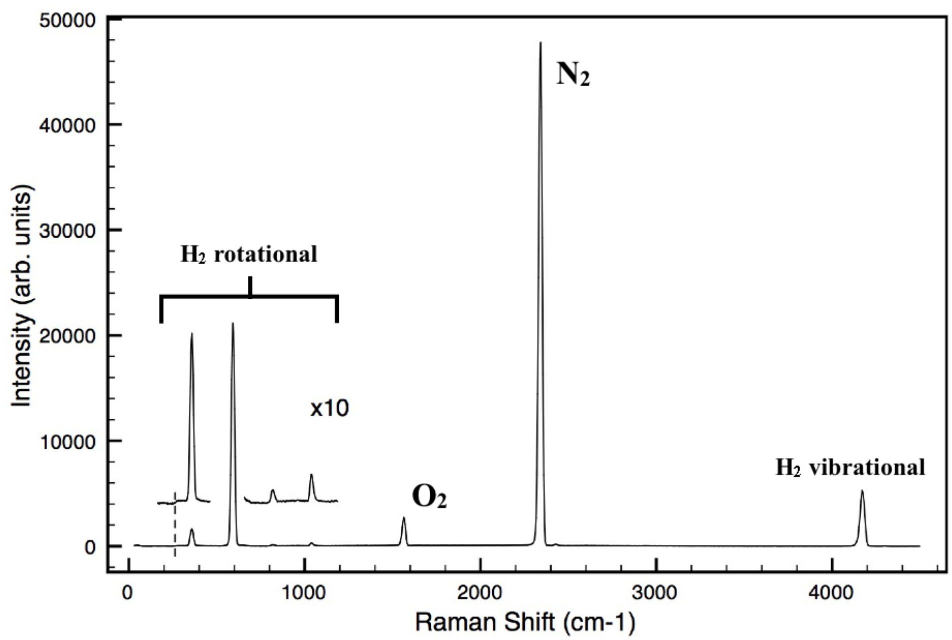

H_2 vibration at 4155cm^{-1} requires
A <8 femtoseconds feature for impulsive excitation

PRL 103, 075005 (2009) PHYSICAL REVIEW LETTERS week ending 14 AUGUST 2009

Characterizing Spectral Phase and Amplitude in a Filament via Transient Grating X-FROG

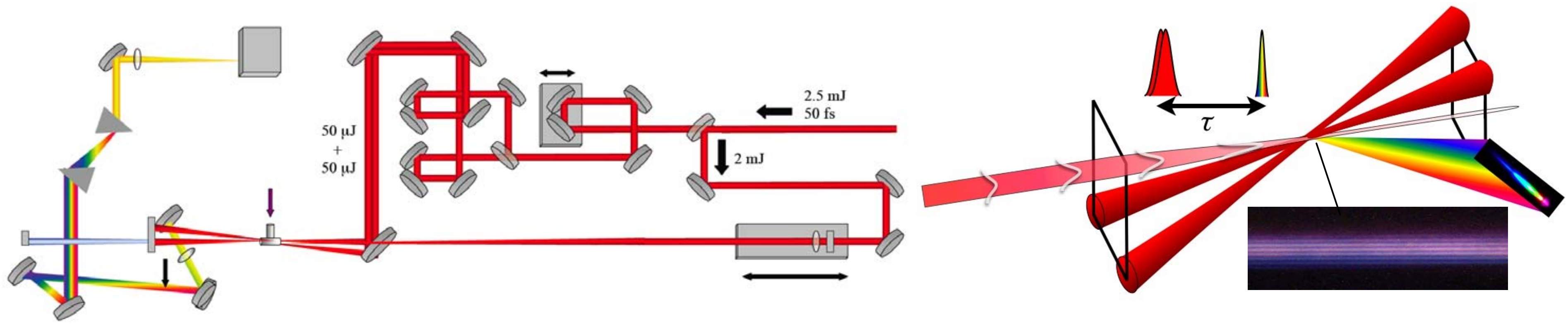

- **The filament formed using a 2-m lens is diffracted off of an optical grating formed by two reference beams. The spectrally-resolved autocorrelation is then inverted to recover the pulse electric field and spectrum.**

- **Measurements as a function of distance from the lens and input power reveal filament formation and propagation dynamics.**

Optics Letters 37, 1775, 2012

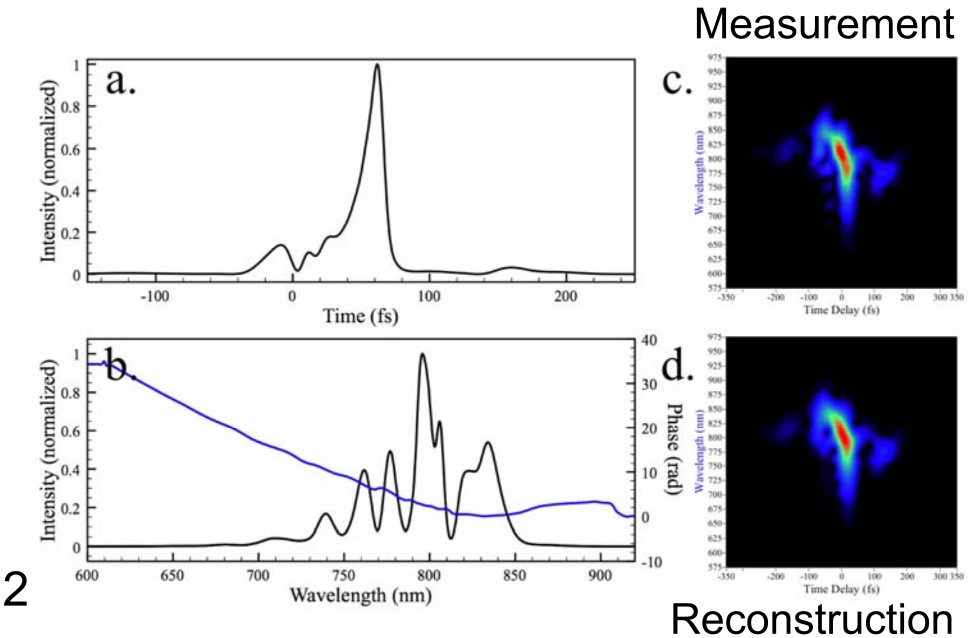

Filament XFROG vs. z Distance

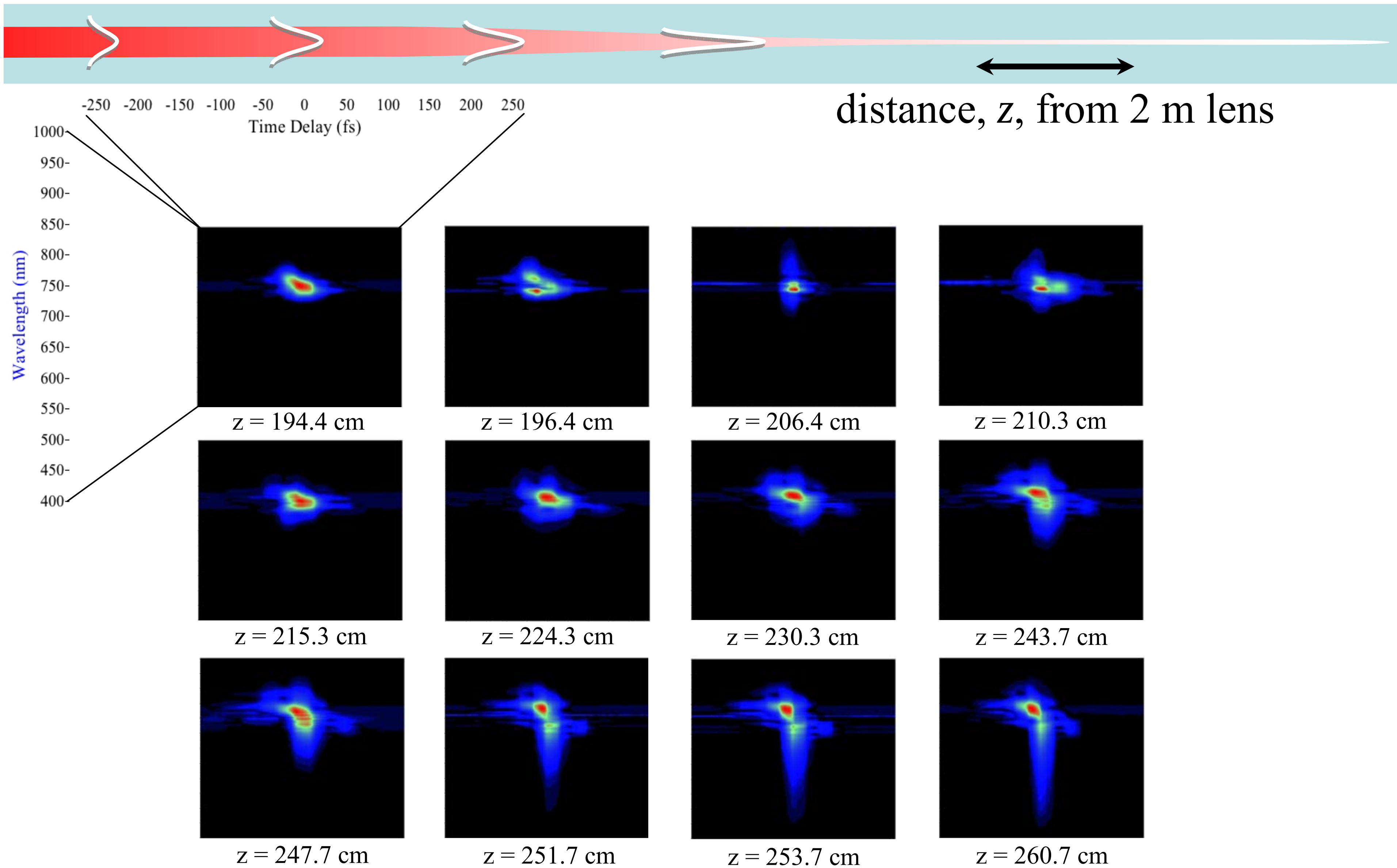

Filament XFROG vs. z Distance

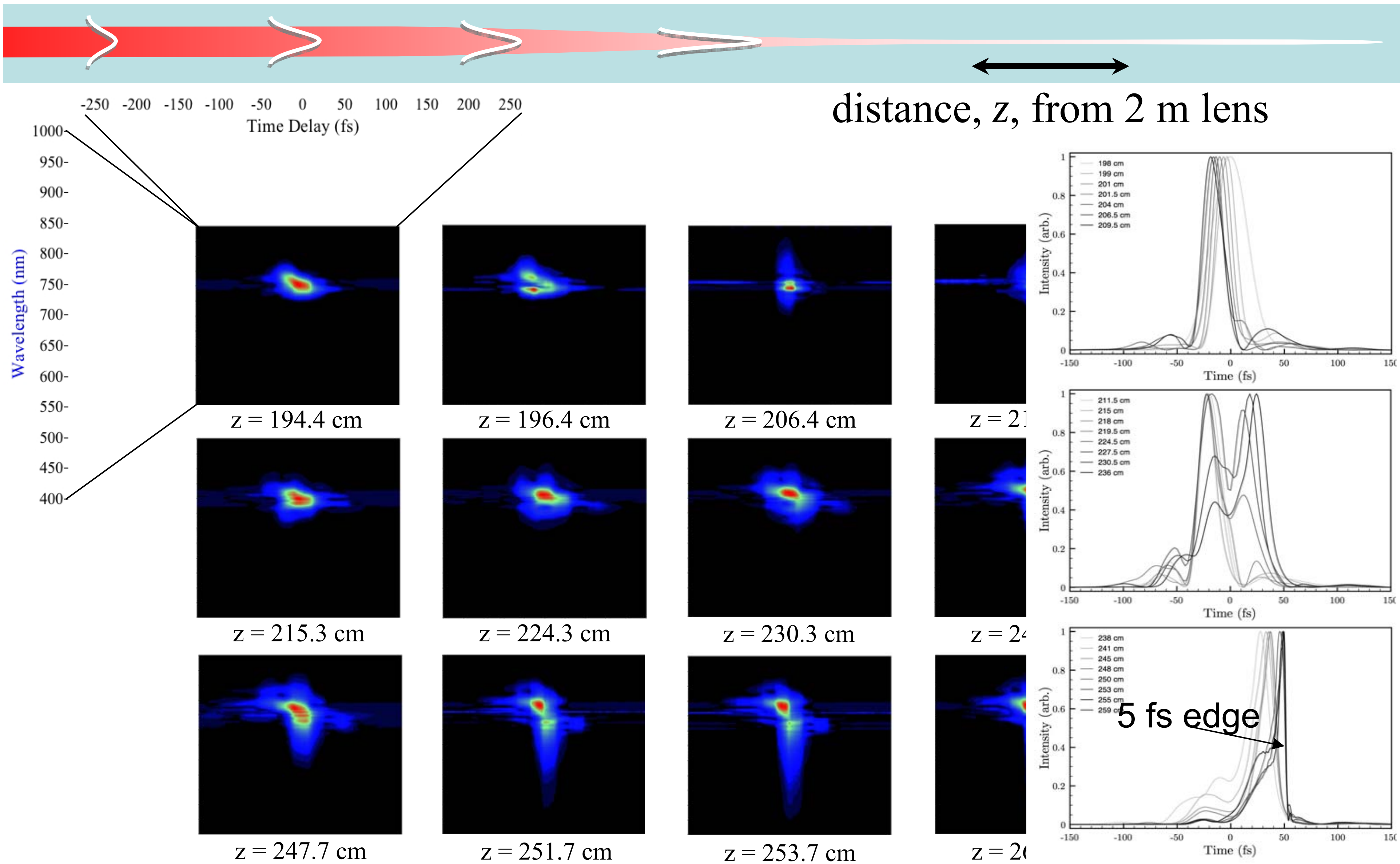

TG-XFROG in Excellent Agreement with Theory

ISSN 1054-660X, Laser Physics, 2010, Vol. 20, No. 5, pp. 1107–1113.

NONLINEAR OPTICS AND SPECTROSCOPY

Plasma Induced Pulse Breaking in Filamentary Self-Compression[1]

C. Brée[a, b, *], A. Demircan[a], S. Skupin[c, d], L. Bergé[e], and G. Steinmeyer[b, f, **]

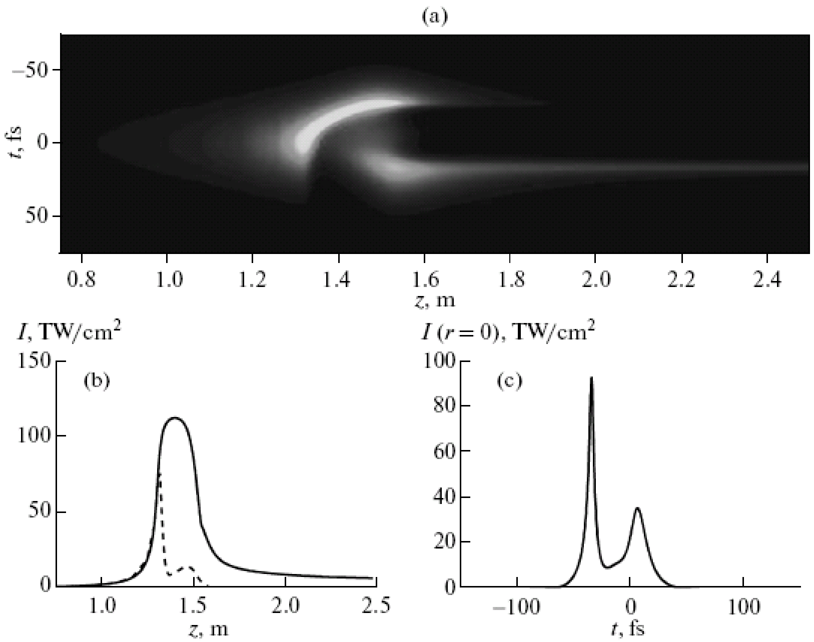

Fig. 1. (a) Evolution of the on-axis temporal profile along z. As soon as plasma defocusing has saturated the optical collapse, a characteristic temporal break-up occurs. (b) Evolution of the peak intensity (solid line) and the on-axis intensity at zero delay (dashed line). (c) On-axis temporal distribution at $z = 1.55$ m exhibiting a typical double hump structure.

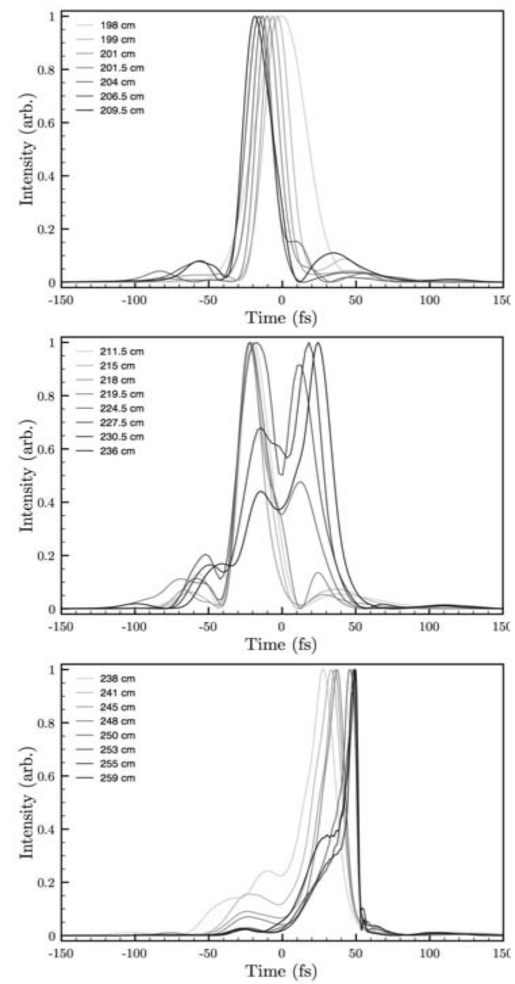

Spectrally-Resolved Transient Birefringence to Determine Mechanism

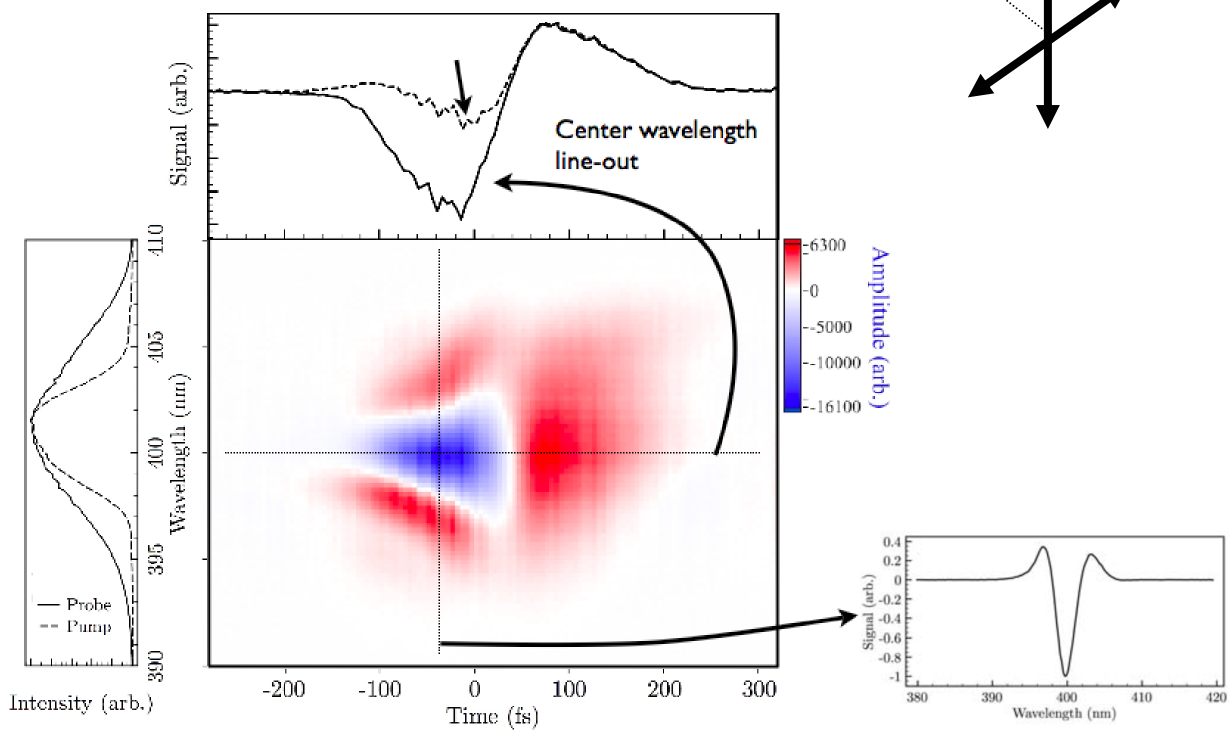

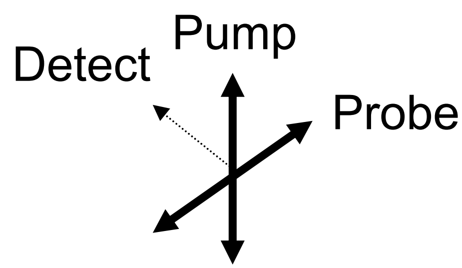

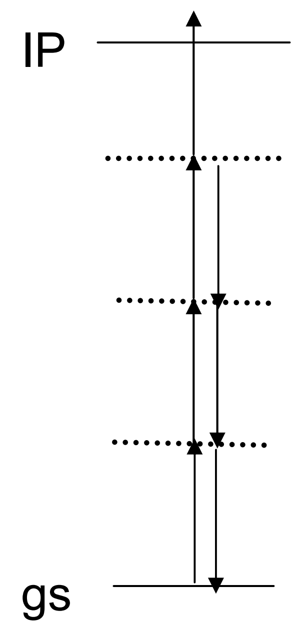

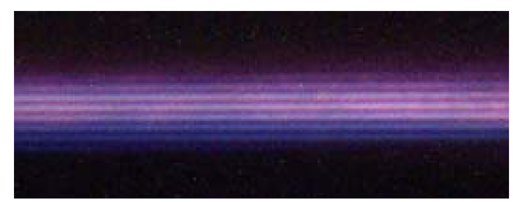

Odhner, et al. PRL **2012, <u>109</u>, 065003**

The Higher Order Kerr Measurement

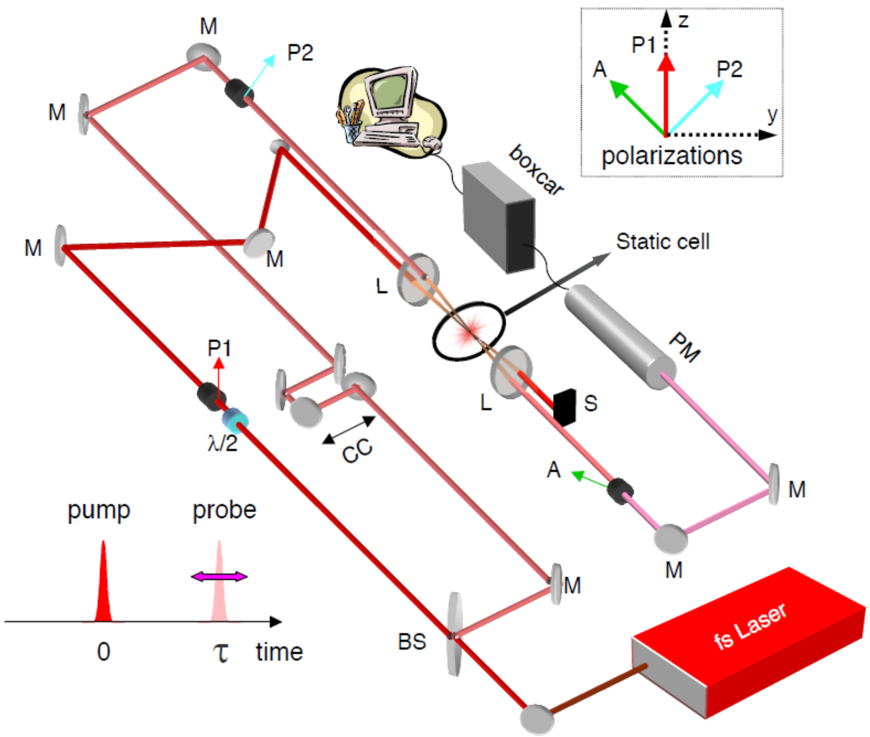

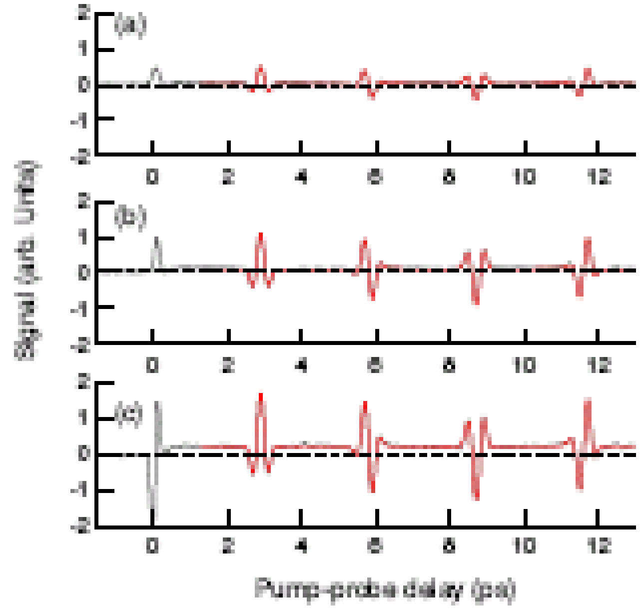

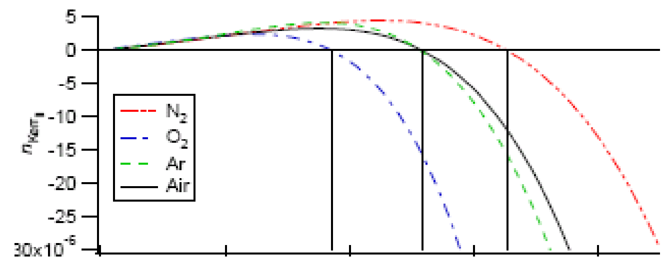

$$S_{\mathrm{hetero}}(t) \propto I_{\mathrm{pr}}(t) \otimes \left(\underbrace{\frac{3\rho\Delta\alpha}{4n_0\varepsilon_0}\left(\langle\cos^2\theta\rangle - \frac{1}{3}\right)}_{\Delta n_{\mathrm{rot}}(t)} + \underbrace{\frac{2}{3}n_2 I + \frac{4}{5}n_4 I^2 + \frac{6}{7}n_6 I^3 + \frac{8}{9}n_8 I^4 + \frac{10}{11}n_{10} I^5}_{\Delta n_{\mathrm{kerr}}(t)} \right)$$

Loriot, V. *et al. Laser Physics*, **2011**, *21*, 1319-1328.

3 August 2009 / Vol. 17, No. 16 / OPTICS EXPRESS 13429

Transient Birefringence in Optical Kerr Effect

An optical transient birefringence experiment measures the anisotropic response of a medium due to the presence of a large optical electric field.

The electric field distorts the potential experienced by electrons bound to atoms and molecules, which changes the degree to which a weak probe field interacts with the medium depending on its polarization.

Filament Polarization

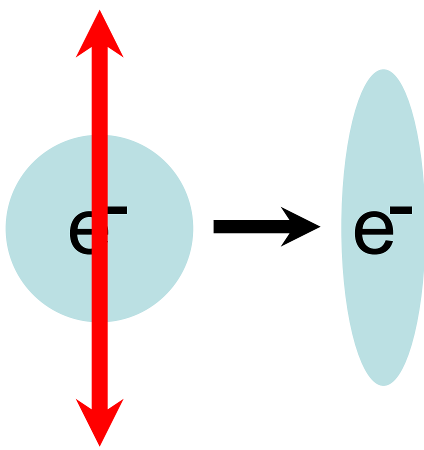

Probe Polarization

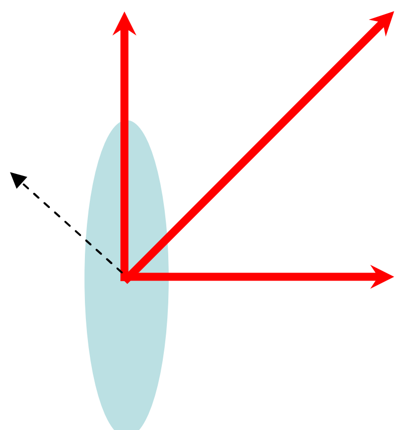

Birefringence

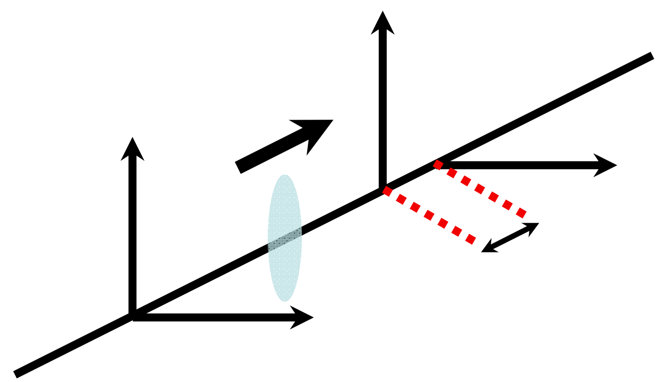

Ionization-Induced Birefringence

Optical Interference

$$I(\mathbf{r},t)=\frac{n_0 c}{8\pi}\left[|E_e(\mathbf{r},t)|^2 + \frac{1}{\sqrt{2}}\left(E_e^*(\mathbf{r},t)E_p(\mathbf{r},t-t_d)e^{i(\mathbf{k}_p-\mathbf{k}_e)\cdot\mathbf{r}}+\text{c.c.}\right)\right].$$

Plus Ionization

$$W(t)=\sigma_m I^m(\mathbf{r},t)$$

Provides Ionization Grating-Induced Phase Accumulation

$$\Delta n_{pl}^g(\mathbf{r},t)=-\frac{n_0 c N_0}{2\sqrt{2}\,\pi N_c}\times\int_{-\infty}^{t}\sigma_m I_e^{m-1}(\mathbf{r},t')E_e^*(\mathbf{r},t')E_p(\mathbf{r},t'-t_d)\mathrm{d}t'.$$

Wahlstrand and Milchberg proposed that the polarization component of the probe pulse parallel to the pump polarization will selectively participate in ionization, leading to an effective birefringence.

OPTICS LETTERS / Vol. 36, No. 19 / October 1, 2011

The Model for Plasma Grating-Induced Birefringence at 400nm Pump Probe

- At 400 nm, four photons are required to ionize O_2
- At low probe intensity, one photon from probe can add to photons to provide an excitation path. In this case interference occurs.
- Interference between pump and probe sets up an intensity grating.
- Interaction or exchange of probe photons in ladder climbing leads to phase accumulation.

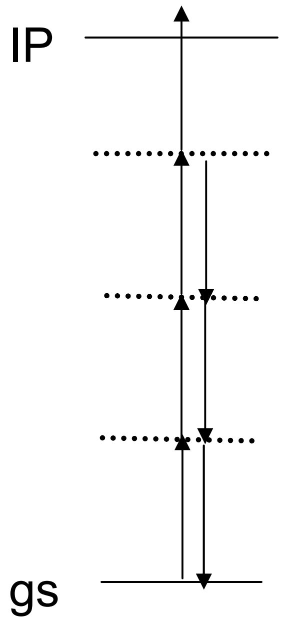

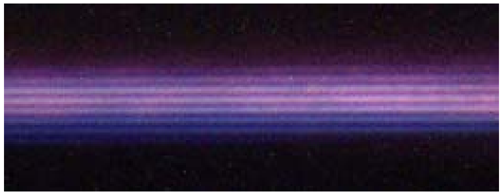

Two-beam phase coupling

OPTICS LETTERS / Vol. 36, No. 19 / October 1, 2011

- Pump (and probe) can diffracts into probe (and pump) direction.
- If frequencies of pump and probe are not degenerate, the grating moves appreciably on the time scale of pulse duration and diffraction washes out.

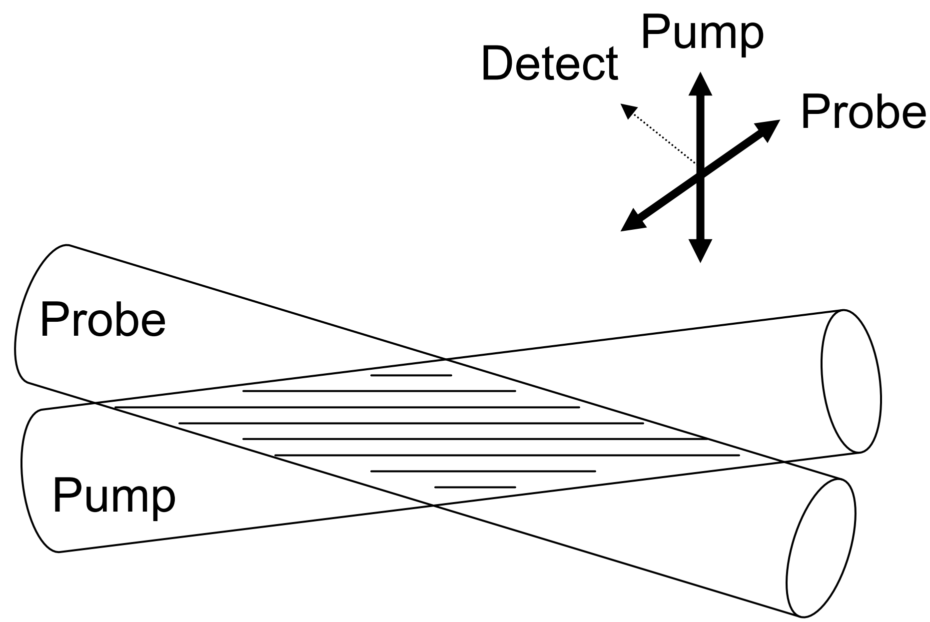

$$\frac{N_e(\mathbf{r},t)}{N_0} = \int_{-\infty}^{t} dt' W\left(E_e(t')\right) + \frac{1}{2}\left(e^{i\mathbf{q}\cdot\mathbf{r}} \int_{-\infty}^{t} dt' E_p(t') W'\left(E_e(t')\right) e^{-i\Delta\omega t'} + c.c.\right)$$

PRL **2012, <u>109</u>, 065003**

ω, 2ω Kerr Birefringence Measurements

- Loriot, et al. showed apparent inversion at high intensity for transient birefringence using 800nm pump and probe.
- We repeated measurements using both 800nm and 400nm probes to test Milchberg hypothesis.

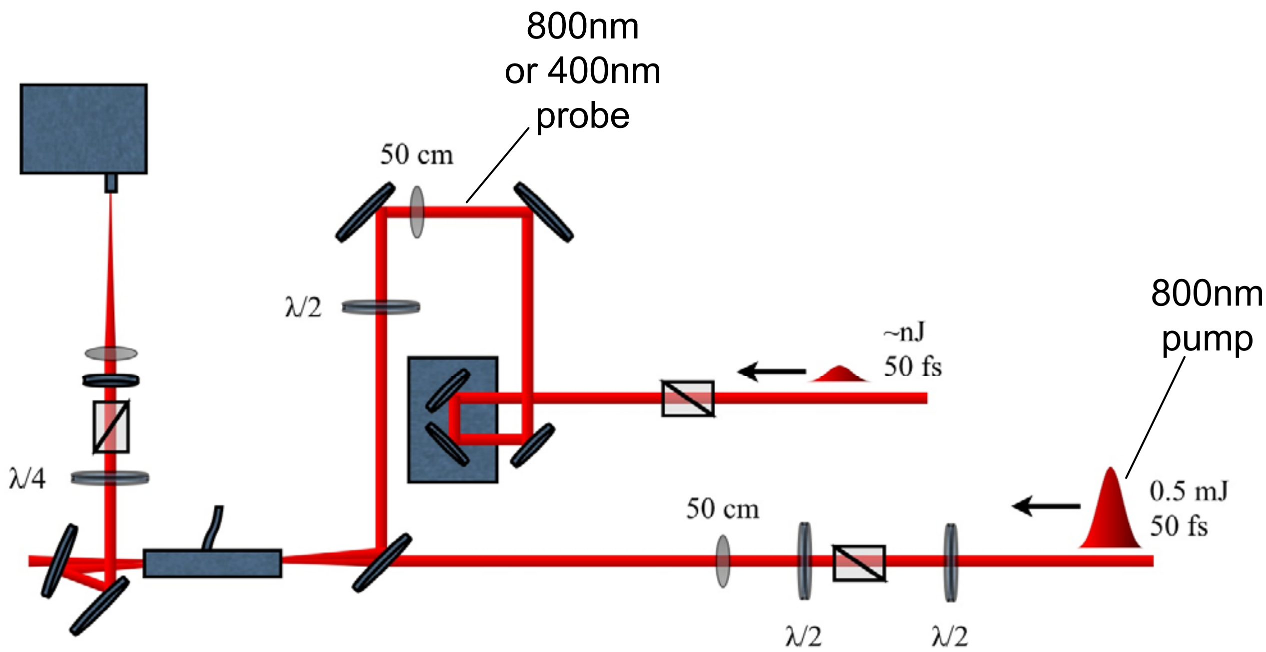

800nm Filament, 400nm Probe Measurement

Initial results of experiments performed at ~40 TW/cm^2 show that no inversion of the birefringence is observed at zero delay in nitrogen using a 400 nm probe pulse, though inversion is observed at 800 nm.

Time-Resolved Birefringence for Degenerate and Nondegenerate Beams

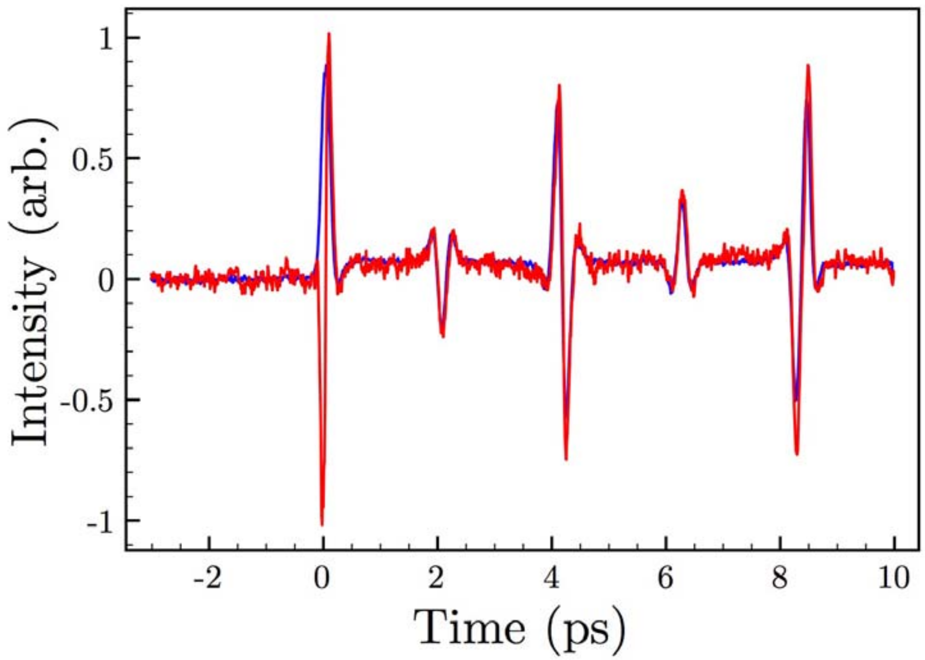

Birefringence Response at t=0 for 800nm, 800nm and 800nm, 400nm

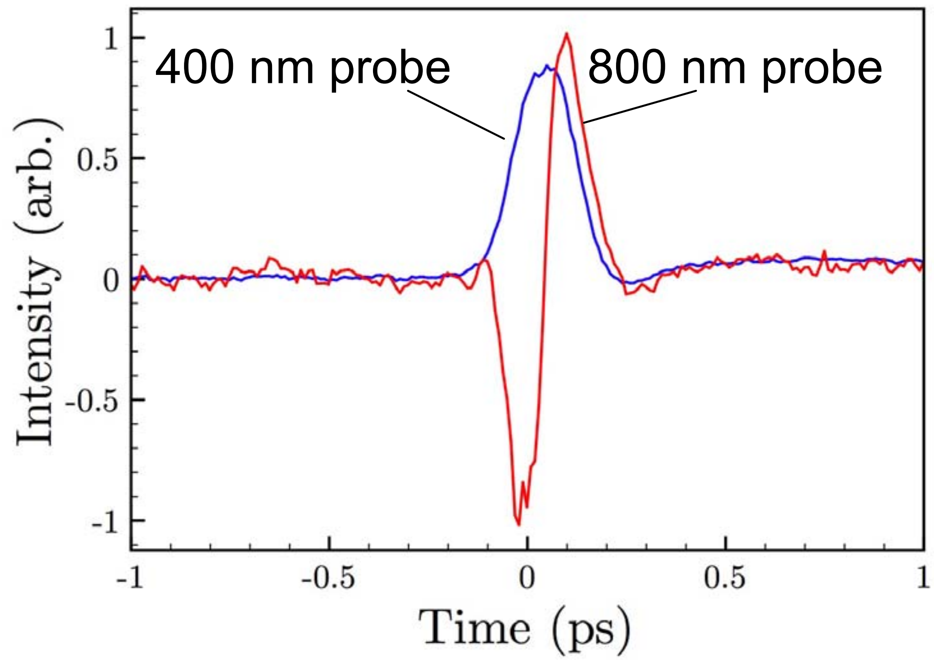

Difference in nonlinearlties between 800nm and 400nm could account for the observation.

Testing the “Ionization Grating” Theory using Nearly Degenerate Beams

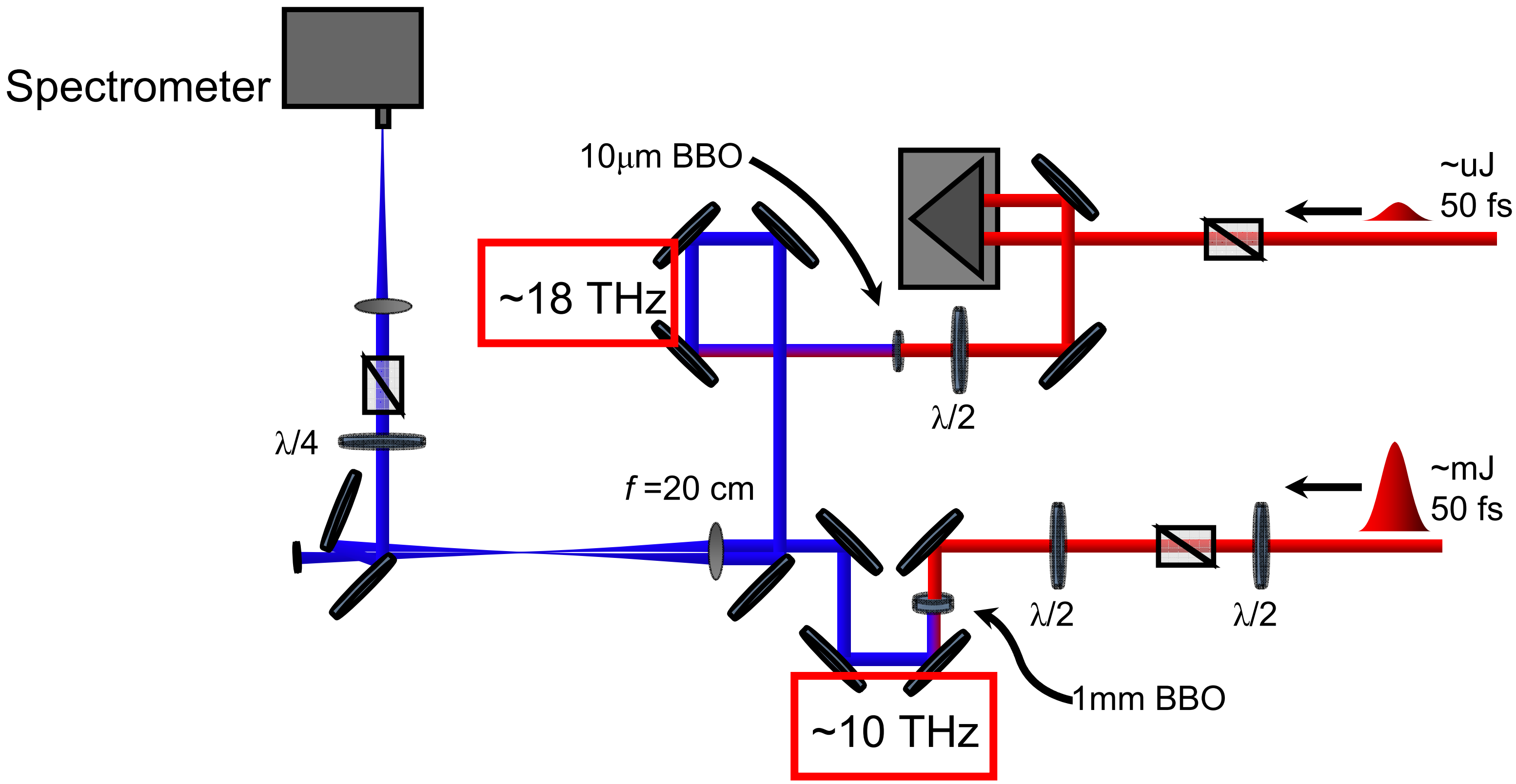

To test the new theory, the spectrally-resolved transient birefringence of air was measured at 400 nm.

Spectrally-Resolved Measurements at 400 nm

- **Double light in two different length BBOs provides different bandwidths**
- **Spectrally-resolving adds new dimension to data, revealing positive sidebands on the leading edge of the pump not otherwise observable.**

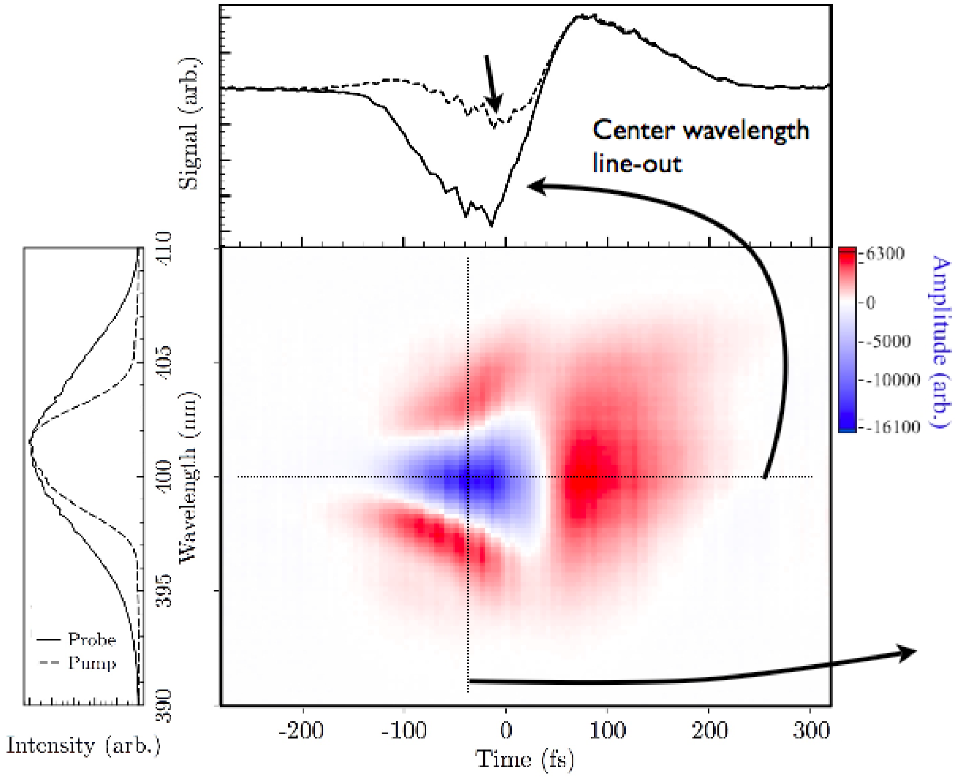

PRL, submitted

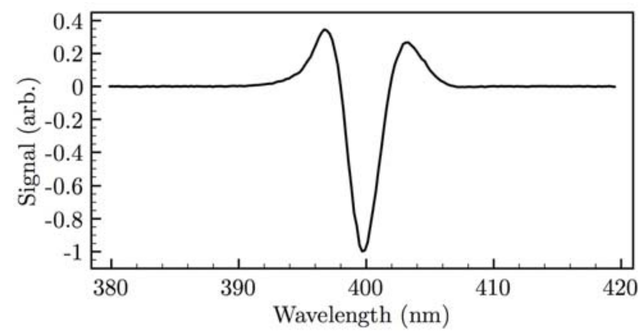

- **Where the frequencies of pump and probe are degenerate there is negative contribution Otherwise there is no inversion as would be expected by HOKE**

Simulating the Two Beam Coupling Geometry

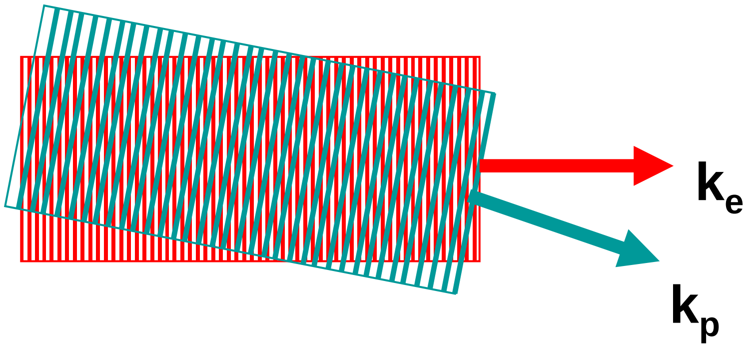

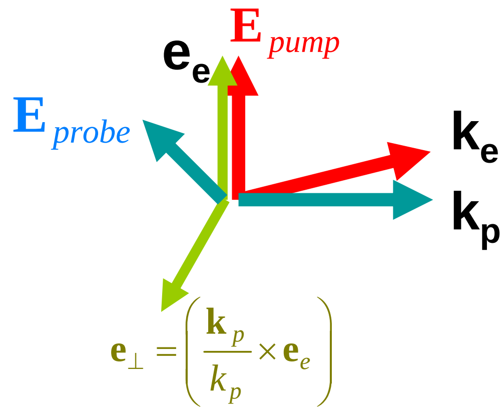

$$\mathbf{E}_{pump} = \mathbf{e}_e \left(I\right)^{1/2} A_e\left(t - \frac{n_0}{ck_e}\left(\mathbf{k}_e \mathbf{r}\right)\right) e^{i\mathbf{k}_e\mathbf{r} - i\omega_e t} + c.c.$$

$$\mathbf{E}_{probe} = \left(I_p\right)^{1/2} \left(\mathbf{e}_e A_{\parallel}\left(t, \mathbf{r}\right) + \mathbf{e}_\perp A_\perp\left(t, \mathbf{r}\right)\right) e^{i\mathbf{k}_p\mathbf{r} - i\omega_p t} + c.c.$$

$$I_p \lll I$$

Basic assumption: A_e **is not changed by the interaction, and it does not undergo noticeable (self)focusing over the interaction length.**

Plasma Nonlinearity I: Conventional Nonlinear Refraction

The plasma is produced by the ionization of the medium at the rate depending on the local field intensity

$$\frac{dN}{dt} = R\left(\left|E\left(t,z\right)\right|\right) N_{neut}$$

Which leads to the corresponding nonlinear variation in the refraction index

$$\Delta n_{pl}\left(t,z\right) = -n_0 \frac{N_{neut}}{2N_c} \int_{-\infty}^{t} dt' R\left(\left|E\left(t',z\right)\right|\right)$$

where $$N_c = \frac{m_e \omega_e^2}{4\pi e^2}$$

is the critical plasma density

In the two-beam coupling setup, this will instigate an equal negative phase shift in both polarization components of the probe pulse.

Plasma Nonlinearity II: Incorporating Multi Photon Ionization

As the ionization rate depends on the total intensity, in the two-beam situation, the generated plasma density will undergo periodic spatial variations due to the small but significant interference term. In the case of multiphoton (*m*-photon) ionization,

$$R\left(\left|E(t,z)\right|\right) = \sigma_m \left(I_{total}\right)^m \approx \sigma_m I^m \left(\left|A_e\right|^{2m} + 2m\sqrt{\frac{I_p}{I}}\left|A_e\right|^{2m-2}\left(A_e^* A_p e^{i(k_p-k_e)z-i(\omega_p-\omega_{ep})t} + c.c \right) \right)$$

OPTICS LETTERS / Vol. 36, No. 19 / October 1, 2011

Accordingly, the plasma-related correction to the refraction index will form a grating capable of initiating scattering between the pump and the probe beams:

$$\Delta n_{pl}(t,z) = -n_0 \sigma_m I^m \frac{N_{neut}}{2N_c}\left(f(t,z) + \underbrace{2m\sqrt{\frac{I_p}{I}}\left(e^{i(k_p-k_e)z}\int_{-\infty}^{t} d\tau \frac{\partial f(\tau,z)}{.\partial \tau}\frac{A_p}{A_e} e^{-i(\omega_p-\omega_{ep})\tau} + c.c \right)}_{\text{Plasma grating terms}} \right)$$

where $f(t,z) = \int_{-\infty}^{t} d\tau \left|A_e(\tau,z)\right|^{2m}$

The Combined Transient Birefrigence Signal from Kerr, Transient Plasma Grating and Rotation

Keeping only the first term in the sum for the plasma heterodyne signal and adding the Kerr-related terms, we obtain the following expression to be compared with the experimental results on the spectrally resolved birefrigence measurements:

$$I_x(\omega) \propto \mathrm{Re}\Bigg[e^{i\omega t_d} \tilde{E}_p(\omega) \times$$

$$iz \int_{-\infty}^{\infty} dt e^{i\omega t} \left(-\frac{k_p n_2}{2n_0} E_p^*(t - t_d) \left(\frac{2}{3} |E_e(t)|^2 + \frac{5}{6} \int_{-\infty}^{t} dt' R(t - t') |E_e(t')|^2 \right) \right.$$

$$\left. + 4\beta e^{iz\beta f(t)} E_e^*(t) \int_{-\infty}^{t} dt' |E_e(t')|^{2m-2} E_e(t') E_p^*(t' - t_d) \right) \Bigg]$$

where:

$$\beta = \frac{2\pi k_p}{m n_0^2} \frac{N_0 \sigma_m}{N_c}; \quad f(t) = \int_{-\infty}^{t} dt' |E_e(t')|^{2m}$$

Simulation Results

Using a Gaussian input pulse with τ_{FWHM}=54 fs, no chirp, and I_e=71 TWcm^{-2} we obtain:

HOKE Simulation

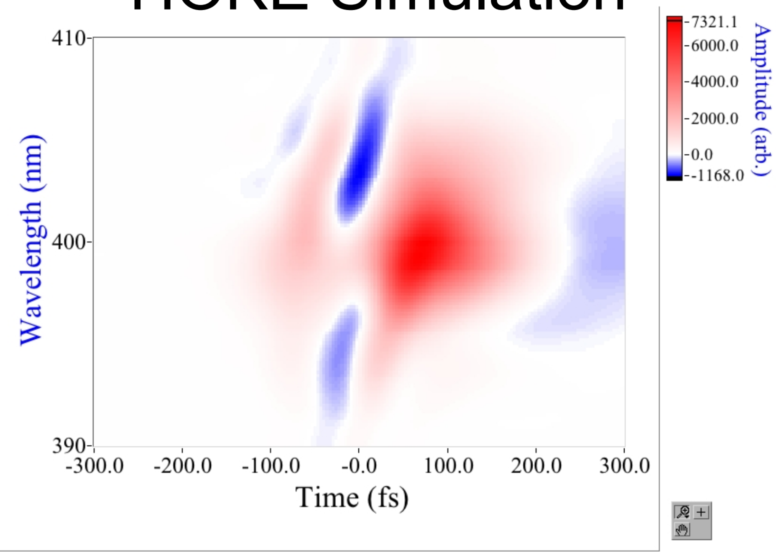

w/ experimental beam parameters

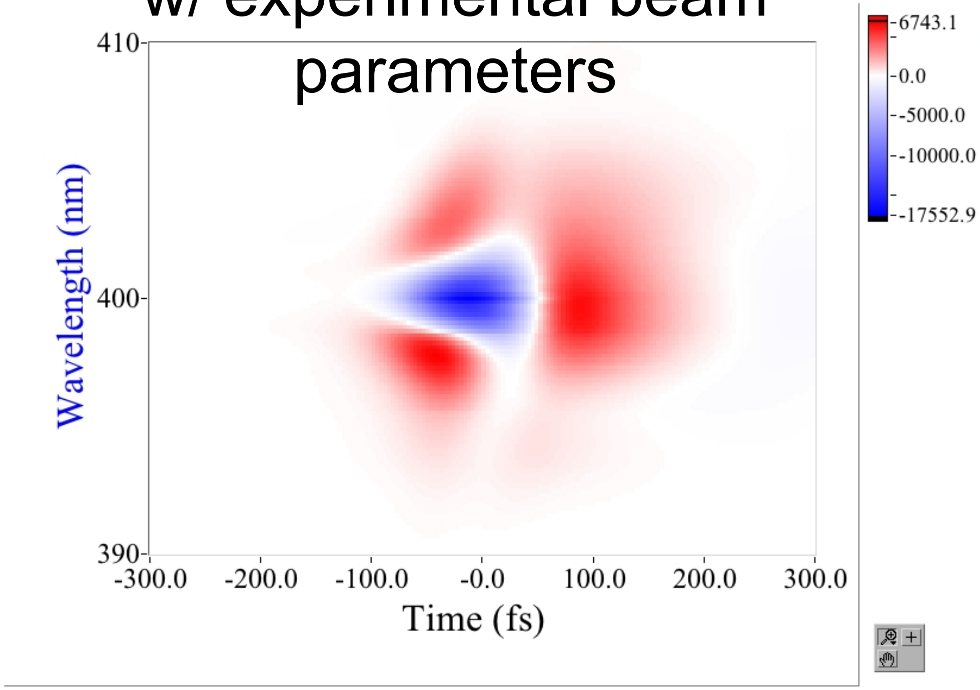

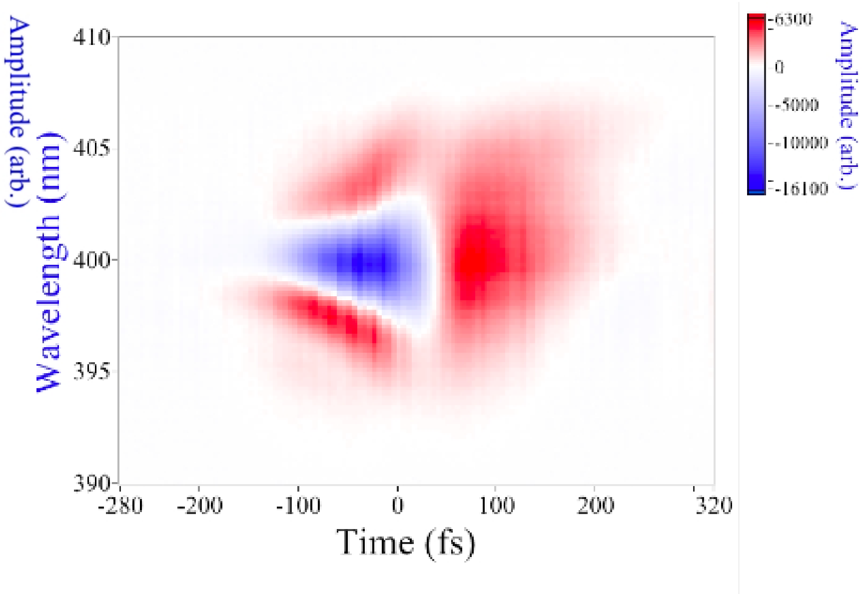

Conclusions for Nonlinear Probing of Filamentation

- Impulsive Raman measurements reveal evidence for ~5fs bandwidth
- TG-XFROG reveals spectral phase and amplitude as a function of propagation length in a filament. Agreement with theory.
- No evidence for HOKE in filamentation at 400nm

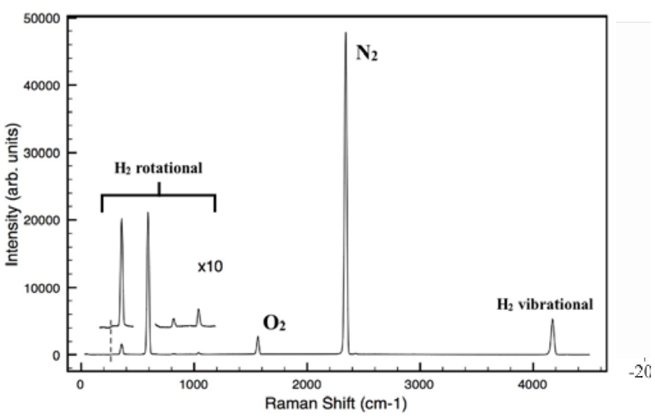

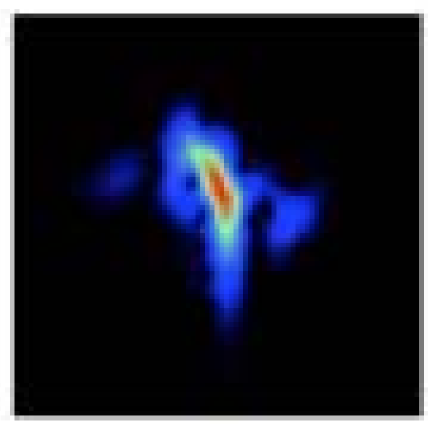

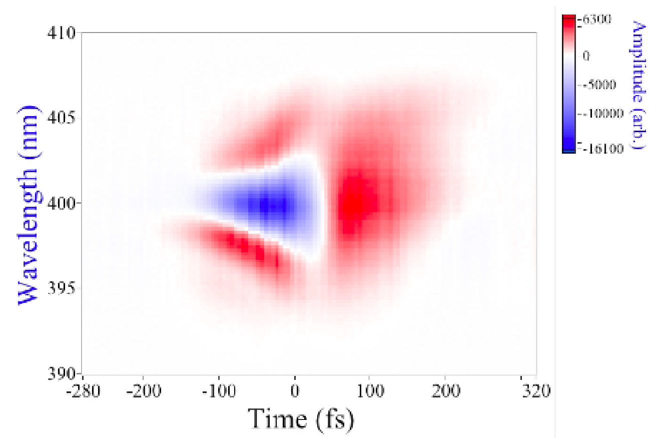

Femtosecond Laser Electrospray Mass Spectrometry (LEMS)

- Biomolecule Mass Spectrometry
- Universal Laser Vaporization
- LEMS Analysis, Laser Electrospray Mass Spectroscopy of Biomolecules

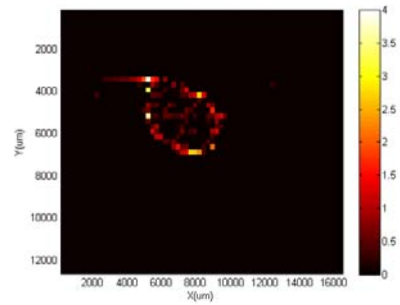

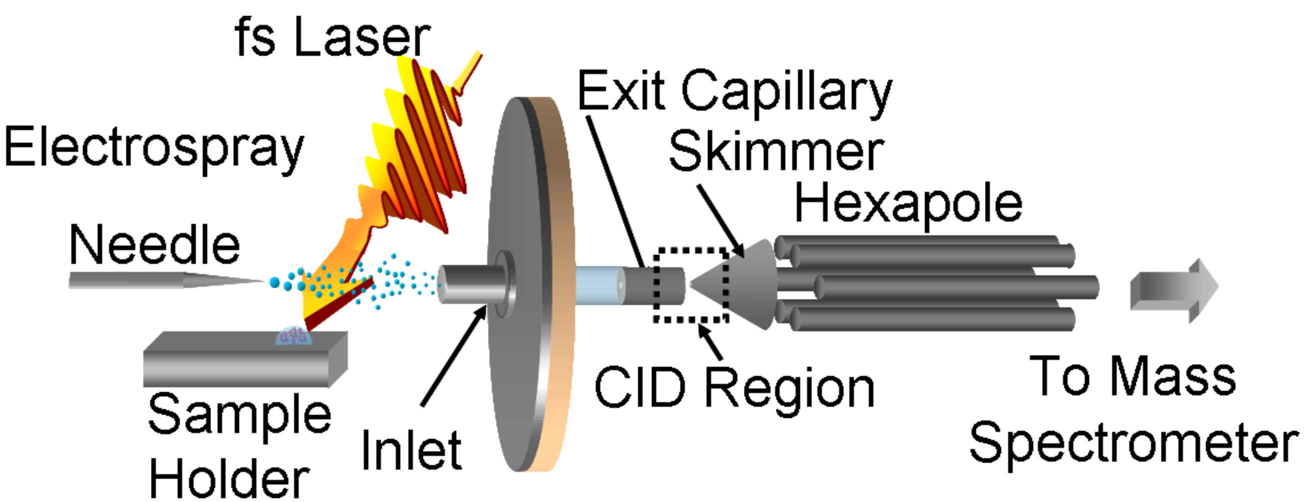

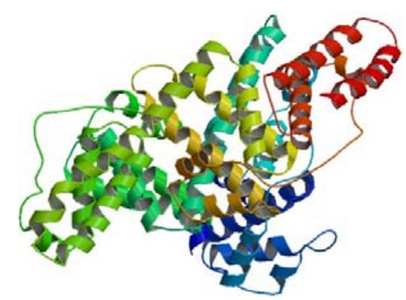

Vaporization of Biomolecules I: MALDI

Early 80's → How to volatilize nonvolatile, fragile molecules?

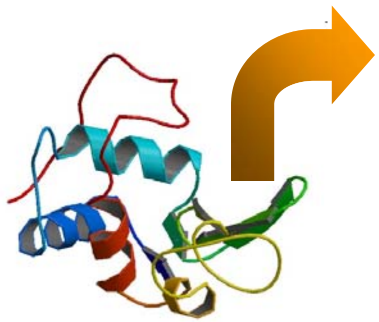

Gas Phase

biomolecule of interest

Laser Beam

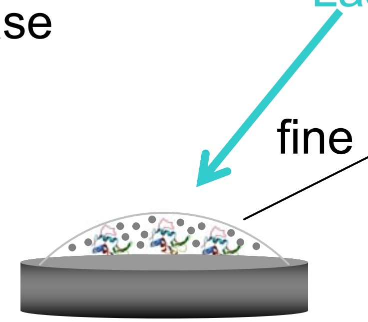

Tanaka's 1993 discovery,
fine cobalt powder + glycerol + lysozyme

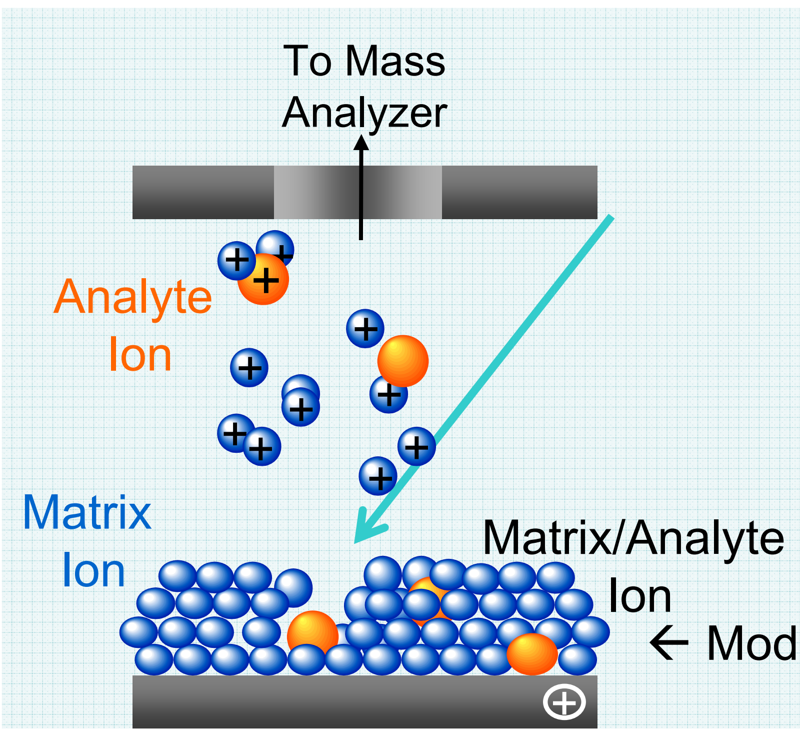

← Modern MALDI Employs Organic Acid Matrix

Mass Spec Detection of Nonvolatile Lysozyme

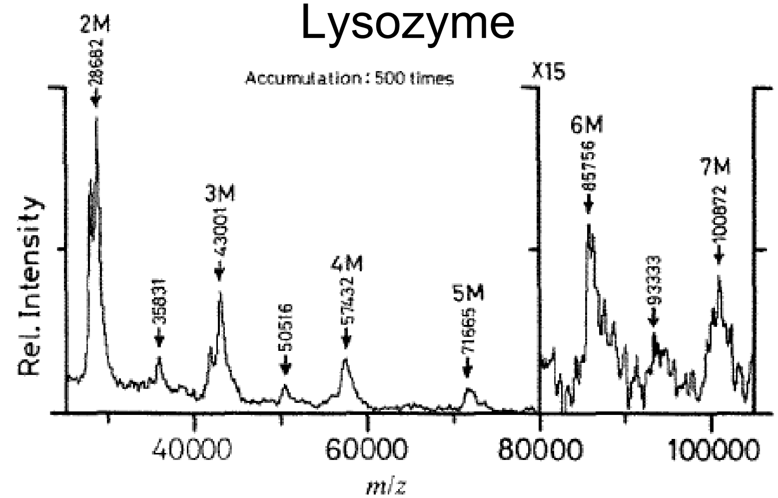

Tanaka, K. RCMS, 2, 8, 1993, 151-153

fs Nonresonant Laser Vaporization

- Couples into all molecules via multiphoton excitation
- No functional group limitation so far
- Eliminates sampling induced decomposition concern
- Noncovalent interactions preserved

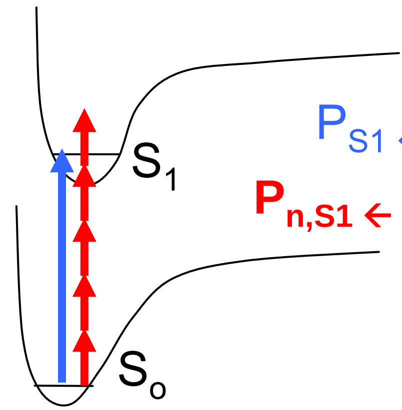

$P_{S1 \leftarrow S0} = I\, \sigma_{S1 \leftarrow S0}$

$\mathbf{P_{n,S1 \leftarrow S0} = I^n\, \sigma_{n,S1 \leftarrow S0}}$

Vaporization of Gramicidin

J. Am. Soc. Mass Spectrom. (2011) 22:762–772

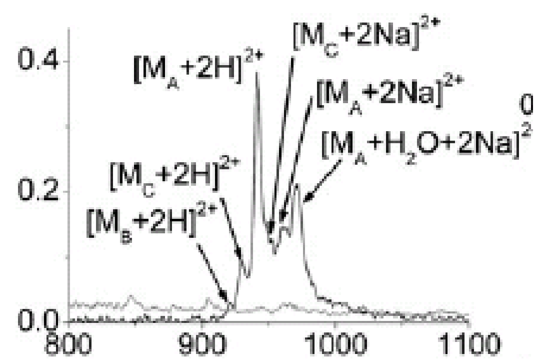

Vaporization of Biomolecules Part II: ESI

Schematic of Electrospray Ion Source

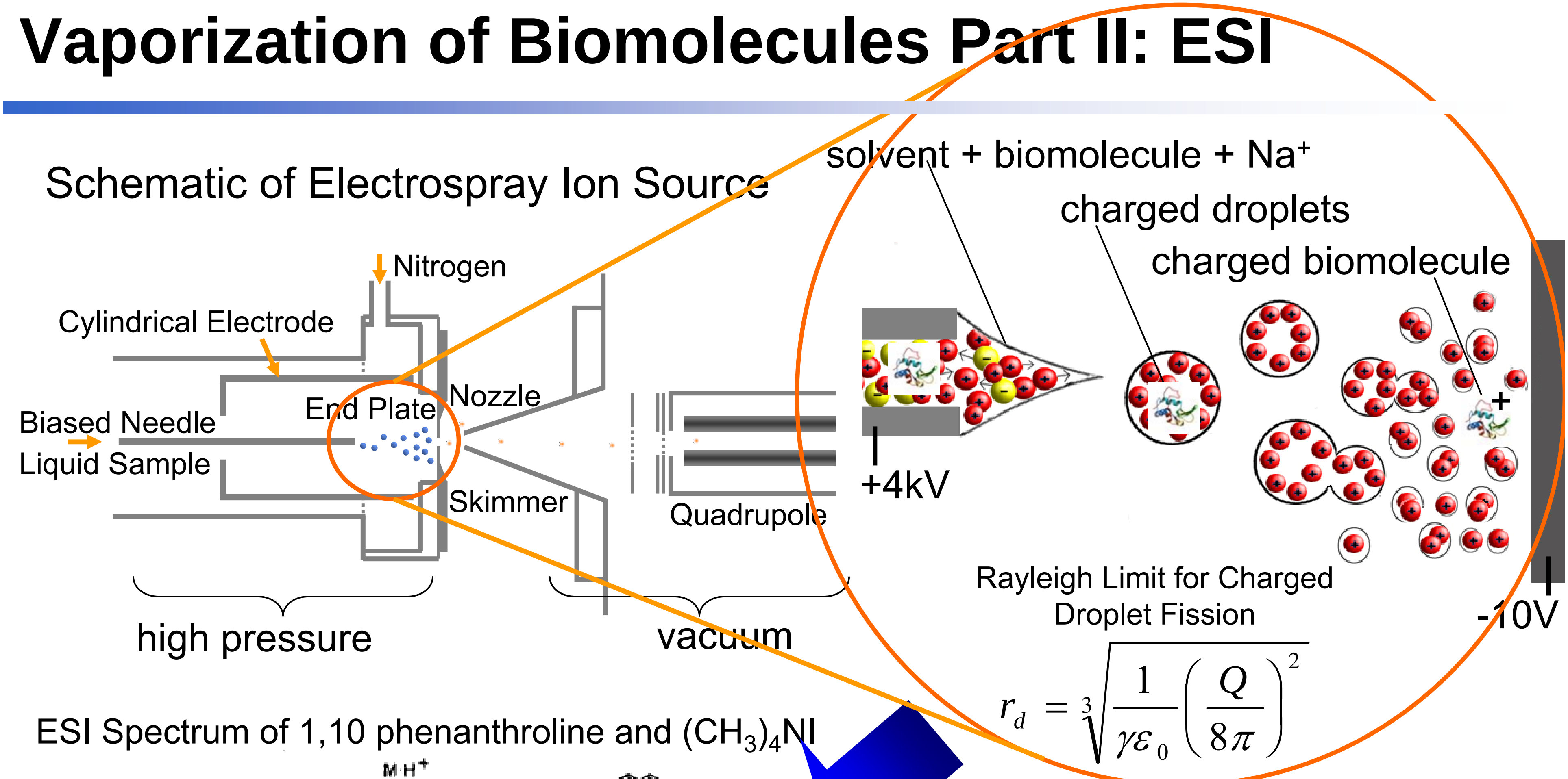

$$r_d = \sqrt[3]{\frac{1}{\gamma\varepsilon_0}\left(\frac{Q}{8\pi}\right)^2}$$

r_d: radius of droplet; γ: surface tension; ε_0: permittivity constant

ESI Spectrum of 1,10 phenanthroline and $(CH_3)_4NI$

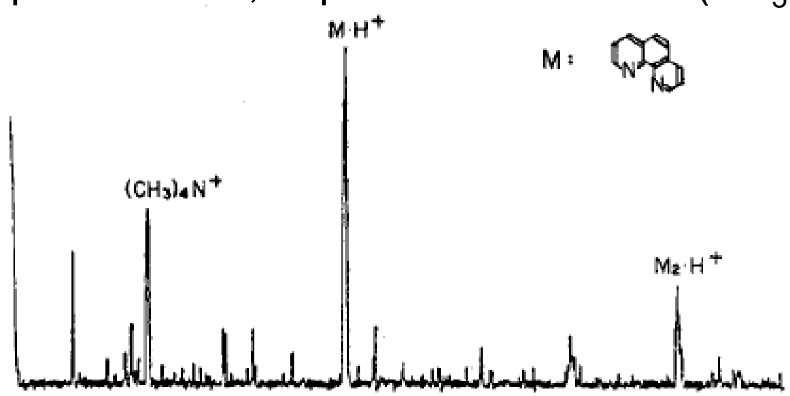

Fenn, J.B., *J. Phys. Chem.* **1984**, *88*, 4451-4459

Laser Electrospray Mass Spectrometry (LEMS)

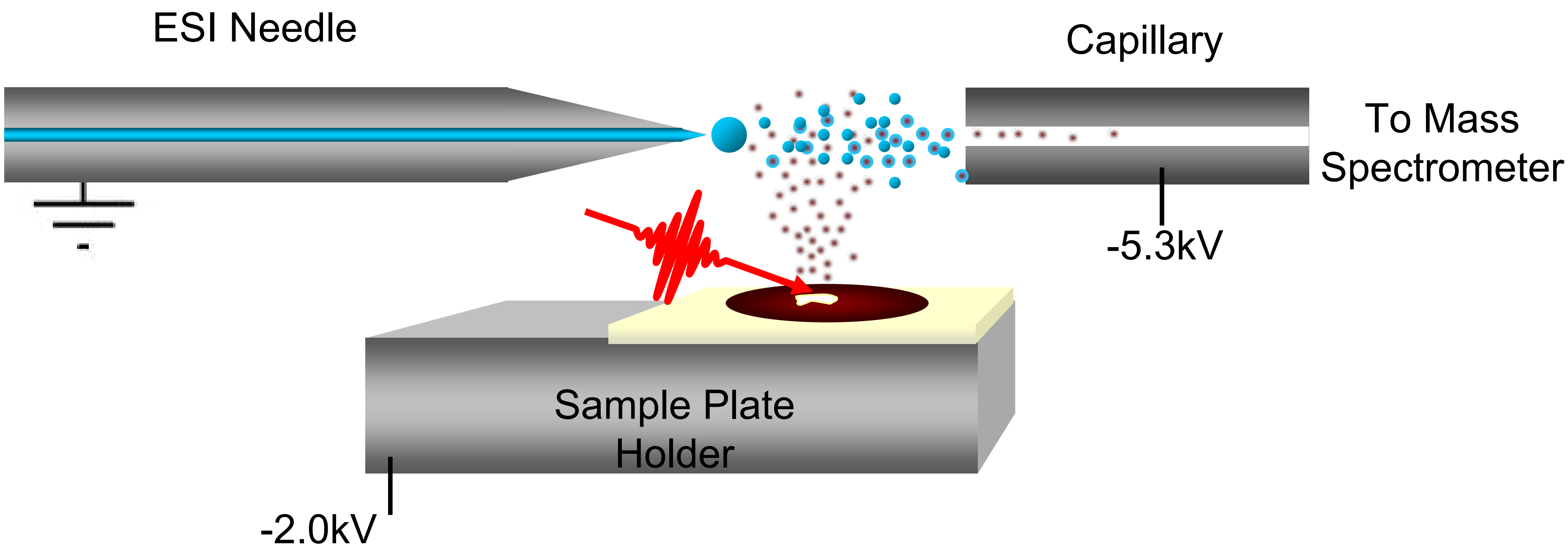

- Neutrals are vaporized from a sample surface using a fs laser.
- The neutrals interact with the electrospray where they undergo ionization.
- The ions then travel to the inlet of the mass spectrometer.

Brady, J.J., Judge, E.J., Levis, R.J., Rapid Commun. Mass Spectrom., **23**, 3151-3157, 2009

The LEMS System

Side View

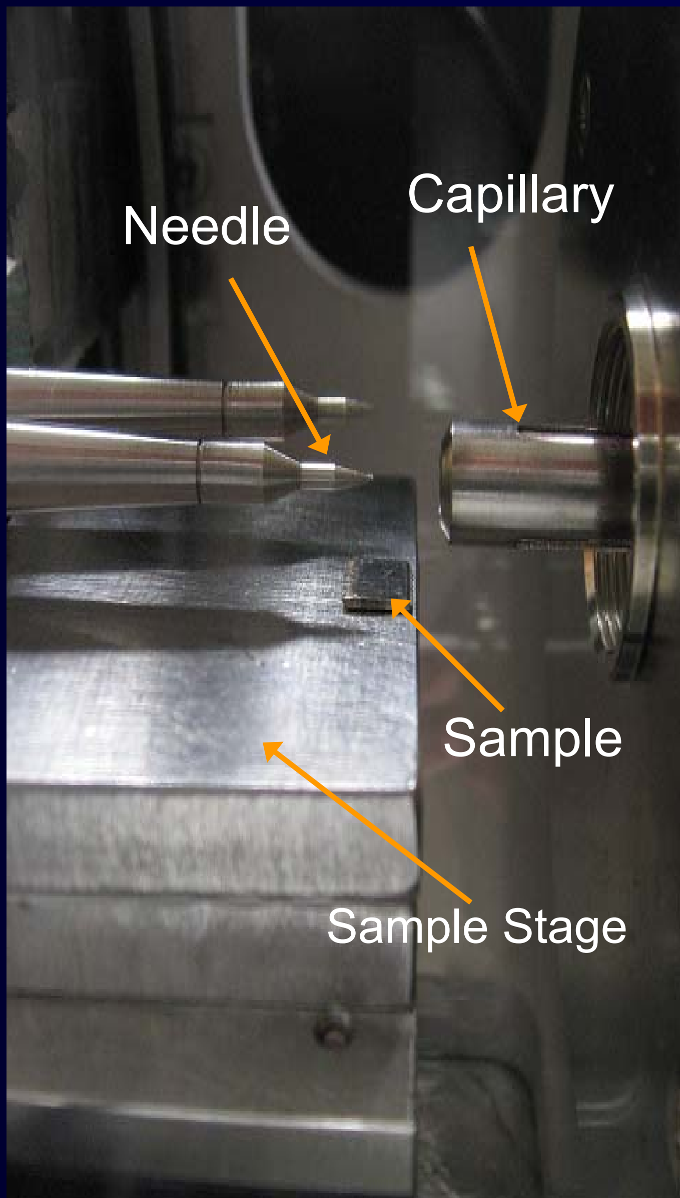

Top View

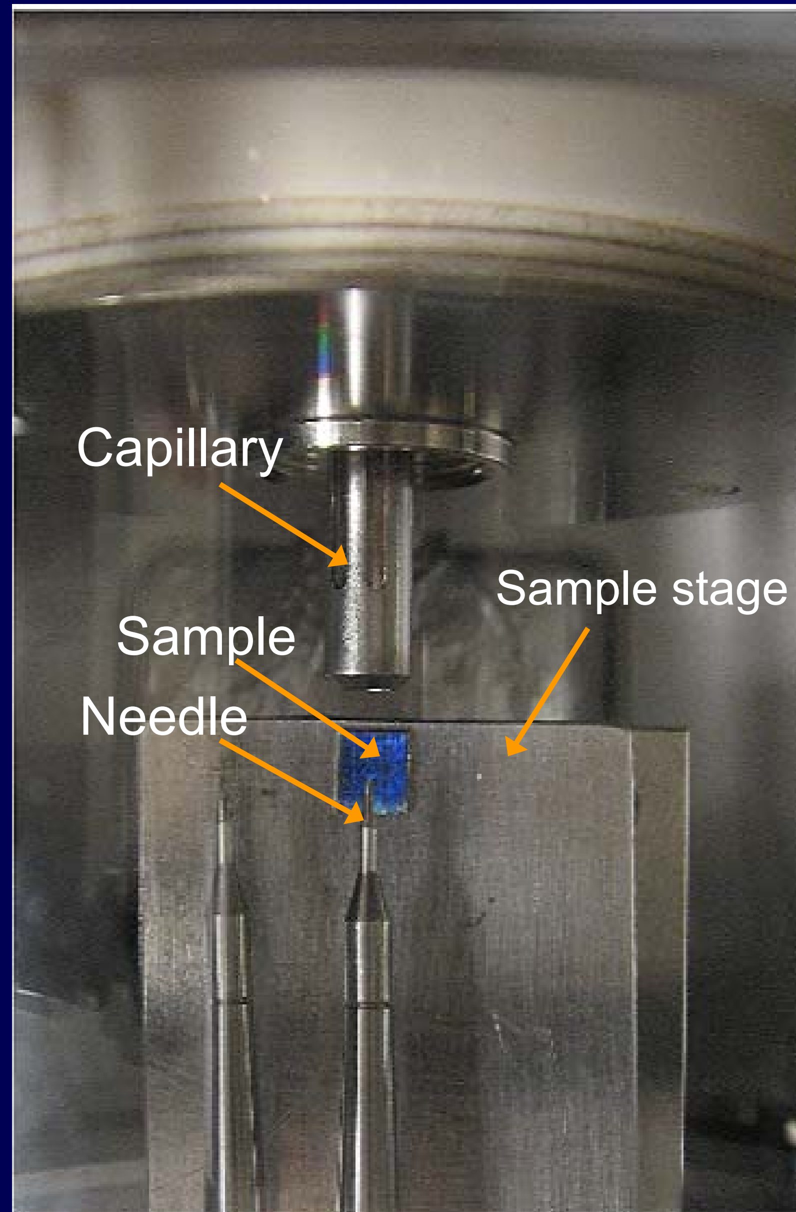

Laser Electrospray Mass Spectrometry System

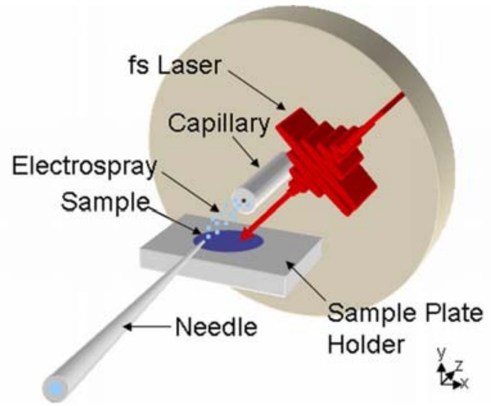

focus 1 mJ, 50fs pulse to 150 micron diameter spot

10^{13} W cm^{-2}

Laser-ESI Source

Pulsed Extraction TOF-MS

1. API Needle
2. Source Chamber Electrode
3. Sample Plate
4. Capillary Electrode
5. Dry Nitrogen
6. Nebulizing Nitrogen
7. Glass Capillary
8. Capillary Electrode
9. Skimmer
10. Hexapole Ion Guide
11. DC Lens
12. DC Lens
13. RF Hexapole Ion Guide
14. DC Lens
15. DC Lens
16. X Steering Plates
17. Ground Plate
18. Extraction Plate (mesh)
19. Acceleration Plate (mesh)
20. Ground Plate (mesh)
21. X Steering Plates
22. Y Steering Plates
23. MCP Entrance Screen Grid
24. MCP Bias Plates
25. Microchannel Plates
26. Anode

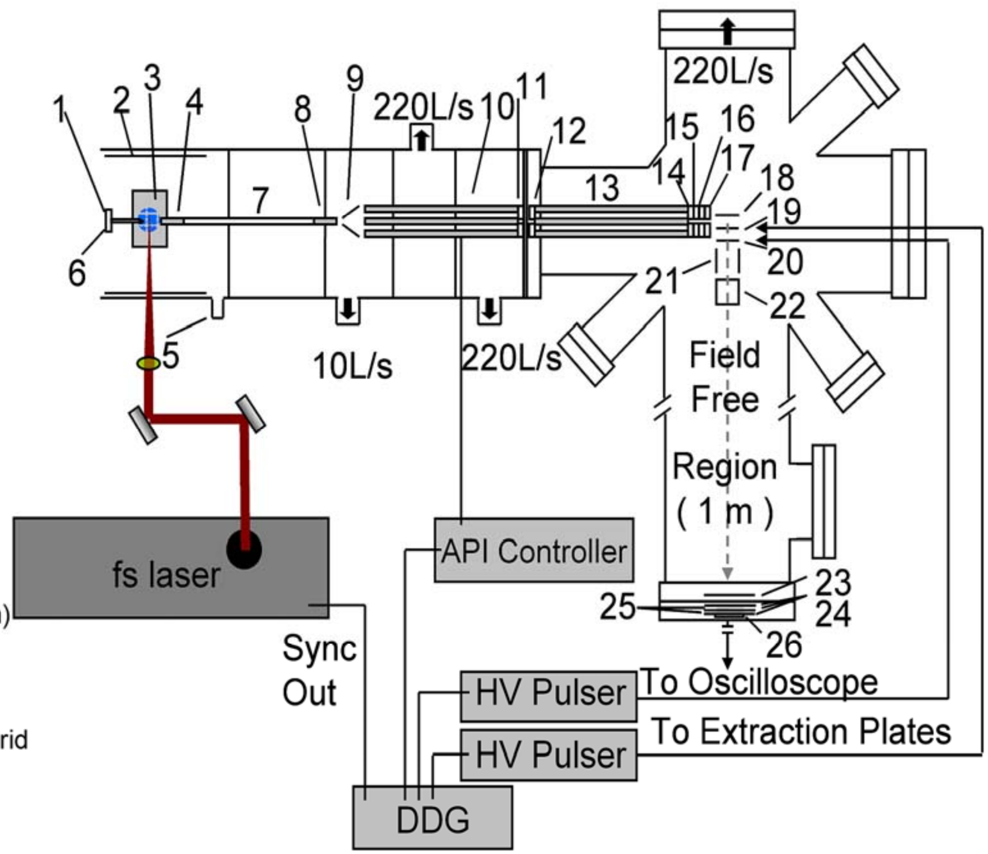

Brady, J.J., Judge, E.J., Levis, R.J., Rapid Commun. Mass Spectrom., **23**, 3151-3157, 2009

Non-Resonant Laser Vaporization of Explosive Taggants on Steel

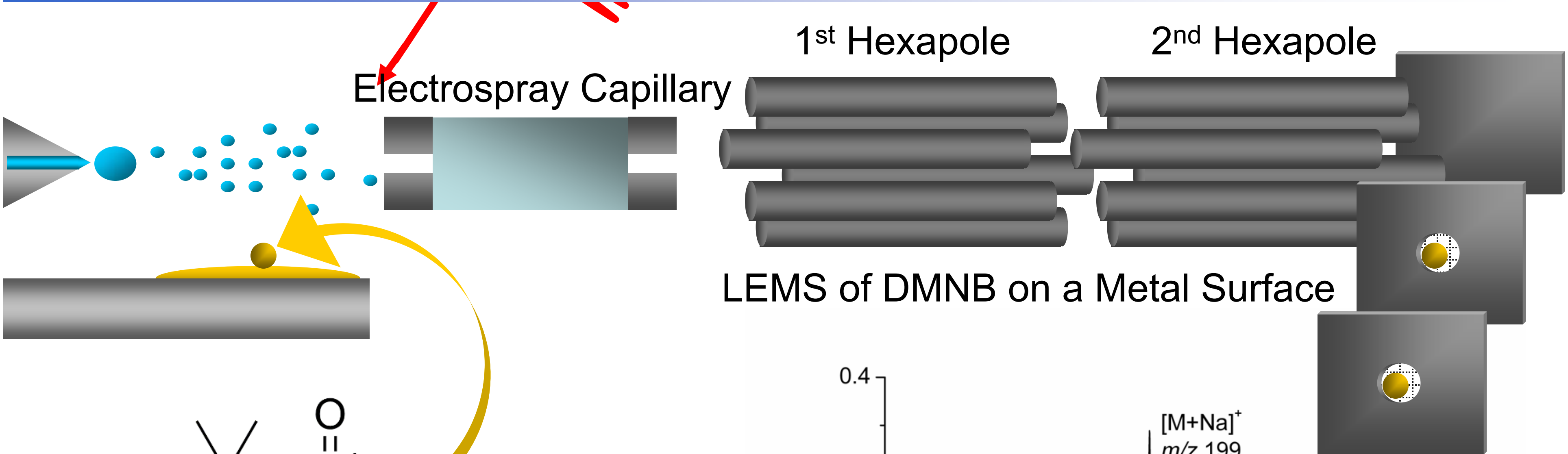

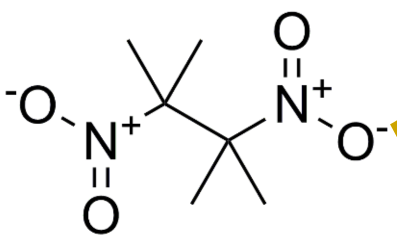

2,3 Dimethyl 2,3 Dinitrobutane
(DMNB)

Sample Deposited	**5 nmol/cm^2**	**880 ng/cm^2**
Sample Analyzed	**1.67 nmol**	**293 ng**

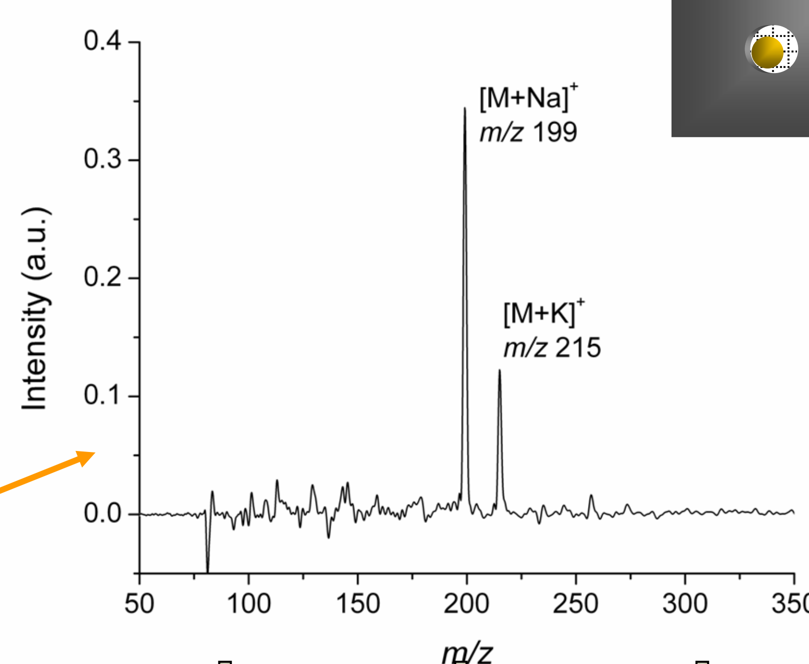

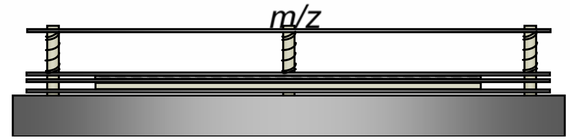

Brady, J.J., Judge, E.J., Levis, R.J., Rapid Commun. Mass Spectrom., **24,**1-6, 2010

LEMS of Trace RDX Explosive Deposited on a Steel Surface

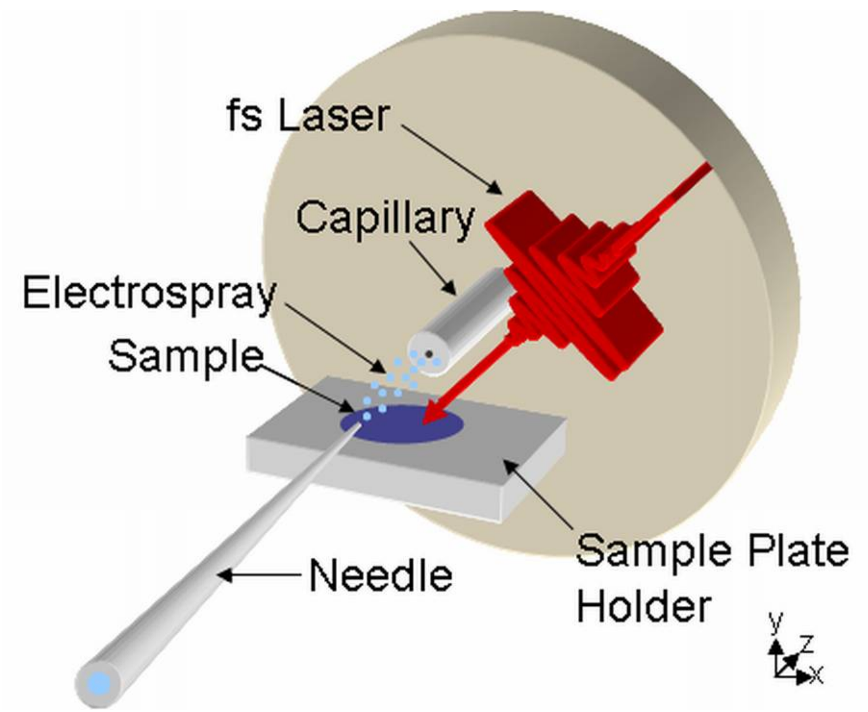

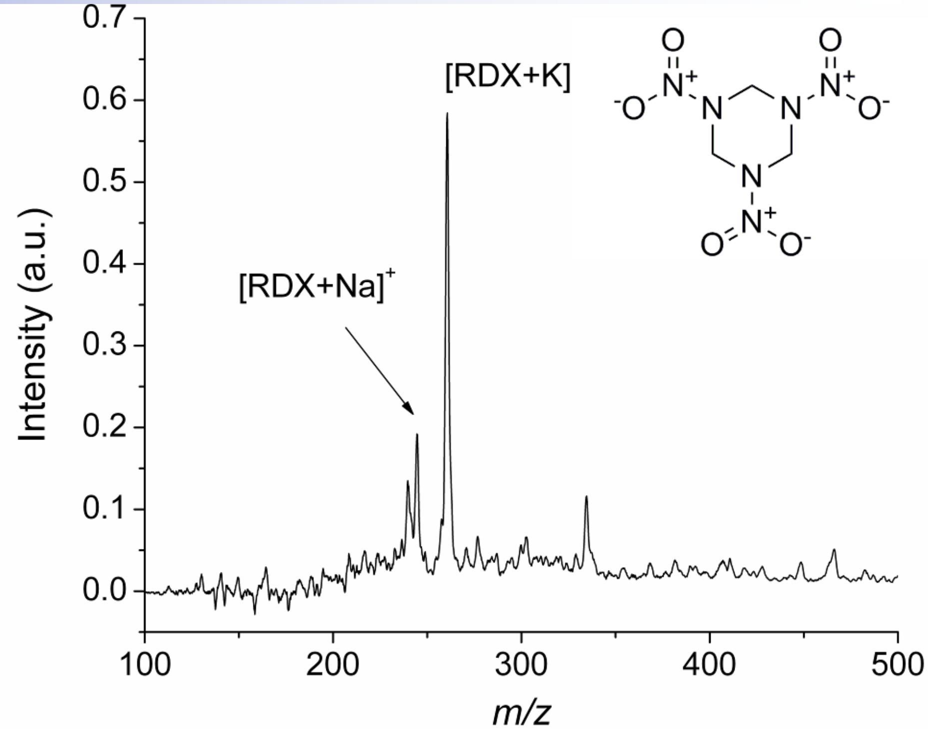

Sample Deposited	**25 nmol/cm^2**	**5.55 µg/cm^2**
Sample Analyzed	**8.33 nmol**	**1.85 µg**

- RDX, cyclotrimethylenetrinitramine, can be detected from a steel surface using non-resonant femtosecond vaporization and ESI ionization
- Does LEMS have the capability to detect complex mixtures of explosives?

Brady, J.J., Judge, E.J., Levis, R.J., Rapid Commun. Mass Spectrom., **24,**1-6, 2010

LEMS of Intact Propellant Formulations

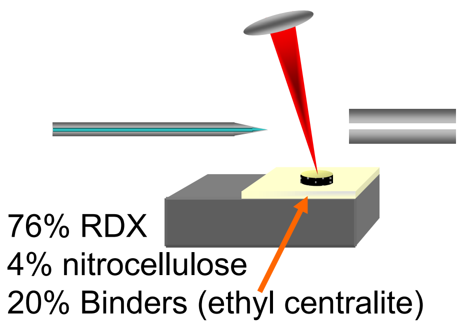

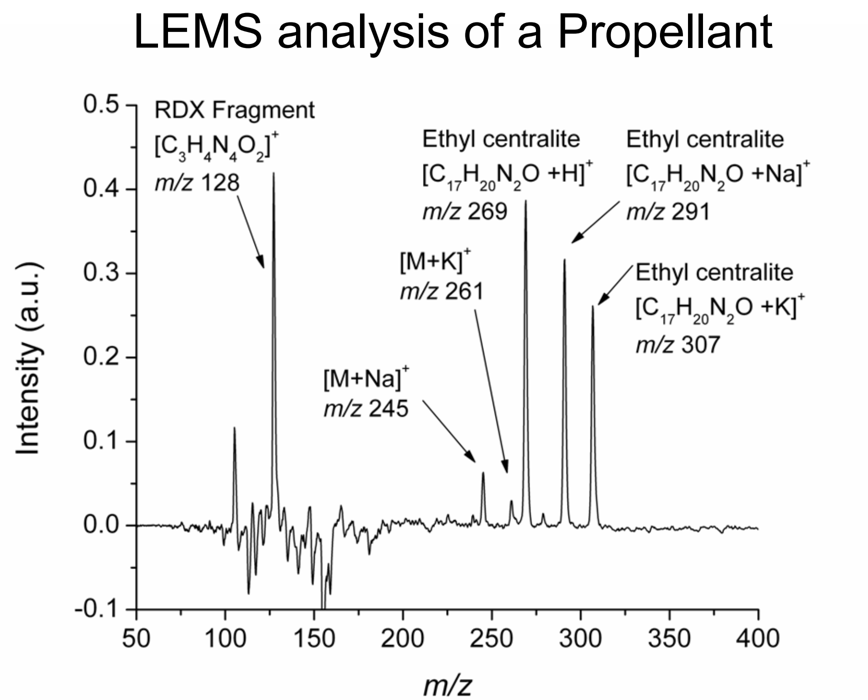

- Ethyl centralite binder is a signature for explosive detection.
- Sodium and potassium adducts of RDX are also detected.

Brady, J.J., Judge, E.J., Levis, R.J., Rapid Commun. Mass Spectrom., **24,**1-6, 2010

Vaporization of Monoolein

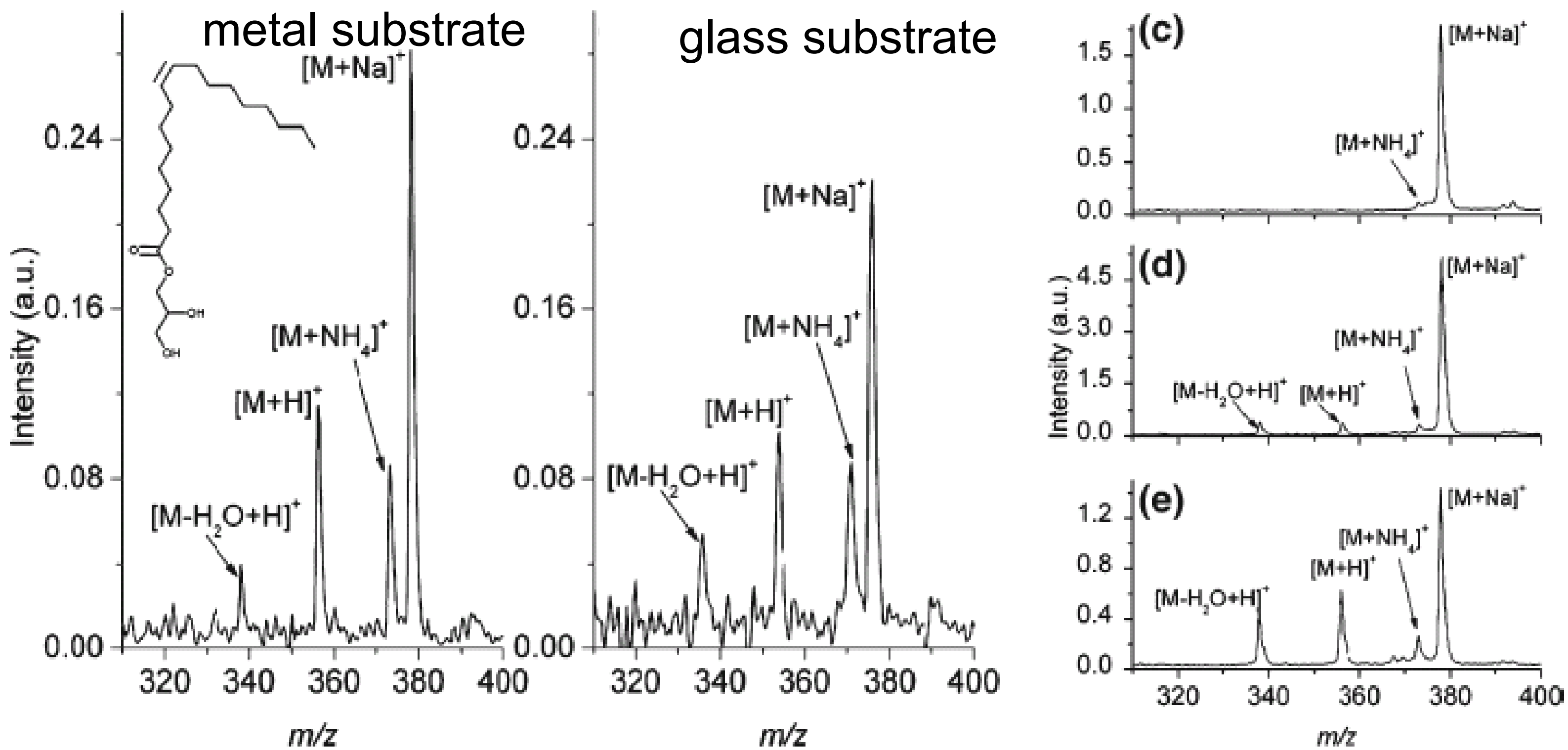

Figure 1. The background subtracted mass spectra of 1-monooleoyl-rac-glycerol (monoolein) vaporized from (a) metal and (b) glass and post-ionized in the electrospray plume. The inset in (a) shows the molecular structure of monoolein. The conventional ESI-MS of a 1×10^{-5} M solution of monoolein dissolved in 1:1 (vol:vol) water:methanol containing (c) 0%, (d) 0.1%, and (e) 1.0% acetic acid

Brady, J. J.; Judge, E. J.; Levis, R. J. *J. Am. Soc. Mass. Spectrom.* **2011**, *22,* 762.

Vaporization of DHPC and DMPC

1,2-dihexanoyl-sn-glycero-3-phosphocholine

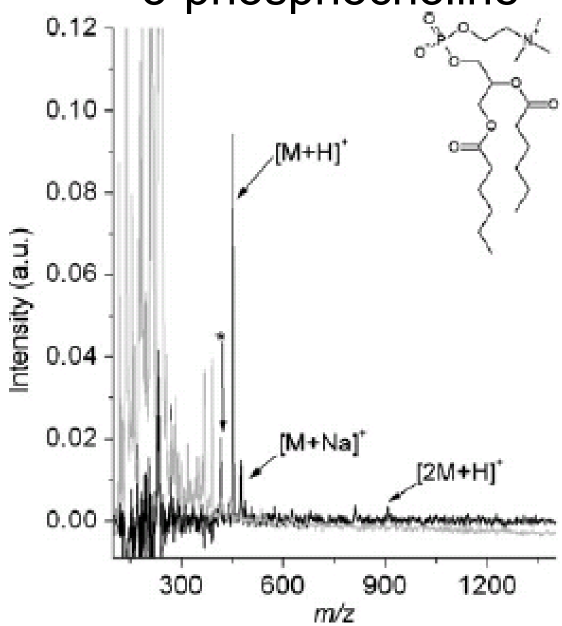

1,2-dimyristoyl-sn-glycero-3-phosphocholine

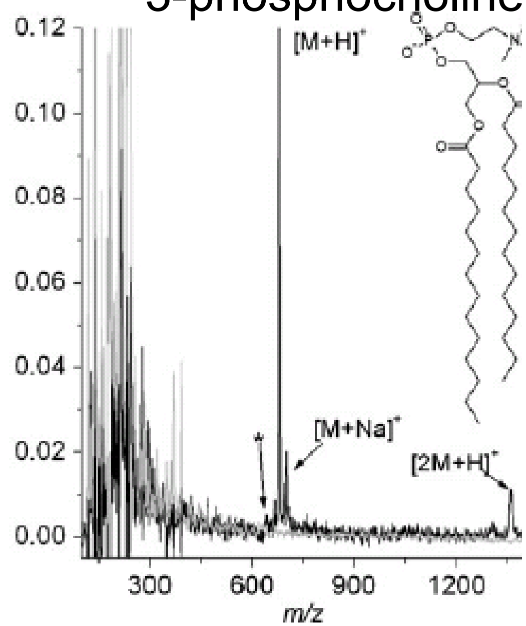

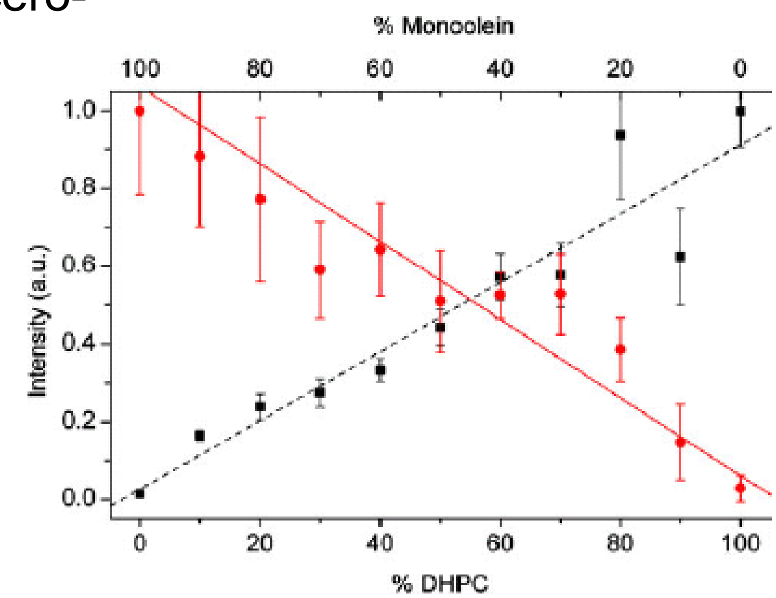

Figure 3. Plot of the average total integrated ion signal from the $[M-H_2O+H]^+$, $[M+H]^+$ and $[M+Na]^+$ ions of monoolein (filled circle ●, solid red line) and $[M+H]^+$ and $[M+Na]^+$ ions of DHPC (filled square ■, dashed black line) as a function of mixture composition

Brady, J. J.; Judge, E. J.; Levis, R. J. *J. Am. Soc. Mass. Spectrom.* **2011**, *22,* 762.

Bulk Analysis: Pharmaceutical Tablets

Active ingredient in Claritin is loratadine (10 mg)

(50mg)

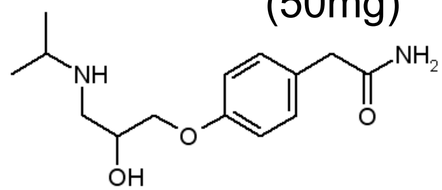

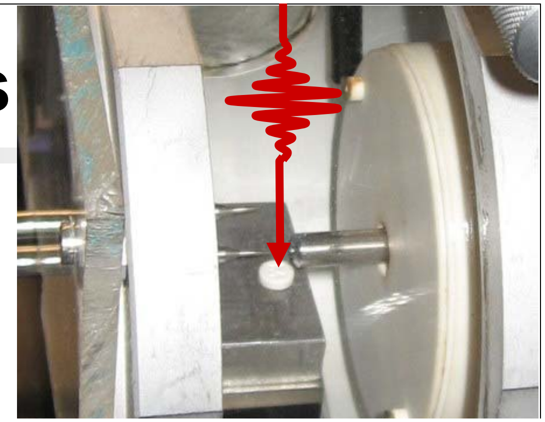

LEMS of Claritin Tablet

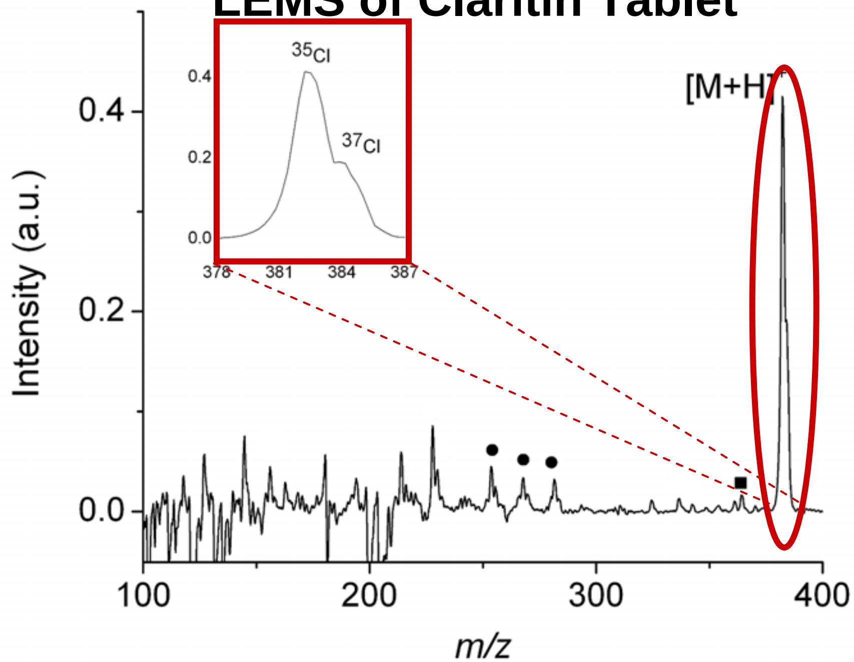

■ lactose monohydrate m/z = 361
● magnesium stearate related peaks

LEMS of Atenolol Tablet

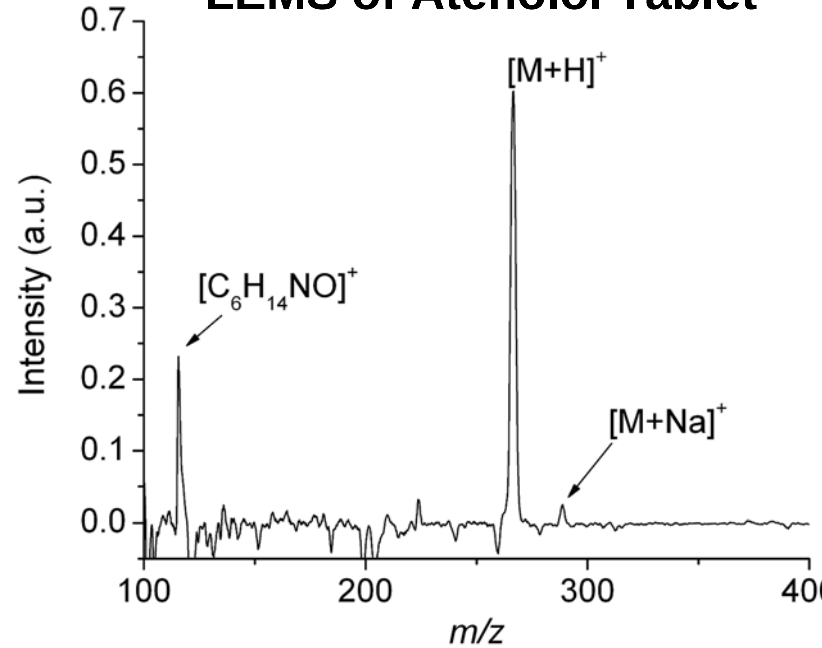

Analysis time < 1 second
Amount vaporized < 1 μg

Judge, E.J., Brady, J.J., Dalton, D., Levis, R.J., *Analytical Chemistry,* **2010**, *82*, 3231

LEMS Signatures for Simulated Inorganic IED

Inorganic Ion IED	Composition
Chlorate, perchlorate, sugar	$KClO_4$, $NaClO_3$, NaCl, Sucrose
Ammonium nitrate	NH_4NO_3
Pre-blast black powder	Black powder pellet (KNO_3, S, C)
Post-blast black powder	NH_4NO_3, $MgSO_4$, KSCN, $Na_2S_2O_3$, Na_2S, $NaHCO_3$, KOCN

Characteristic anions, cations, and neutrals were detected for each respective IED

Could these 4 IEDs be classified?

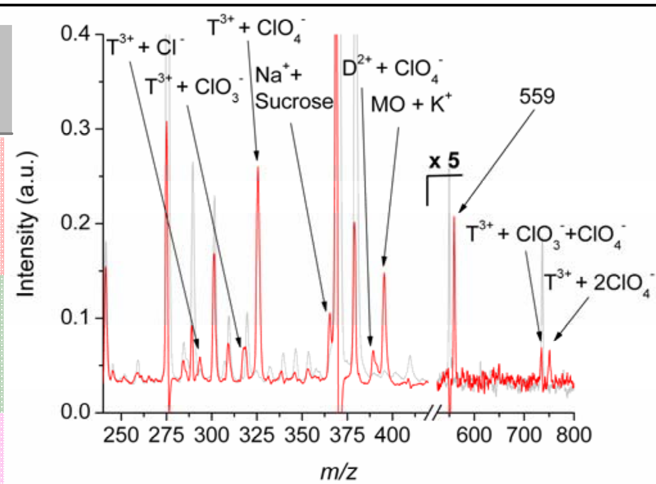

Chlorate, perchlorate, sugar

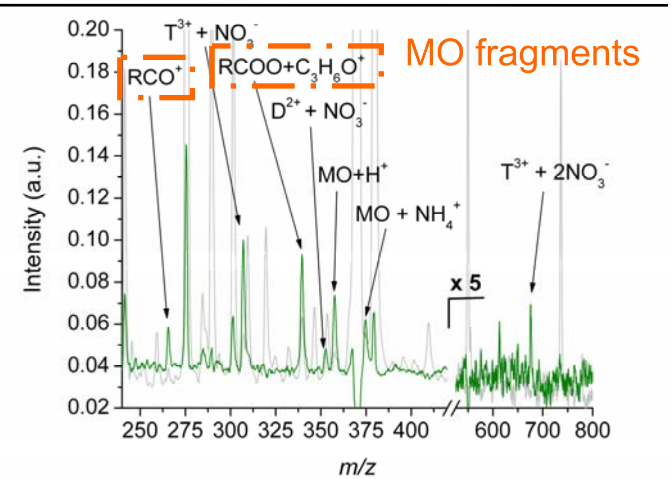

Ammonium nitrate

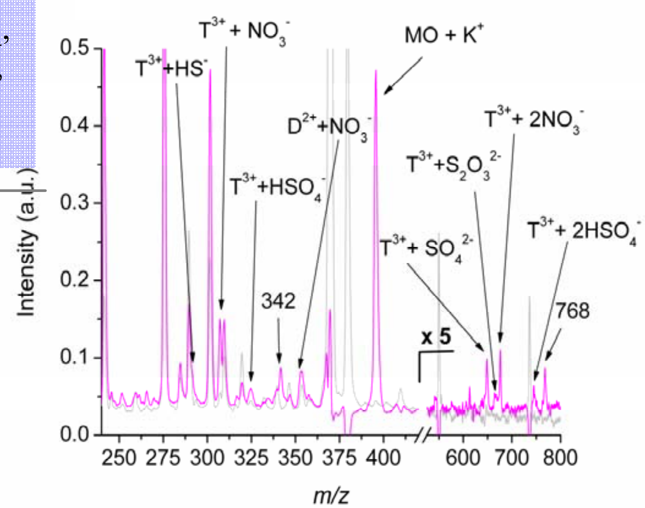

Pre-blast black powder

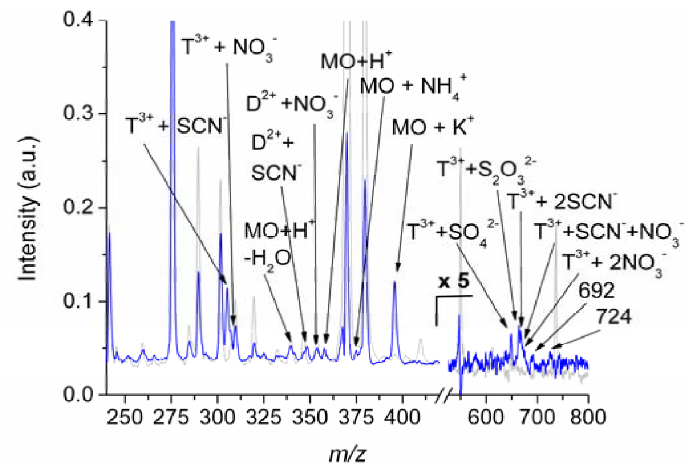

Post-blast black powder

Flanigan, P.M.; Brady, J.J.; Judge, E.J.; Levis, R.J. *Anal. Chem.* 83 (**2011**), 7115–7122.

Classification of Inorganic IEDs

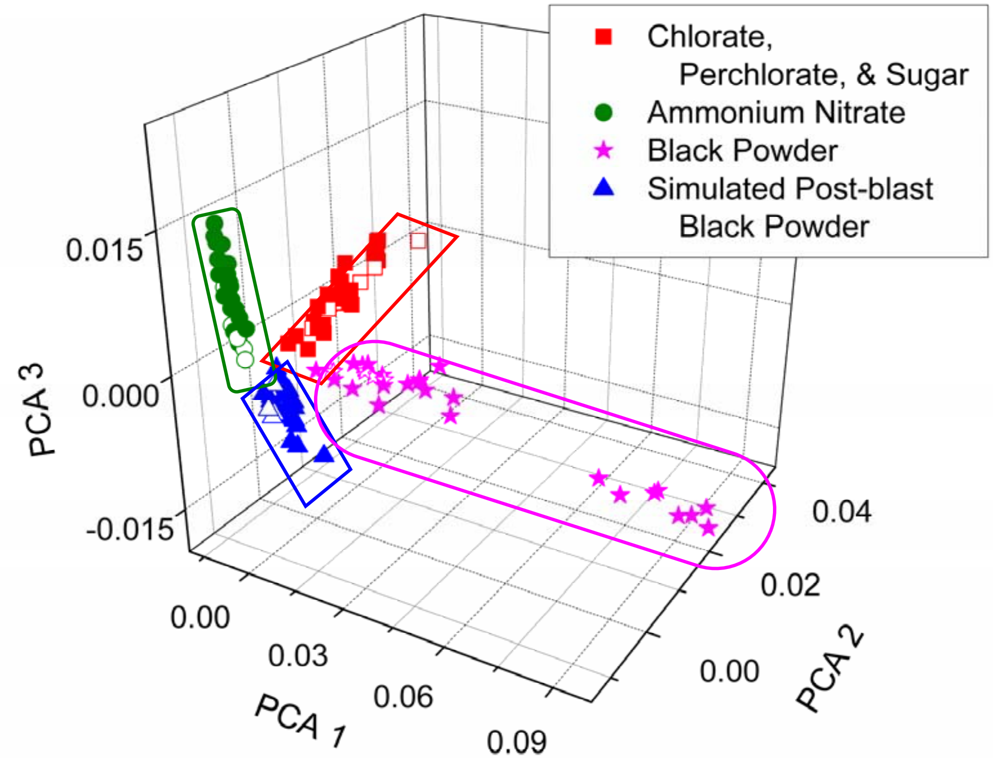

Training set: 6 spectra from each IED
(Unfilled symbols □○☆△)
Testing set: 24 spectra from each IED
(Filled Symbols ■●★▲)

High fidelity classification;
99% Accuracy overall

Inorganic Ion IED	Training Set Size	Samples Correctly Characterized	
Chlorate, perchlorate, sugar	6	23/24	96 %
Ammonium nitrate	6	24/24	100 %
Pre-blast black powder	6	24/24	100 %
Post-blast black powder	6	24/24	100 %
Total	24	95/96	99 %

LEMS Characterization of Smokeless Powders from Various Ordinance

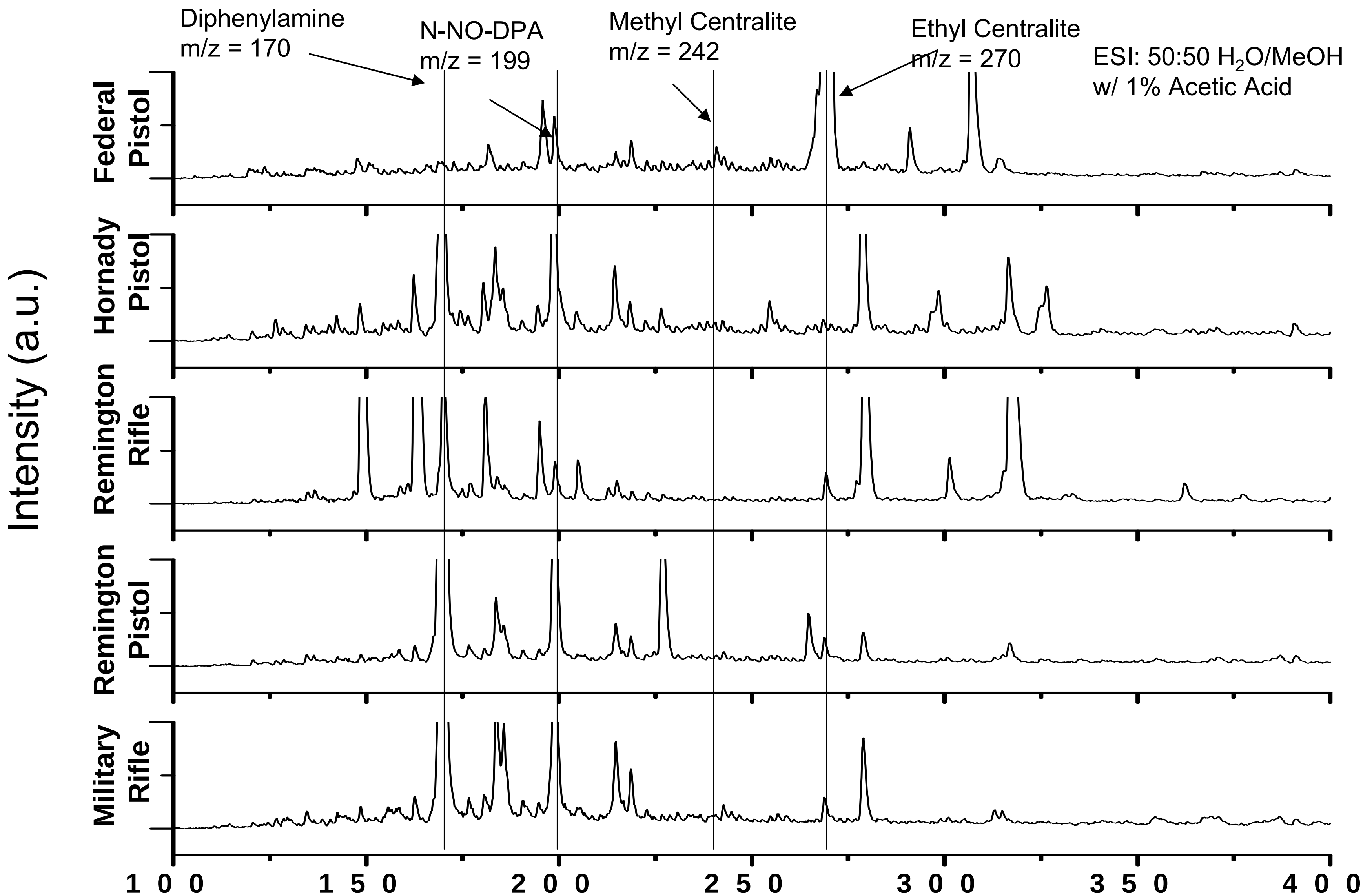

Classification of Black Powder Manufacturer

Projection of the Mass Spectra into the First Three Principal Components

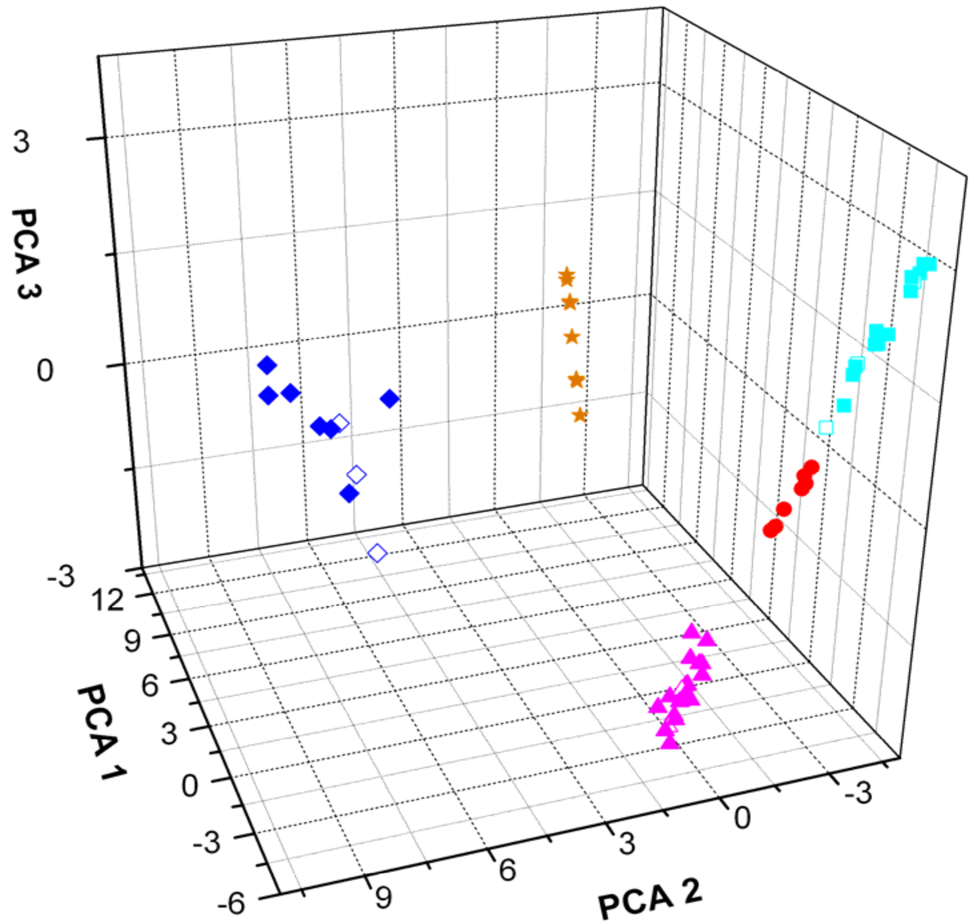

PCA analysis of five different commercially available gun powders projected into three dimensions for Military Rifle (red), Remington Rifle (blue), Remington Pistol (cyan), Hornady Pistol (magenta) and Federal Pistol (orange) which shows separation between manufactures' gunpowder. The open symbols and the filled, colored symbols represent the training and testing sets for each IED, respectively.

Femtosecond Laser Excitation Leads to Universal Vaporization through Nonresonant Excitation

- Ultrashort pulse durations cause less thermal damage to sample and less fragmentation.
- Femtosecond laser couples into any system through resonant and non-resonant mechanisms.

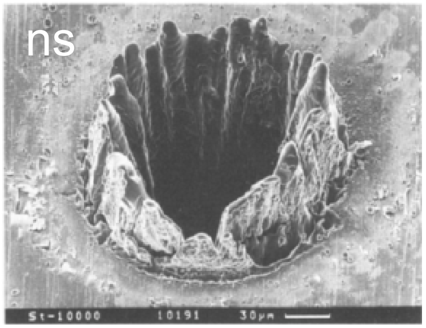

SEM of 100 μm thick steel foil after exposure to 3.3 ns, 1 mJ, F = 4.2 J/cm^2 laser pulses at 780 nm

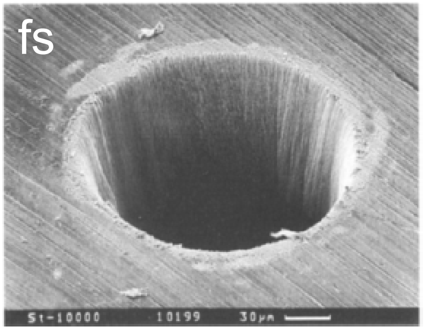

SEM of 100 μm thick steel foil after exposure to 200 fs, 120 μJ, F = 0.5 J/cm^2 laser pulses at 780 nm

B.N. Chichkov, et al., *Appl. Phys. A.* (1996) 63, 109-115

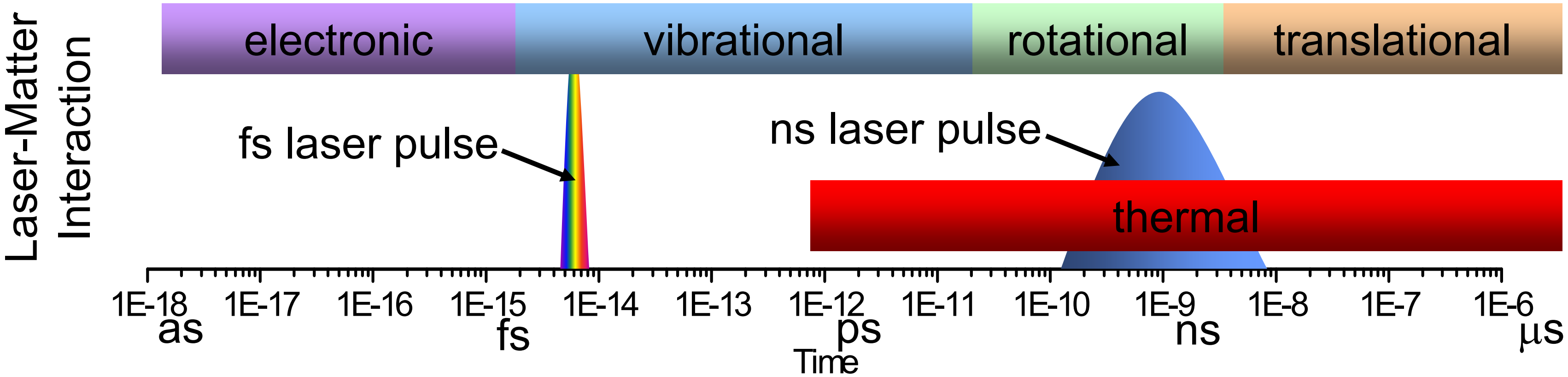

Non-resonant Femtosecond Desorption

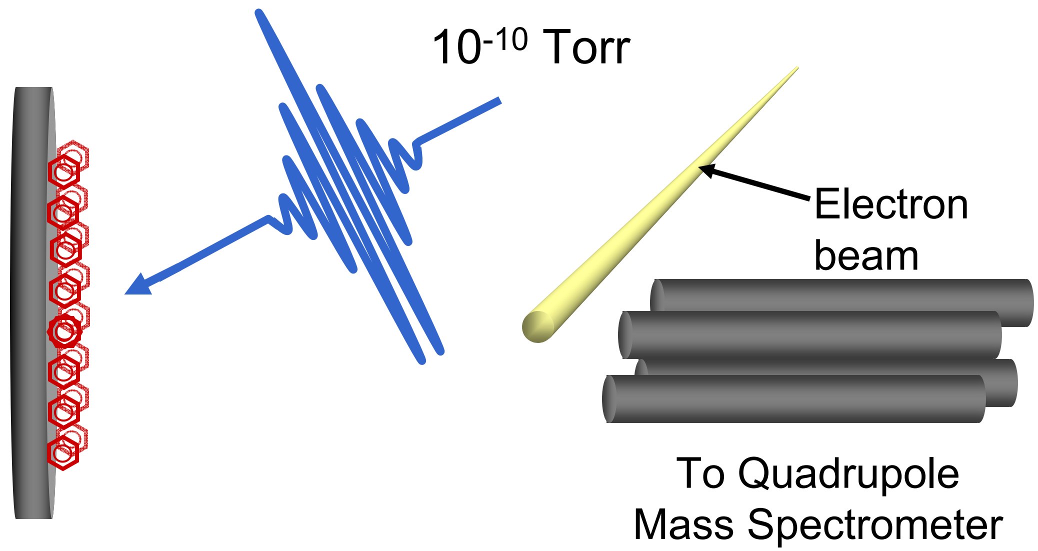

Pt(111) single crystal covered with cryogenic benzene multilayer

Desorption as a function of pulse duration and sample thickness

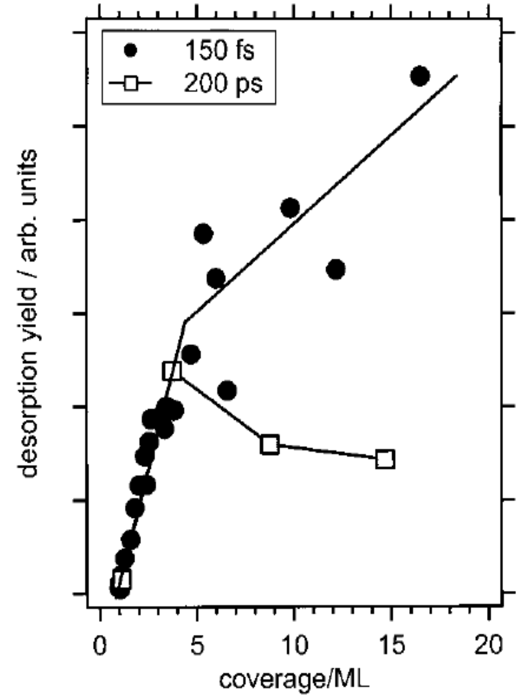

- Desorption has been demonstrated without fragmentation.
- Suggests that fs desorption can be extended to atmospheric pressure.

Arnolds, H.; Levis, R. J.; King, D. A. Chemical Physics Letters 2003, 380, 444-450.
Arnolds, H.; Rehbein, C.; Roberts, G.; Levis, R. J.; King, D. A., JCP B 2000, 104, 3375-3382.
Arnolds, H.; Rehbein, C. E. M.; Roberts, G.; Levis, R. J.; King, D. A. Chemical Physics Letters 1999, 314, 389-395.

LEMS Spatially-Resolved Molecular Imaging Microscopy Modality for Pharmaceuticals in Tablets and Narcotics

Optical Photograph of Dried Droplet
500 pmol oxycodone

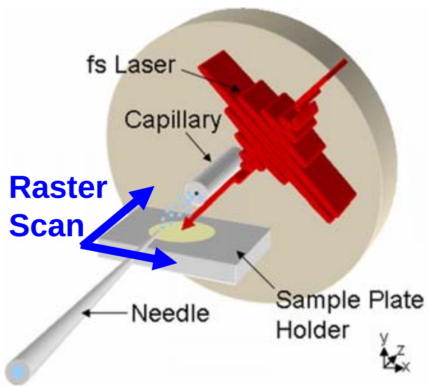

Ion signal for parent molecular ion
m/z = 316 vs position

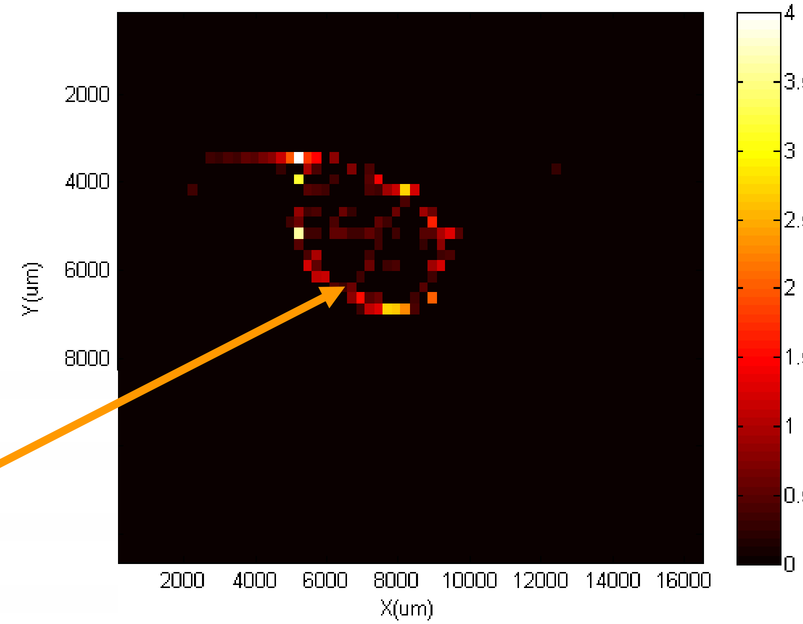

Optical Photograph
After Scanning LEM

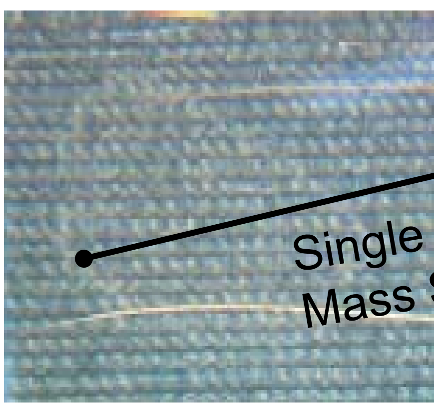

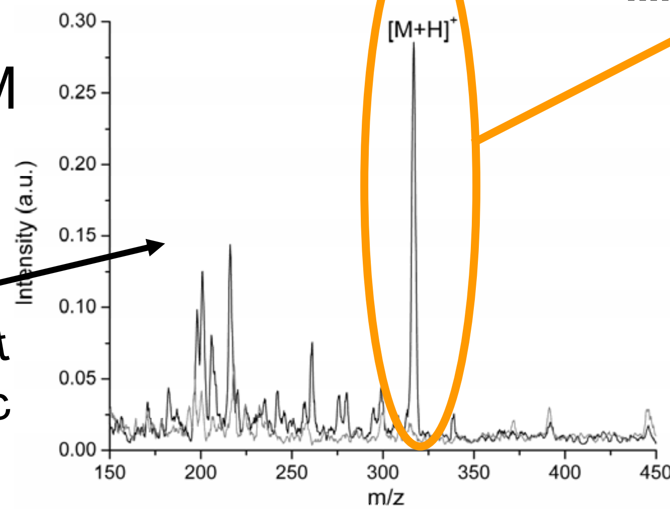

1 mJ/pulse
focused to a 100 μm spot
with 250 mm steps.

Judge, E.J., Brady, J.J., Dalton, D., Levis, R.J., *Analytical Chemistry,* **2010**, *82*, 3231

Femtosecond Laser Electrospray Mass Spectrometry (LEMS)

- Ultrafast, Strong Field Laser Molecule Interactions
- Biomolecule Mass Spectrometry
- Universal Laser Vaporization
- LEMS Analysis, Laser Electrospray Mass Spectroscopy of Biomolecules

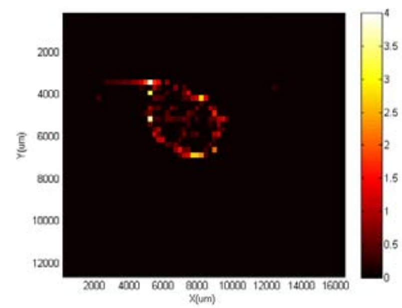

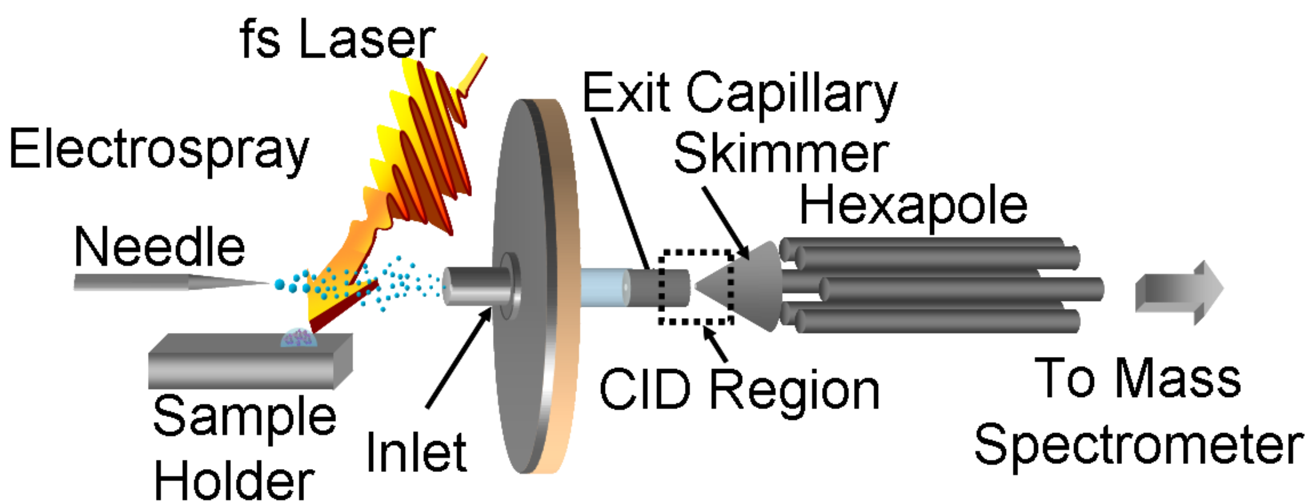

Femtosecond Non-Resonant Laser Vaporization of Protein Films Provides Universal Analysis

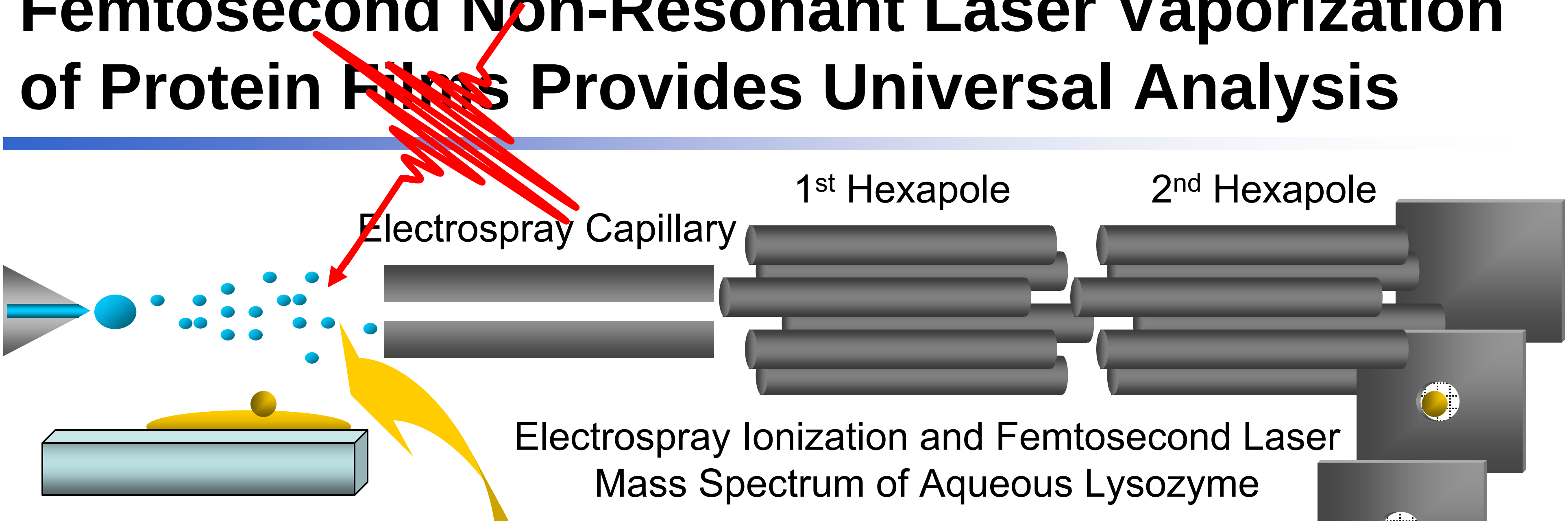

Electrospray Ionization and Femtosecond Laser Mass Spectrum of Aqueous Lysozyme

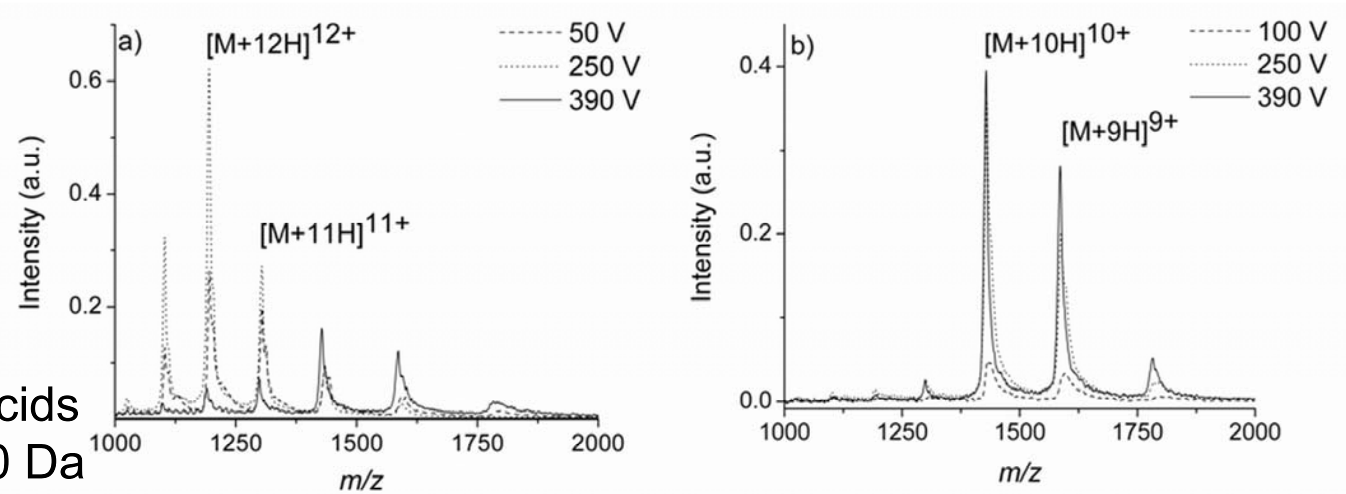

Lysozyme 129 Amino Acids
molecular weight 14,300 Da
20 basic AA, 20 acidic AA

No Matrix, Nonresonant Desorption

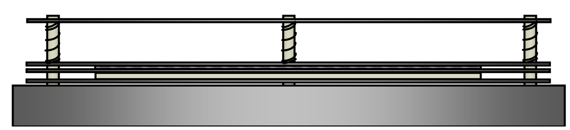

Brady, J. J.; Judge, E. J.; Levis, R. J. *PNAS* **2011**, *108,* 12217

ESI Measurements of Cytochrome C Conformation as a function of Solvent pH

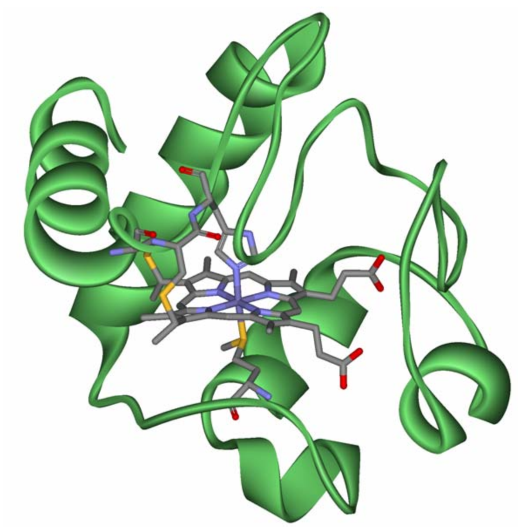

Cyctochrome c is a heme protein found within mitocondria with molecular weight 12,384 Da.

The ESI-MS assignments for cytochrome c are in accord with absorbance, fluorescence and circular dichromism techniques.

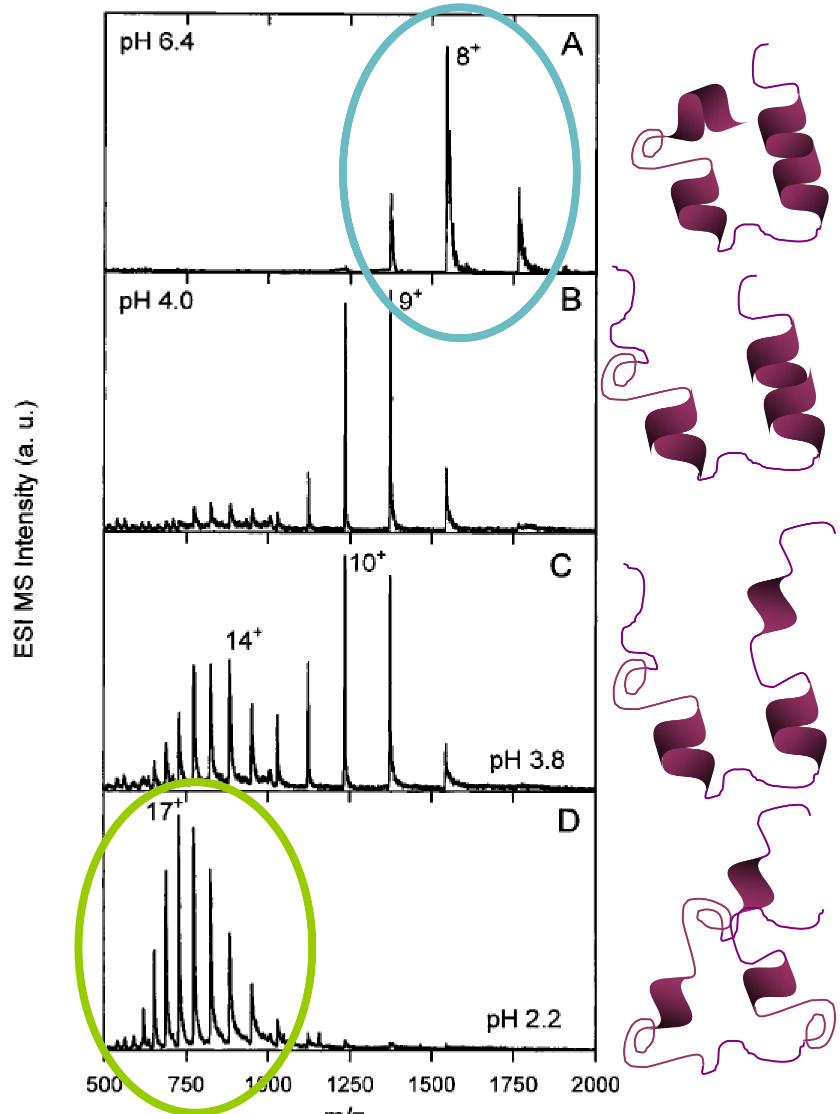

Konermann L., Douglas DJ, *Biochemistry* 1997; **36**: 12296

Lysozyme: Basic and Acidic Site Pairing Controls ESI Charge State

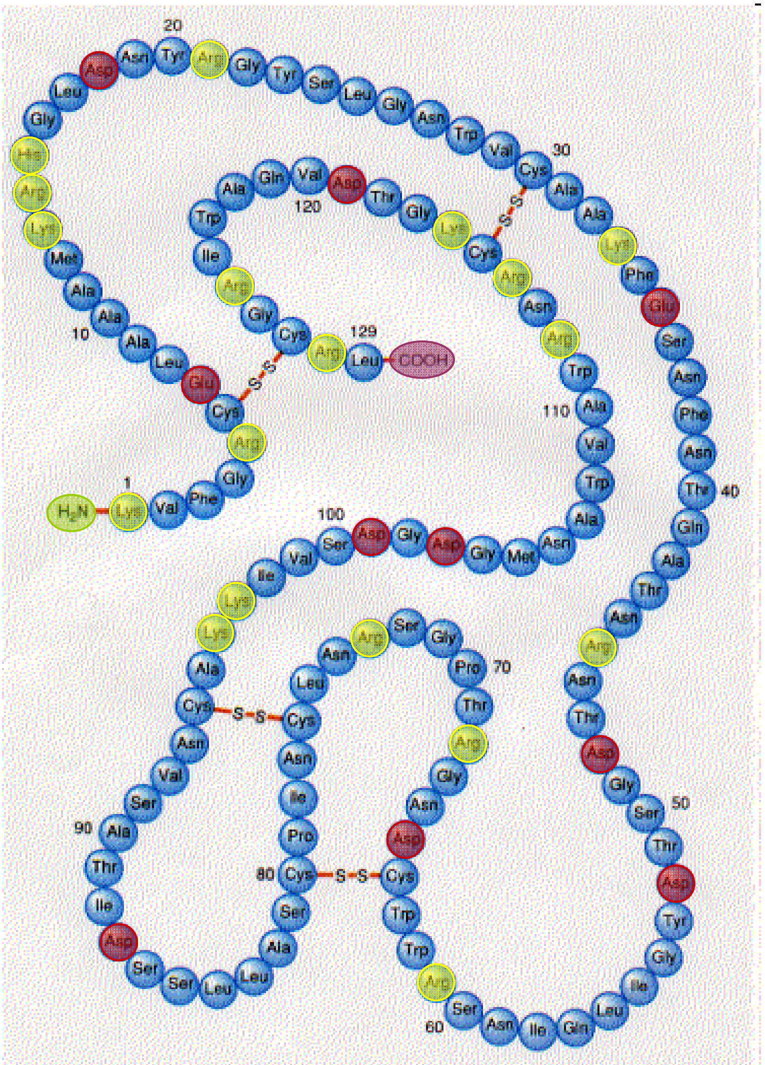

Molecular weight: 14.3 kDa
129 amino acids

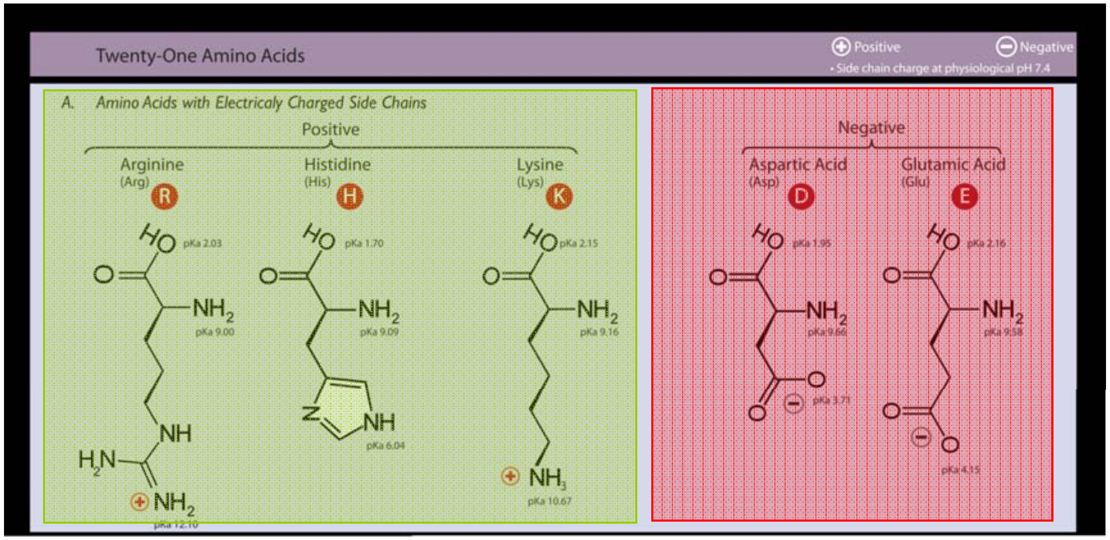

Folded Lysozyme Expected Charge State 9+

Grandori, R. *J. Mass Spectrom.* **2003**, *38*, 11-15

Nelson, D.L., Cox, M.M. *Lehninger Principles of Biochemistry,* W.H. Freeman and Company, New York, 2005

ESI and LEMS Analysis of Cytochrome C

Conventional ESI-MS

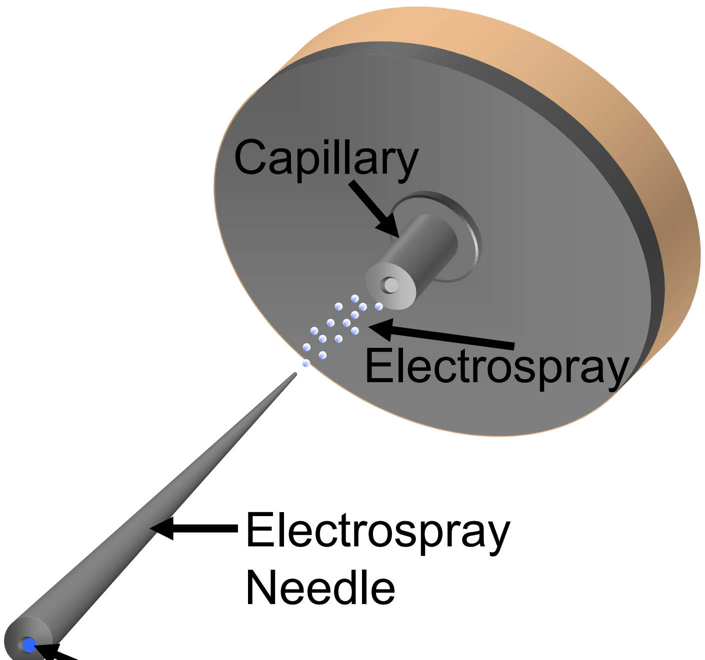

10^{-5} M cytochrome c dissolved in a buffered H_2O:MeOH solvent varying in pH from 7 to 4.

LEMS

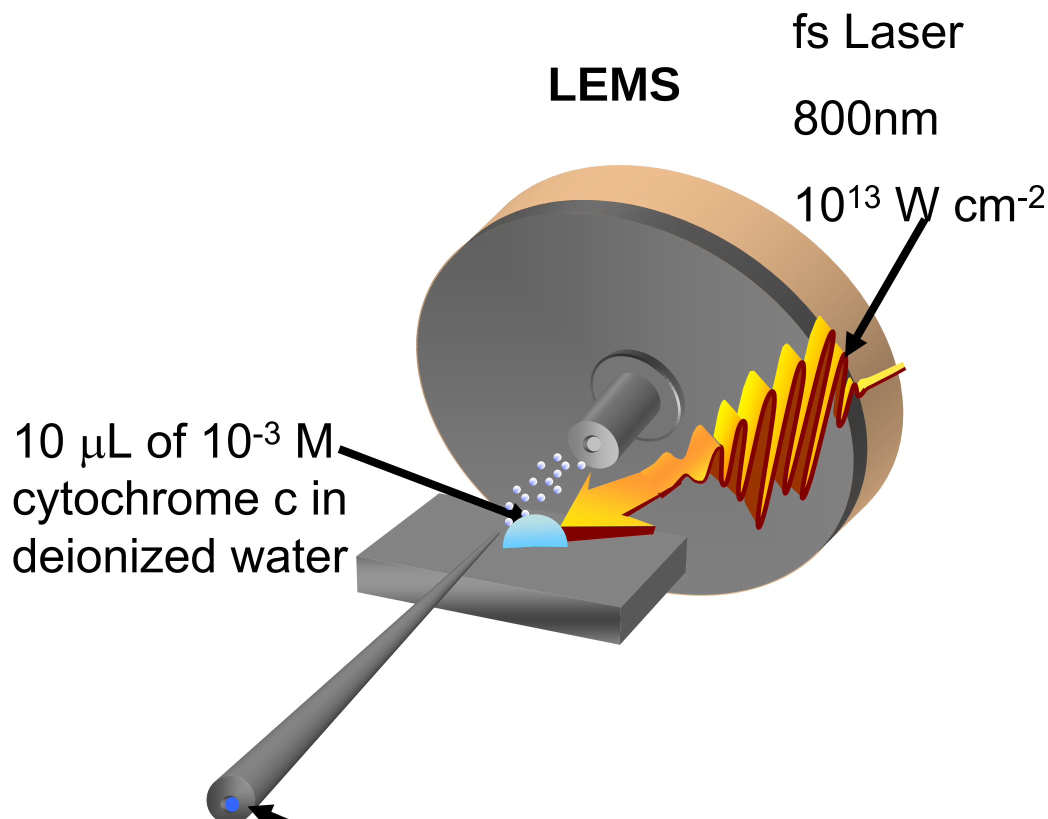

Buffered solvent varying in pH from 7 to 4.

Effect of pH on Cytochrome C Conformation

Conventional ESI-MS of Cytochrome C

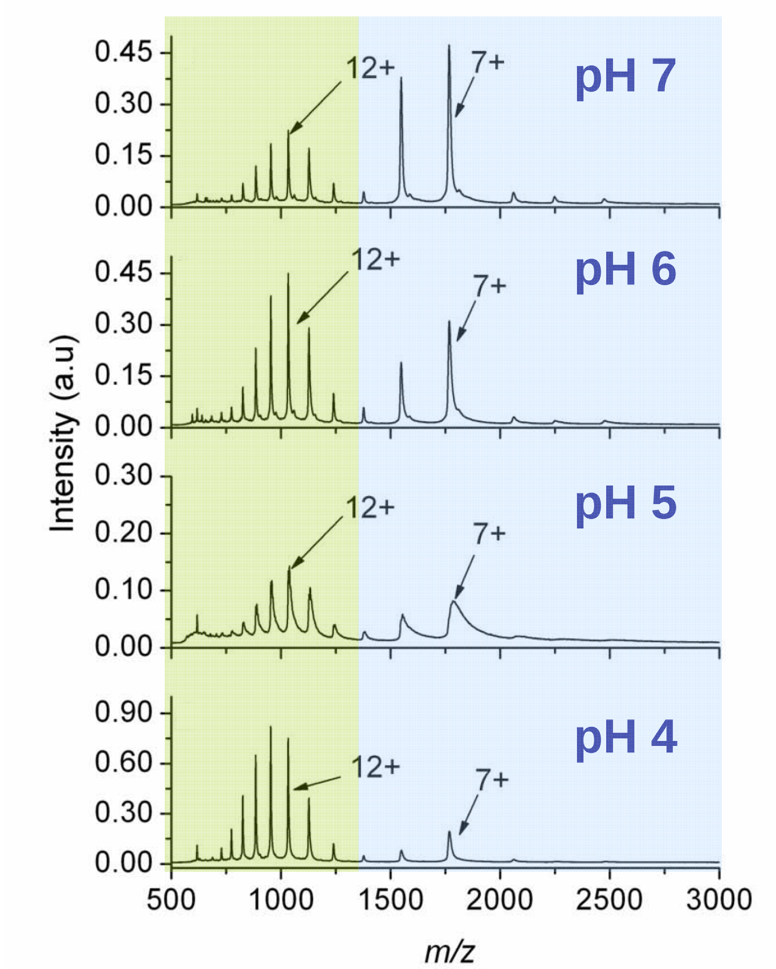

Femtosecond laser vaporization yields more protein in the folded state than conventional ESI-MS

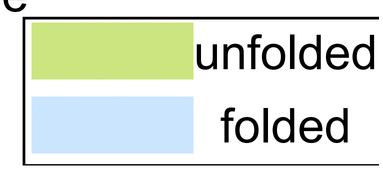

Brady, J. J.; Judge, E. J.; Levis, R. J. *PNAS* **2011**, *108,* 12217

Probing Protein Conformation: Collision-Induced Dissociation (CID)

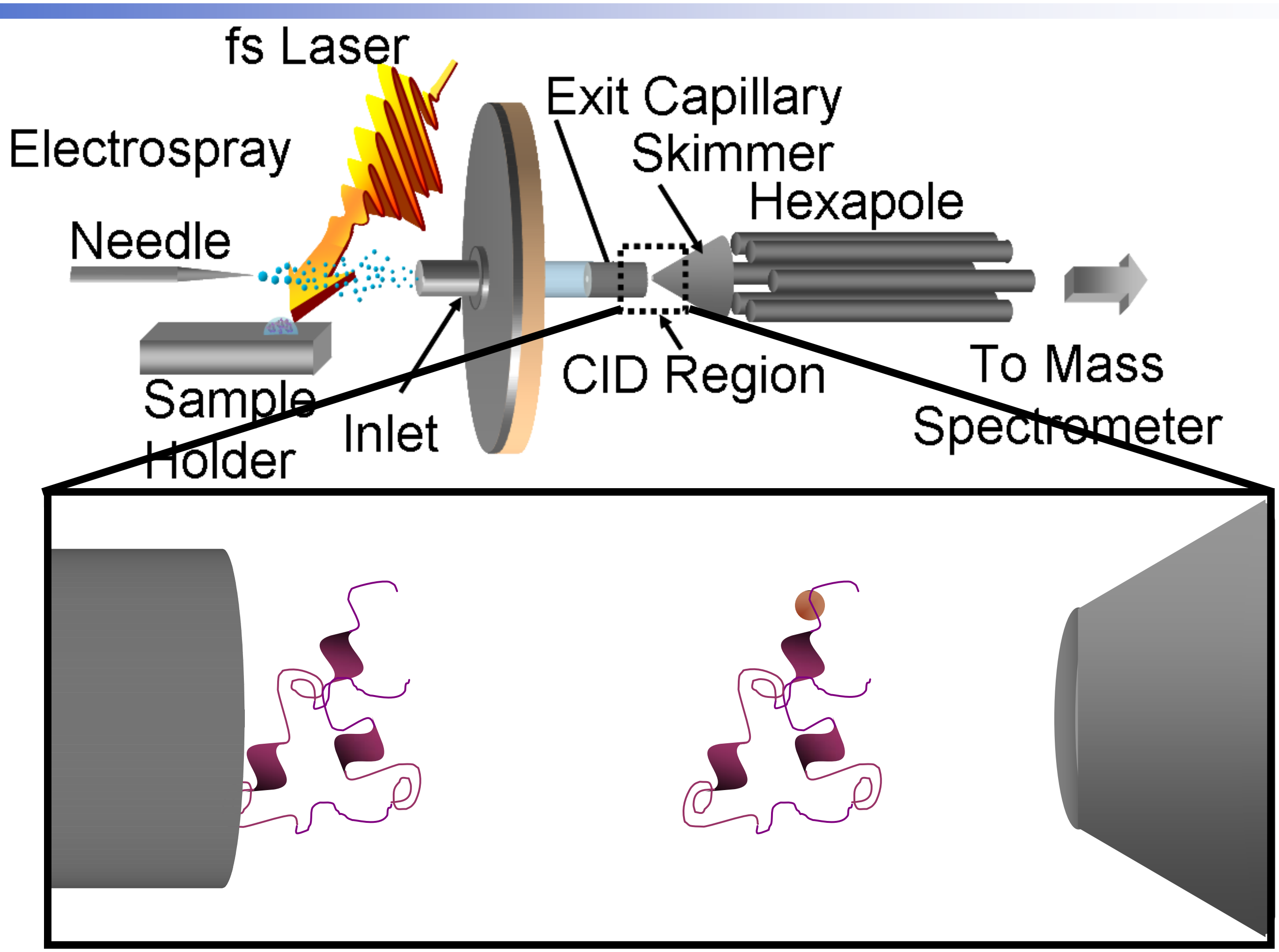

When the analyte ion collides with a background gas molecule, energy can be transferred into the analyte ion leading to dissociation.

Comparing CID for ESI and LEMS

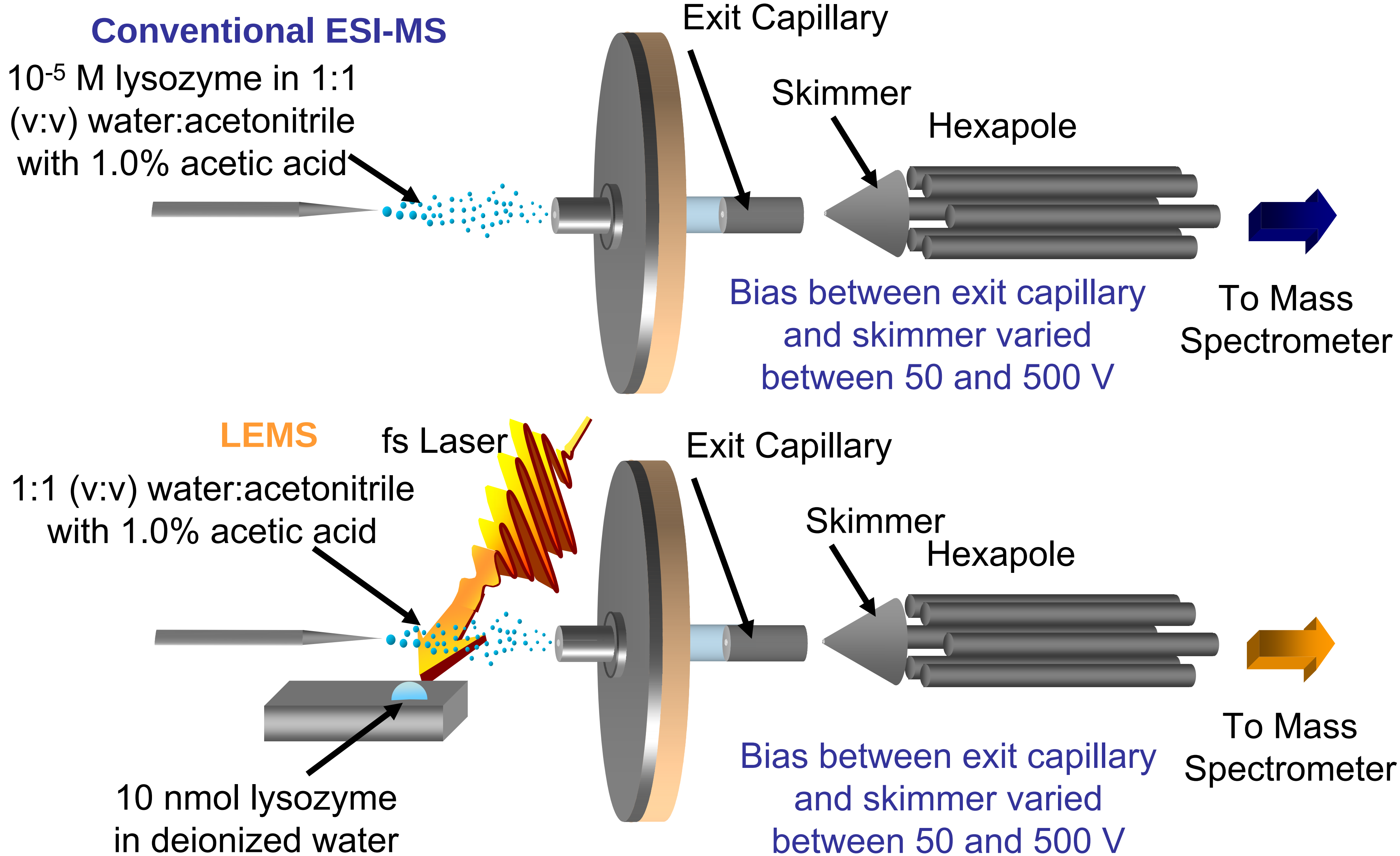

CID of Lysozyme in ESI-MS vs. Femtosecond Laser Vaporization

Conventional ESI-MS

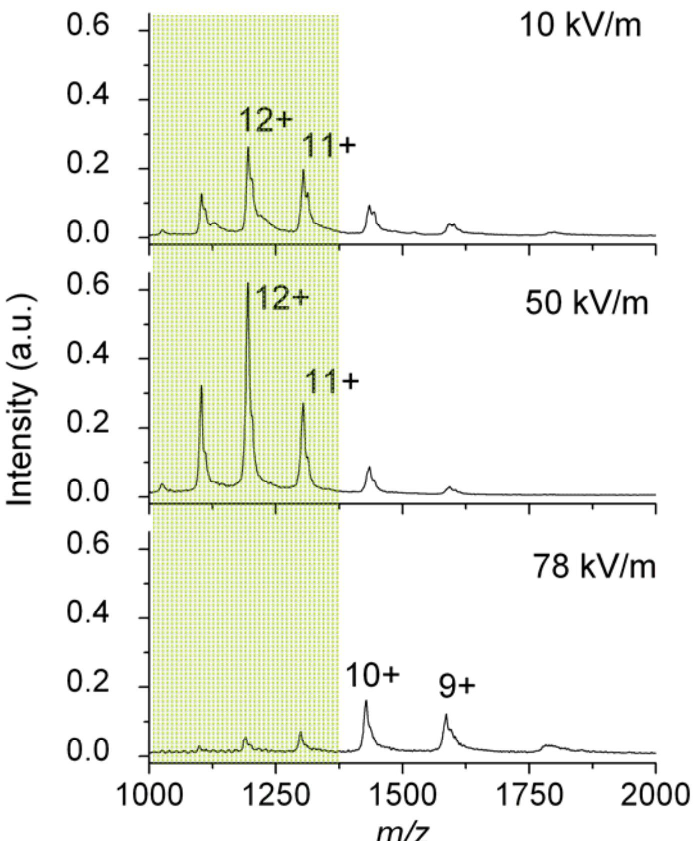

LEMS

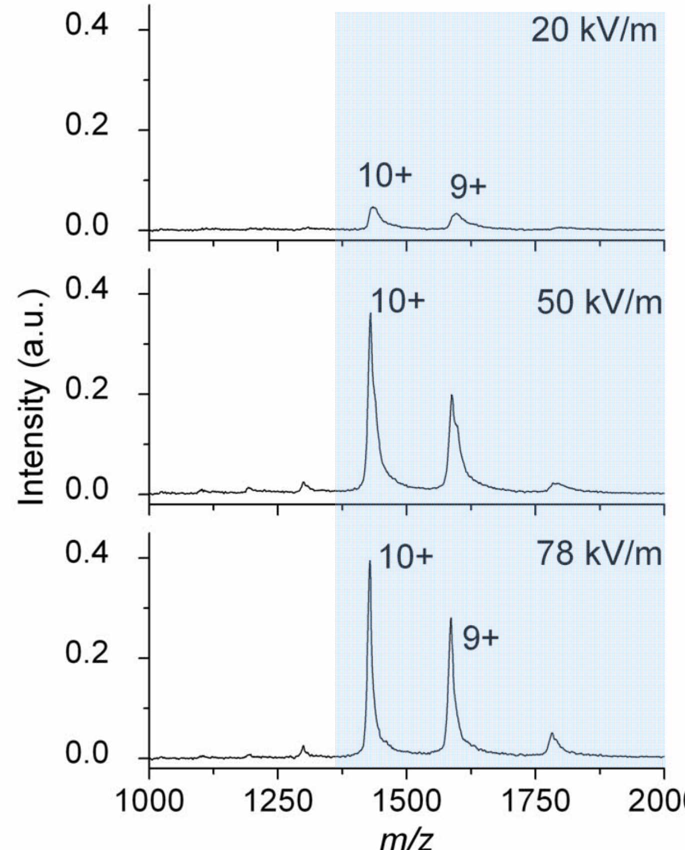

•Noncovalent adducts are removed.
•Charge reduction occurs.
•Large fragmentation cross section.

•Noncovalent adducts are removed and signal intensity increases.
•No observed charge reduction.

Suggests that tertiary structure controls CID probability

unfolded
folded

Brady, J. J.; Judge, E. J.; Levis, R. J. *PNAS* **2011**, *108,* 12217

Noncovalent Interactions During CID

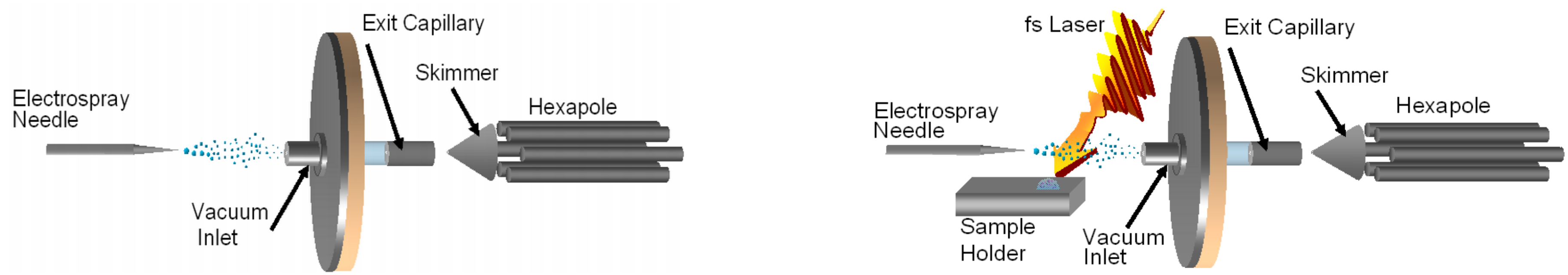

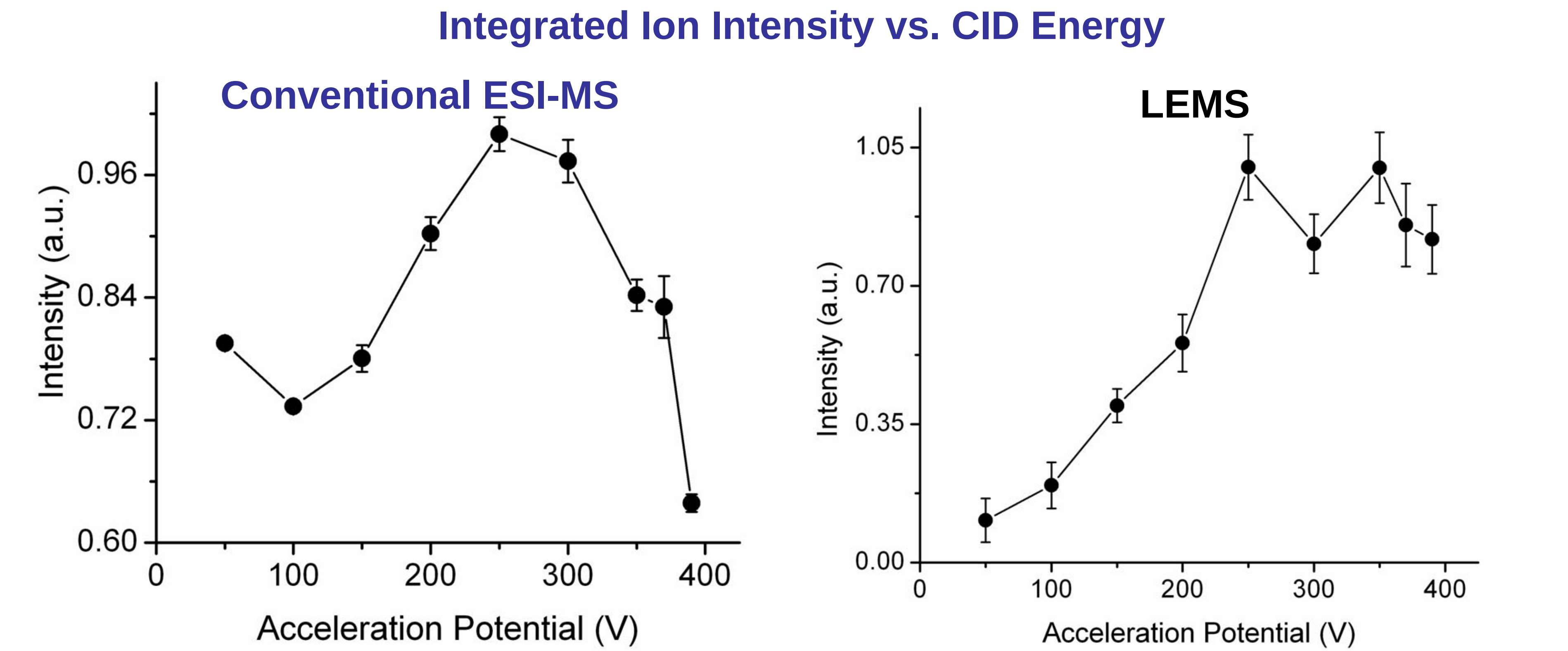

Brady, J. J.; Judge, E. J.; Levis, R. J. *PNAS* **2011**, *108,* 12217

Cytochrome C Vaporization from pH 3 Solution

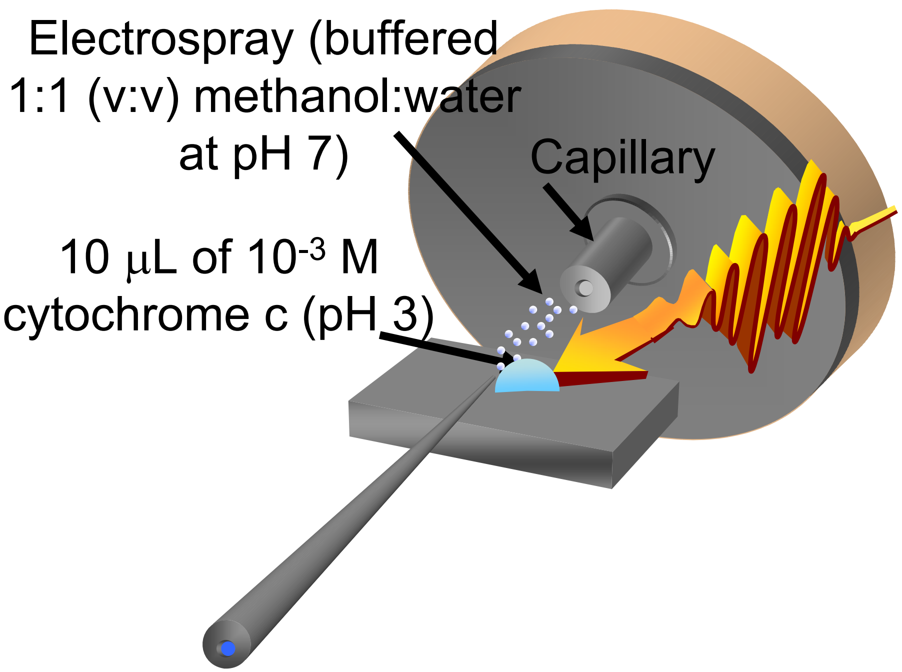

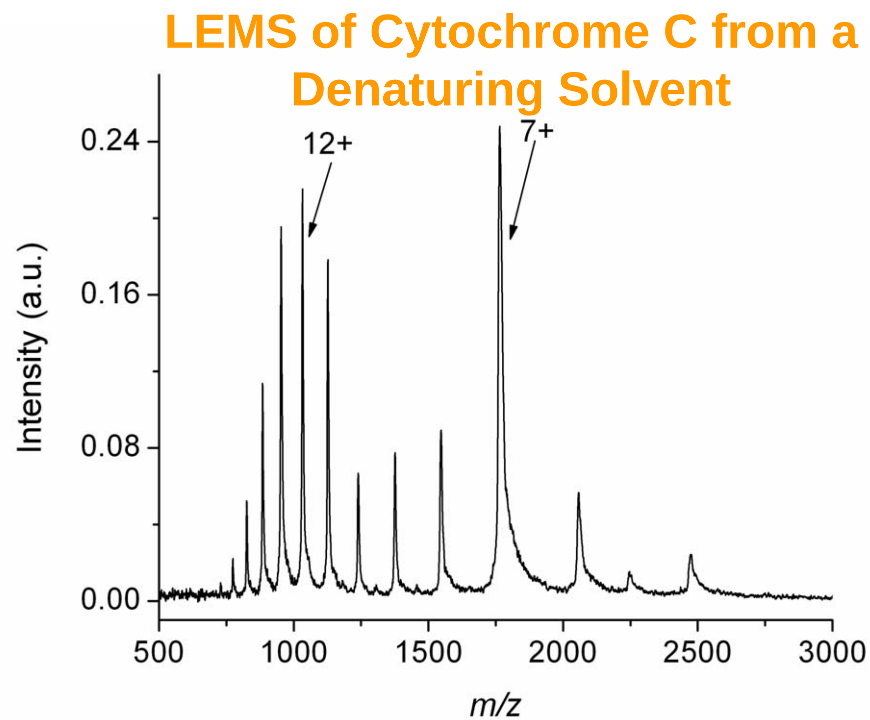

Suggests that nonresonant fs laser vaporization ***preserves*** condensed phase conformation.

Vaporization of (De)Hydrated Lysozyme

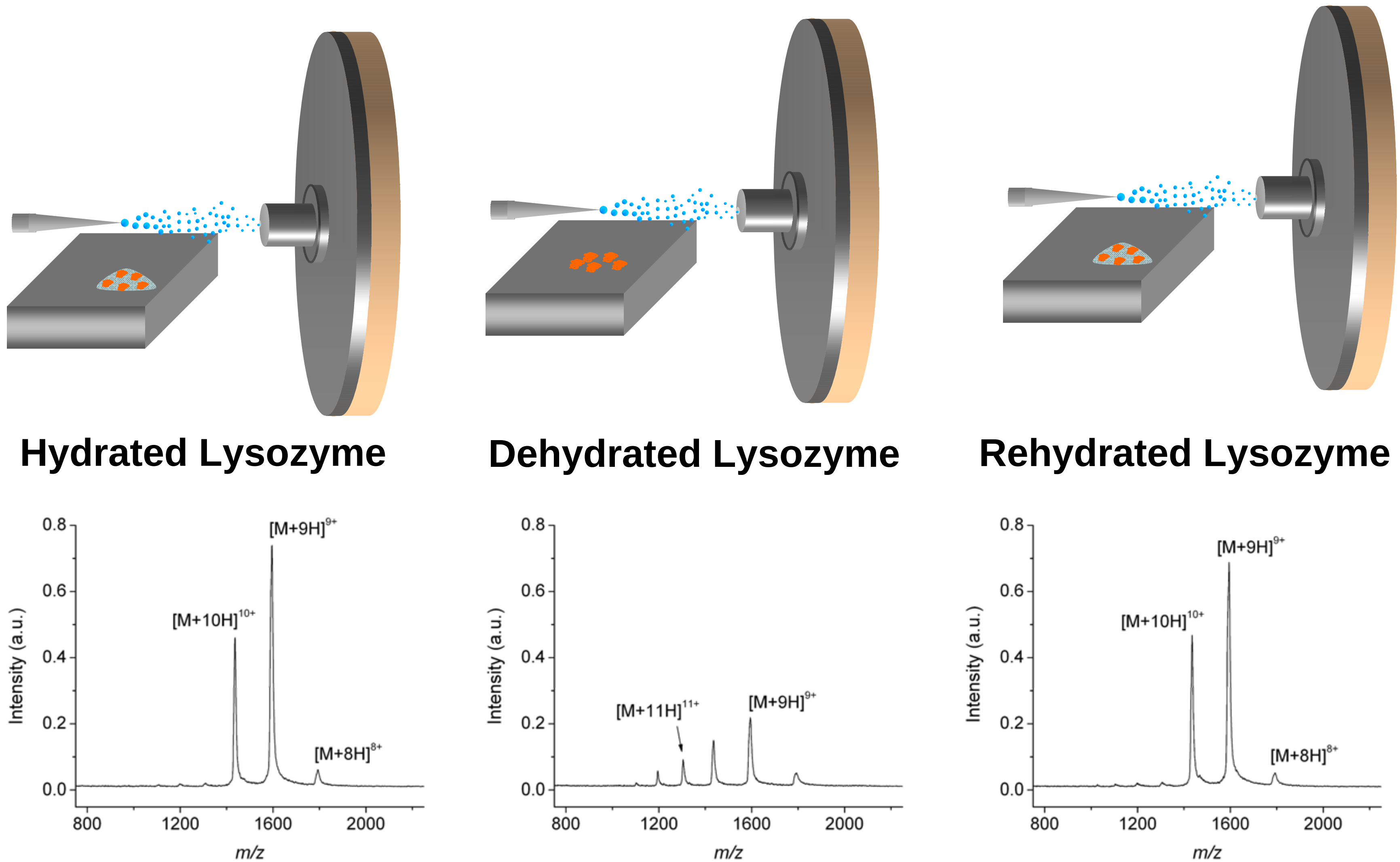

Judge, E.J., Brady, J.J., Levis, R.J., *Analytical Chemistry,* **2010**, *82,* 10203

Mechanism of LEMS Pickup Avoids Equilibria Enabling Quantitative Protein Measurements

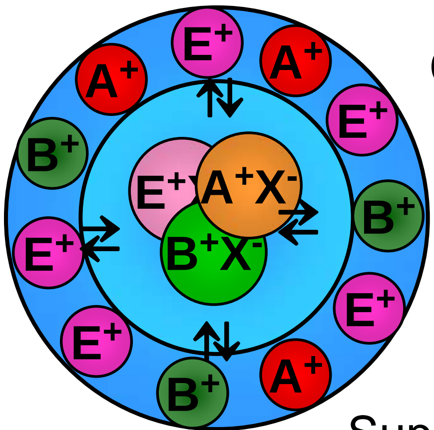

Conventional ESI-MS

Equilibrium

Suppression due to competition for surface

LEMS

Nonequilibrium Surface Interaction

Provides quantitative capability

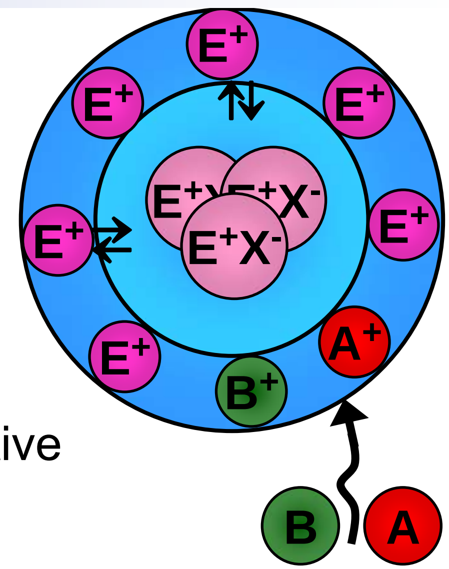

ESI Equimolar Protein Mixtures

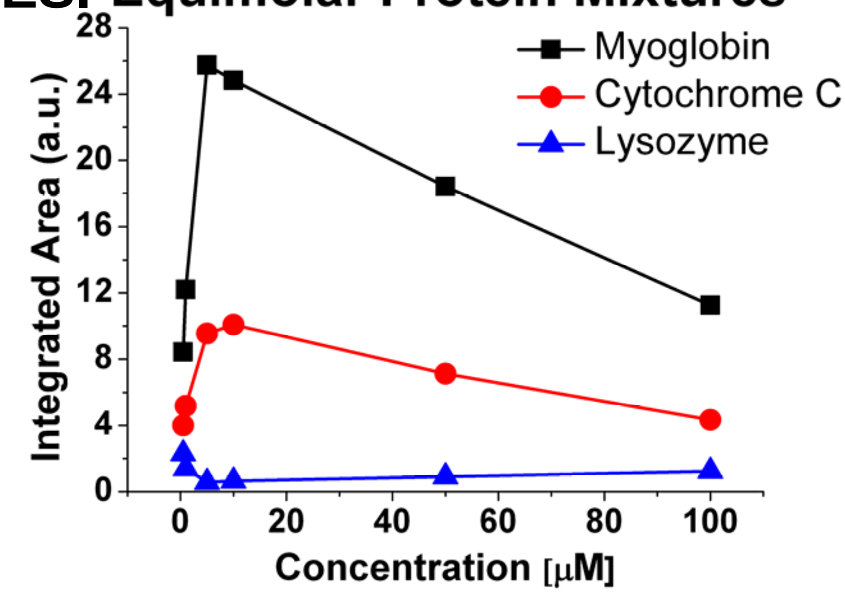

LEMS Equimolar Protein Mixtures

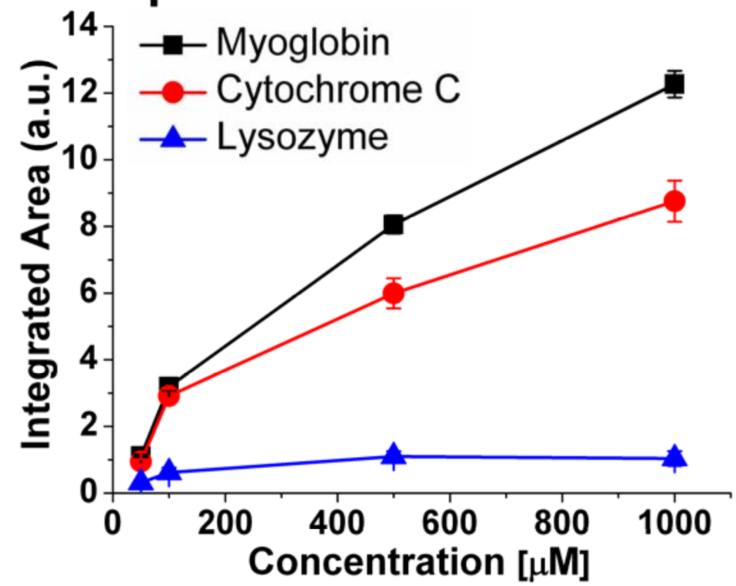

Femtosecond Vaporization of Tissue

Plant Tissue Discrimination Test Bed

- Femtosecond LEMS analysis of an *impatien's* stem, flower and leaf.
- Three clear peaks may be used to differentiate the tissue type at m/z = 190, 609, and 812.

Analytical Chemistry, 2011, 83, 2145

LEMS Analysis of Plant Tissues

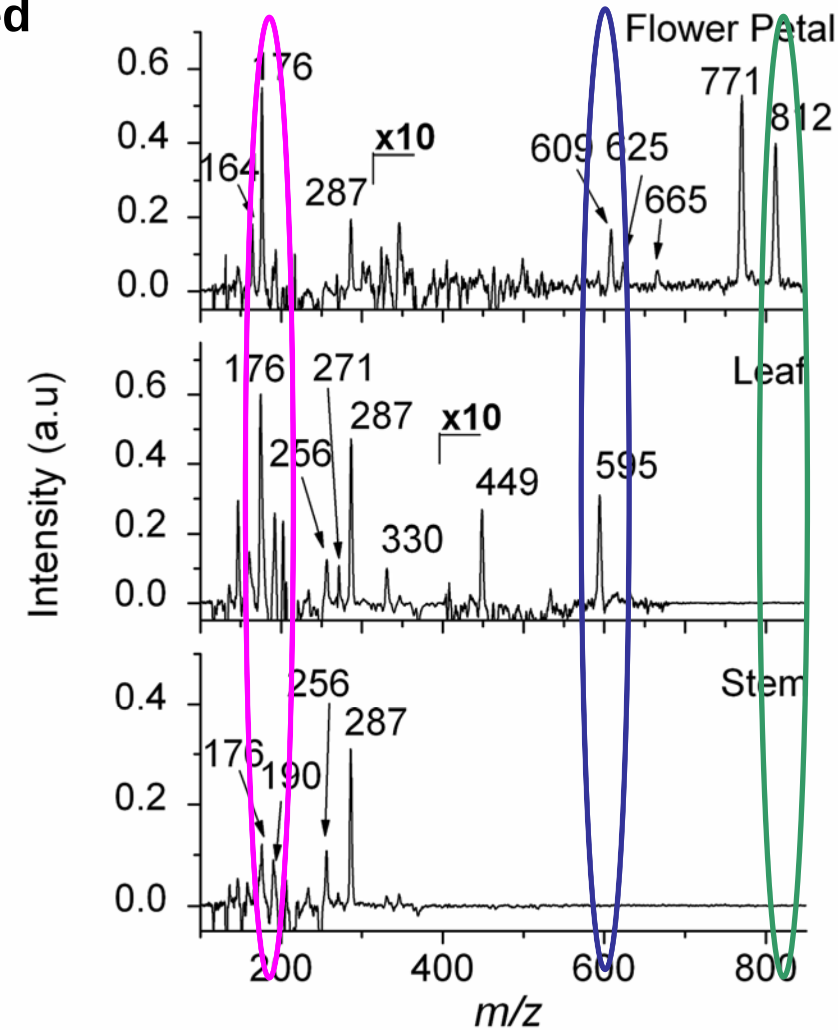

Suggests Diagnostic Applications

Discriminating Tissue for Diagnosis

Statistical demonstration of tissue discrimination

Raw Data

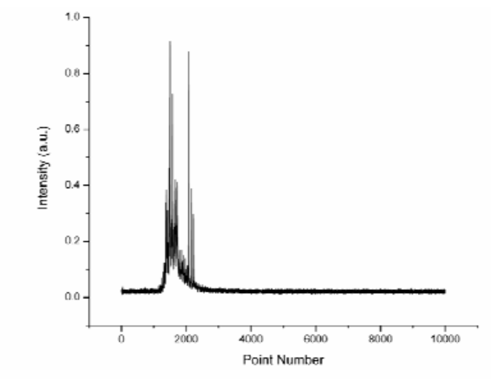

Distill Significant Data

$\Phi: R^{10000} \rightarrow R^{350}$

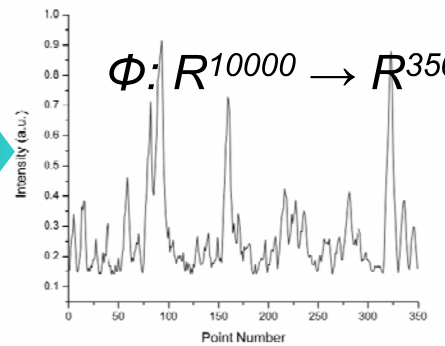

Compress to Smallest Possible Discrimination Space

Manipulate and further compress with optimized T Matrix to generate maximal separation

Example of Data Projected to 3 Dimension

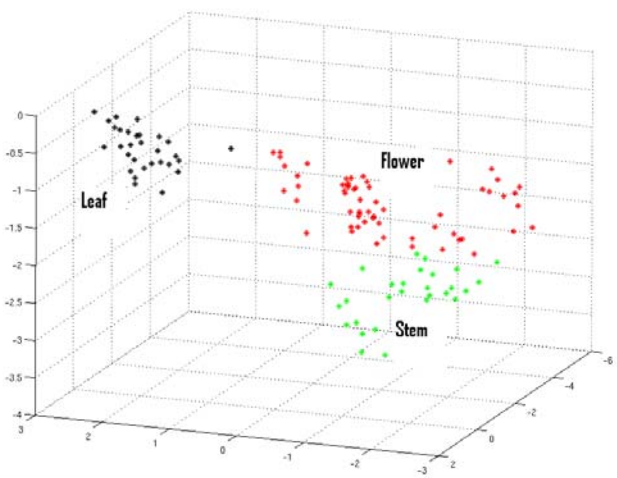

Near Perfect Classification of Plant Tissue

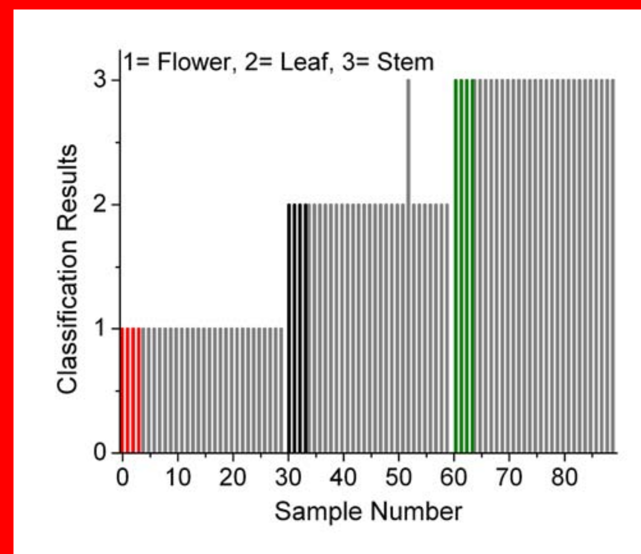

LEMS Analysis of Plant Tissue: Variety of Petal Colors

Anthocyanins: Water soluble plant pigments

164 rhamnose
176 Ferulic acid – H_2O
287 Luteolin/kaempferol/cyanidin
812 Peonidin 3-O-(6-O-*p*-coumaryl)-5-O-diglucoside
801 Malvidin 3-gluoside-coumarate-5-glucoside

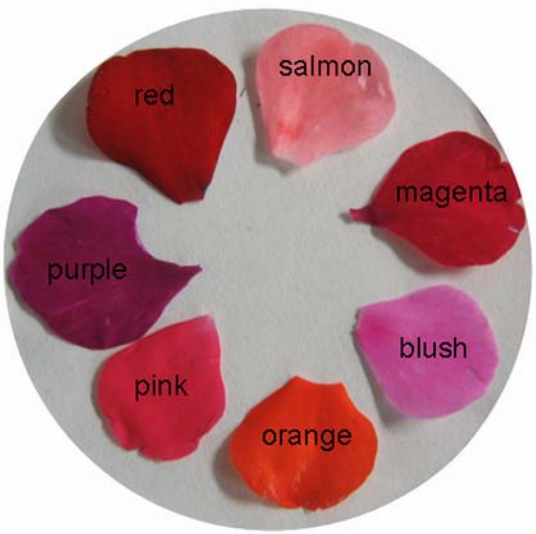

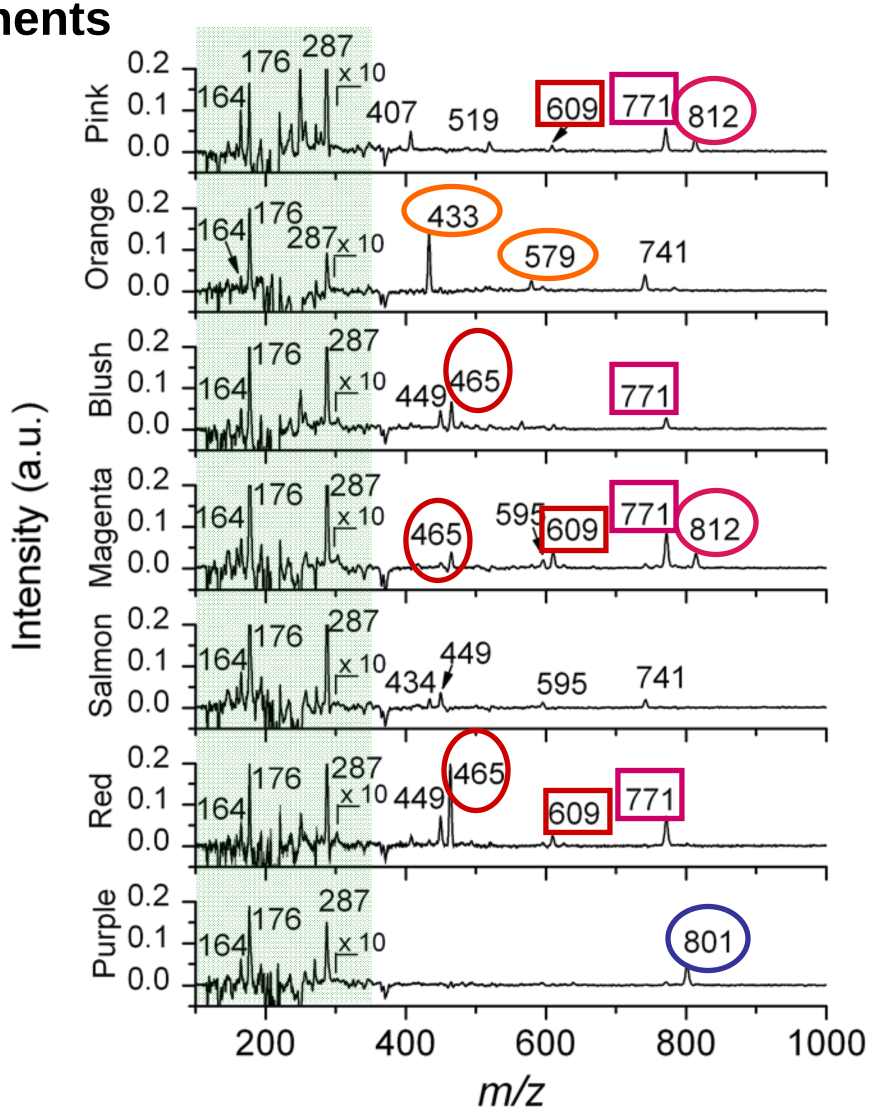

PCA Classification of Eight Phenotypes of a Single Flower Tissue Type

Analytical Chemistry 2012, 84, 6225

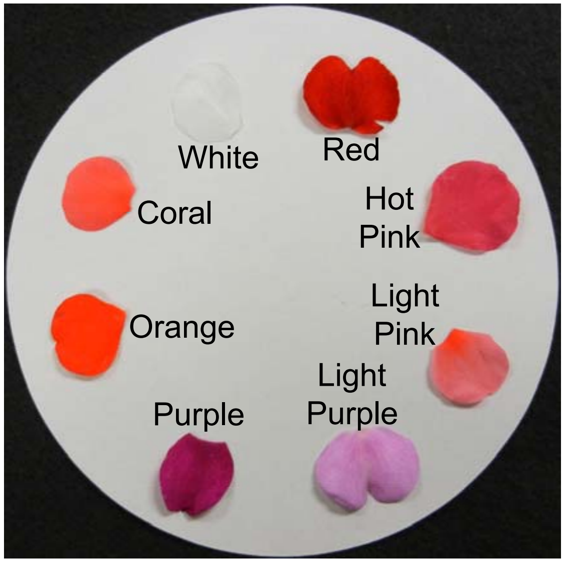

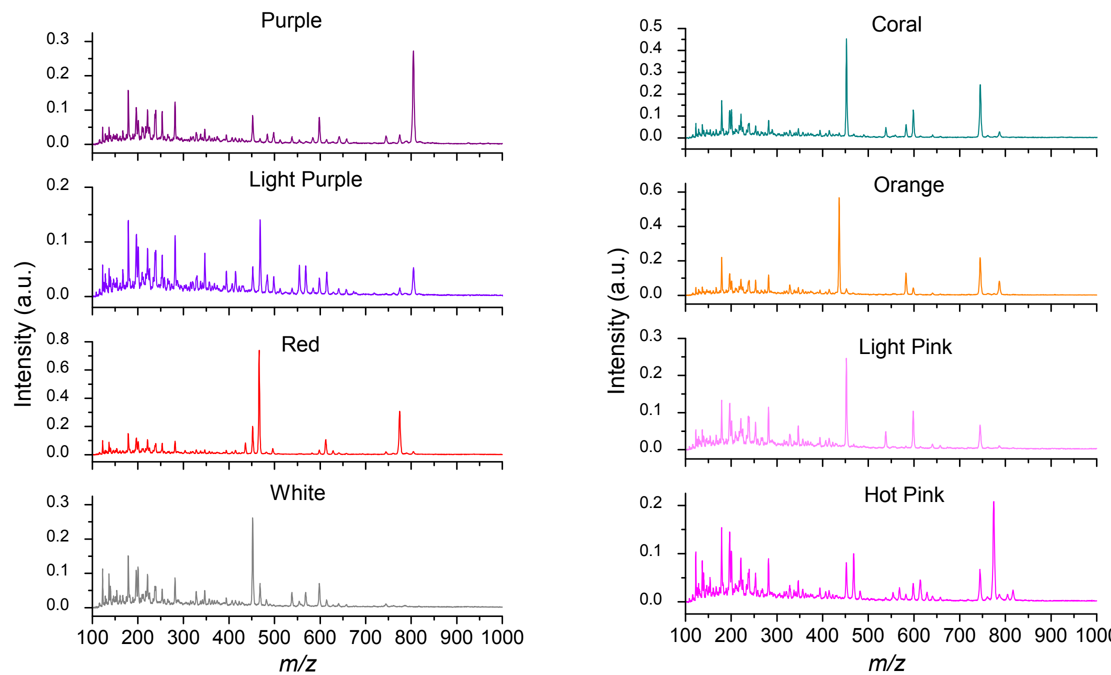

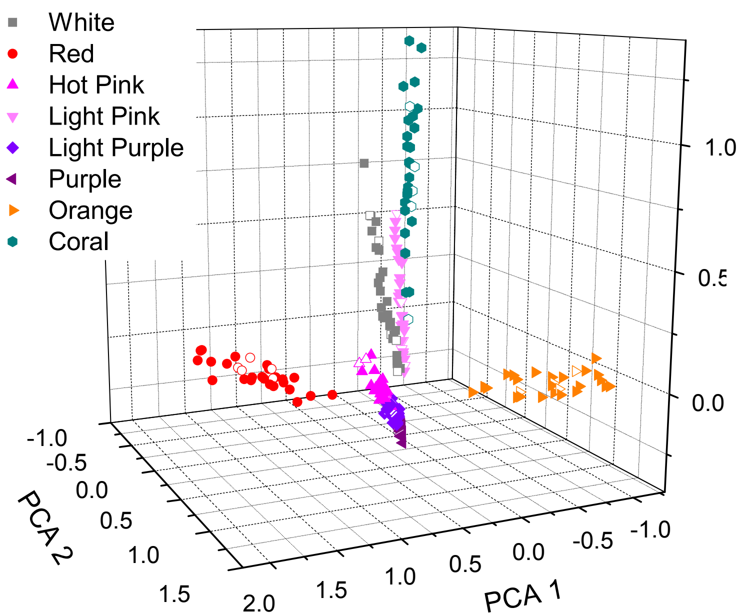

	Nearest Neighbor			LDA		
Color	**Correct**	**Total**	**Percentage**	**Correct**	**Total**	**Percentage**
White	25	25	**100.0%**	22	25	**88.0%**
Red	25	25	**100.0%**	25	25	**100.0%**
Hot Pink	25	25	**100.0%**	25	25	**100.0%**
Light Pink	25	25	**100.0%**	25	25	**100.0%**
Light Purple	25	25	**100.0%**	25	25	**100.0%**
Purple	25	25	**100.0%**	25	25	**100.0%**
Orange	25	25	**100.0%**	24	25	**96.0%**
Coral	23	25	**92.0%**	22	25	**88.0%**
Total	198	200	**99.0%**	193	200	**96.5%**

Laser Vaporization Mass Spec Analysis of Human Blood

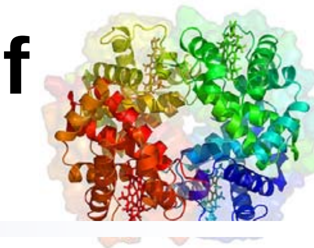

Liquid State Whole Blood | **Solid State Dried Blood**

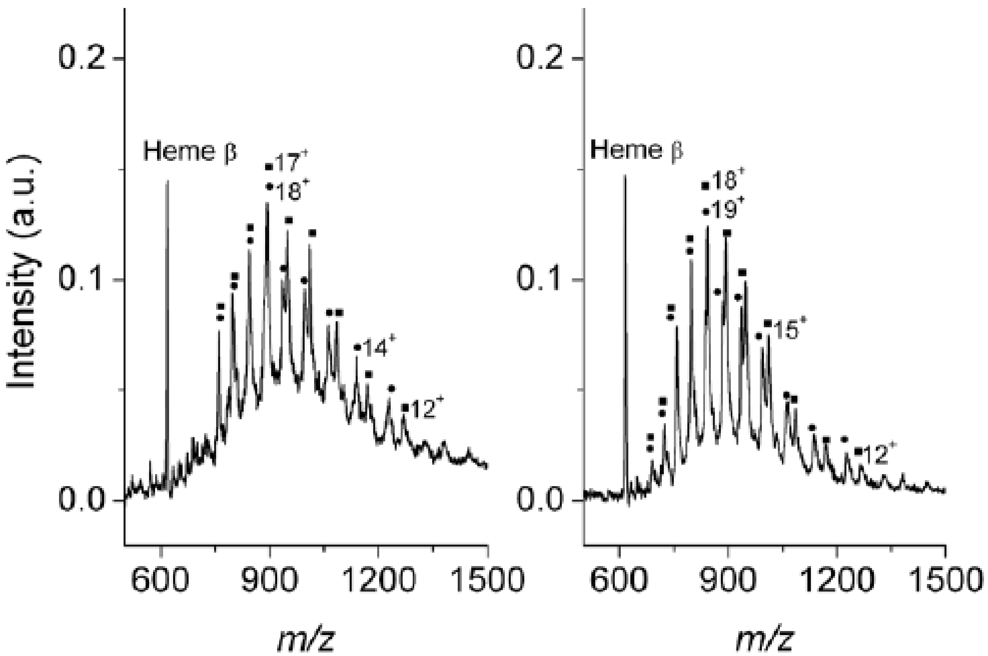

Whole Blood Spiked with One Nanomole of Lipid

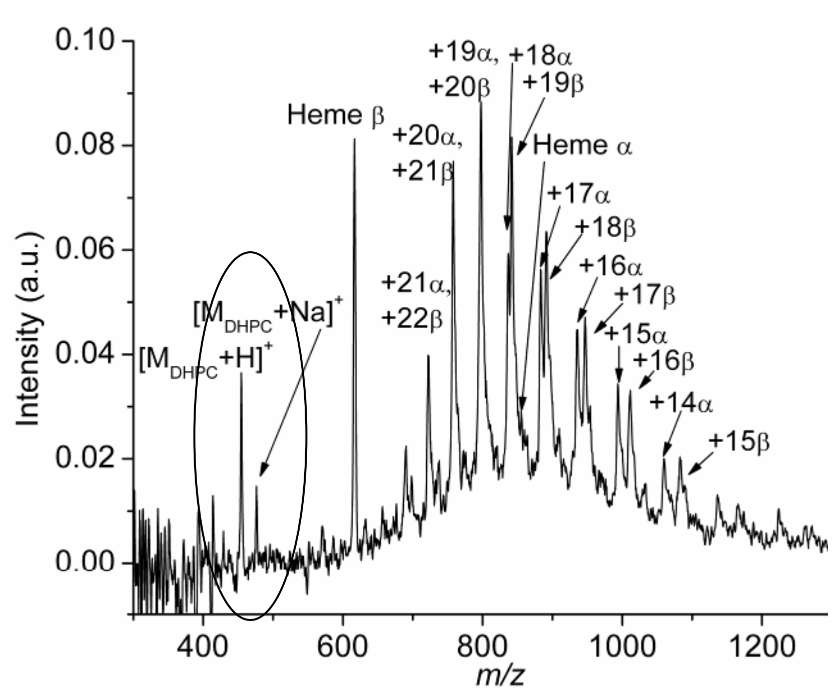

Analytical Chemistry, 2010, 82, 10203

Journal of the American Mass Spectrometry Society, 2011, 22, 762

LEMS Analysis of Mouse Brain Section

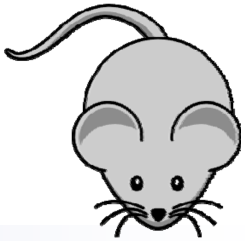

- 10 micron thick section of mouse brain deposited on stainless steel slide
- Laser is raster scanned over the section
- Mass spectra is sum of 50 laser shots

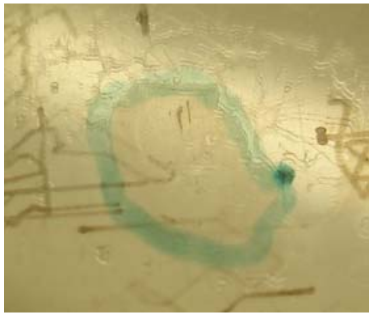

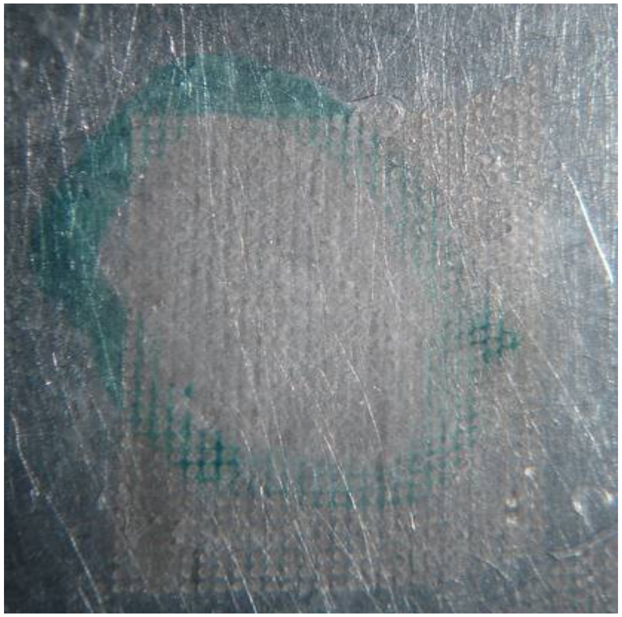

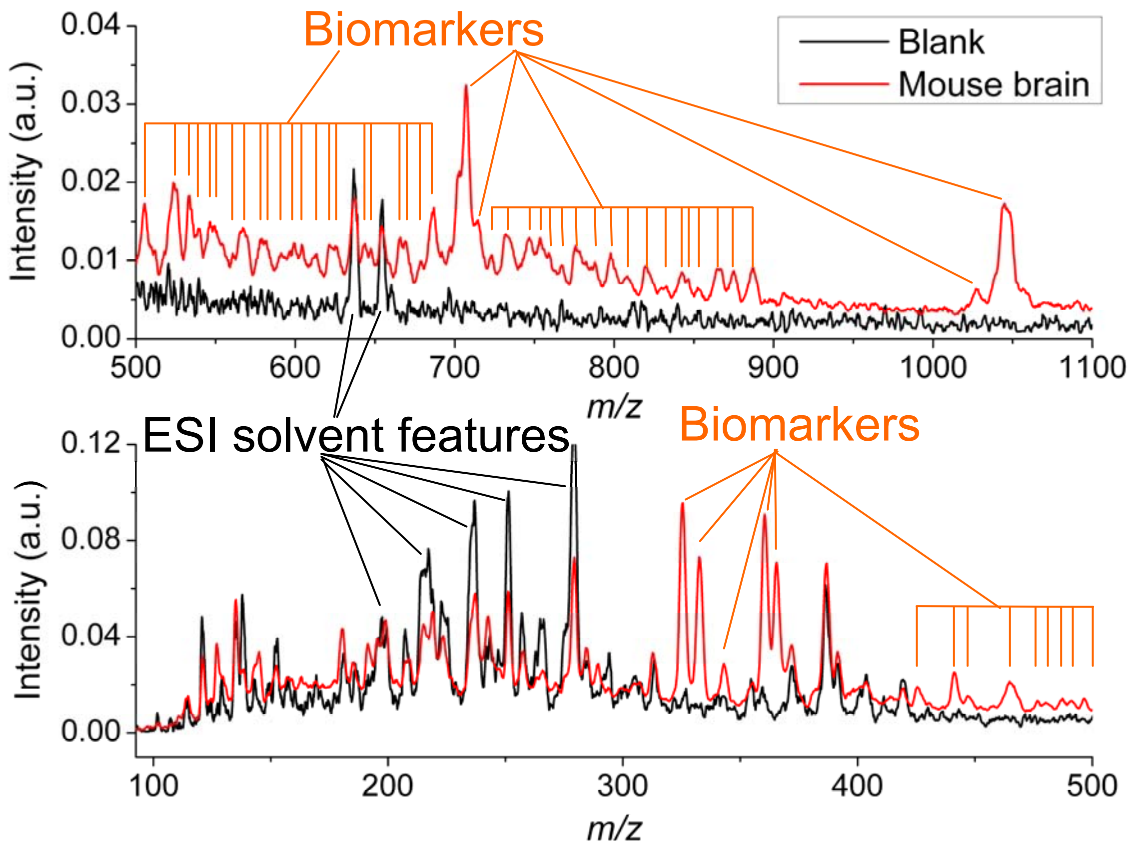

Conclusions

- Femtosecond laser vaporization at atmospheric pressure is a soft vaporization method producing intact neutrals.
- When combined with ESI, a universal vaporization and quantitative detection method can be used to analyze explosives, pharmaceuticals, macromolecules directly from surfaces including metal, glass, wood, cloth, semiconductor and sand.
- LEMS preserves condensed phase protein conformation via nonequilibrium ESI solvent conditio

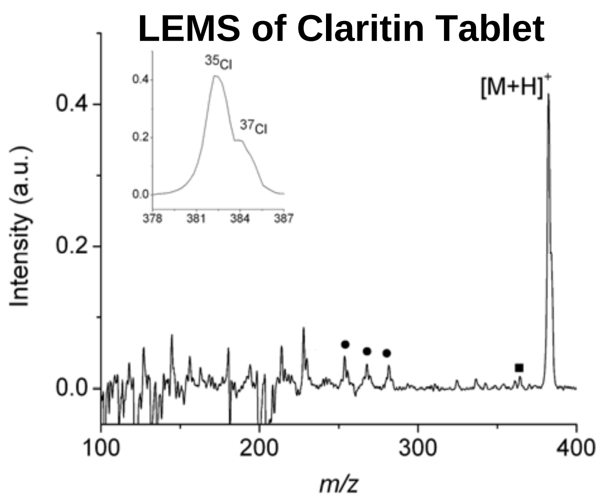

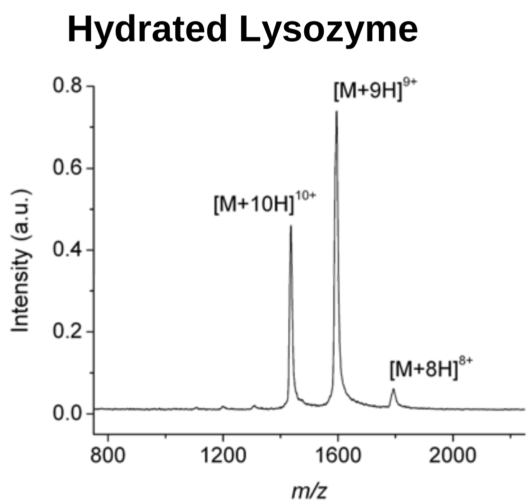

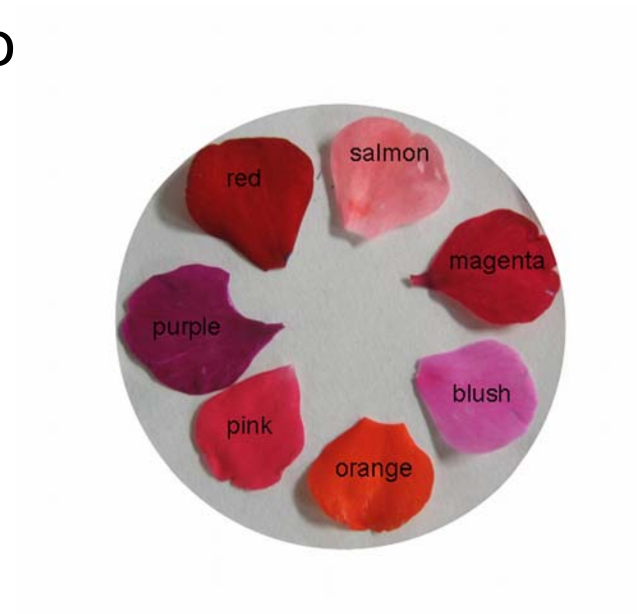

Acknowledgements and Funding

National Science Foundation
WHERE DISCOVERIES BEGIN

DEPARTMENT OF THE NAVY
ONR
Science & Technology

Air Force Office of Scientific Research
The Basic Research Manager of the Air Force Research Laboratory

JOINT IMPROVISED EXPLOSIVE DEVICE DEFEAT ORGANIZATION • 2006 •

MTO DARPA

CAPR
Center for Advanced Photonics Research

TEMPLE UNIVERSITY
INCORPORATED MAY 12, 1888
PERSEVERANTIA VINCIT
Of The Commonwealth System Of Higher Education